Phosphine modified rhodium catalysts for the carbonylation of methanol

A thesis submitted for the degree of Ph.D. by

Gareth William Lamb

Under the Supervision of Dr. Matthew L. Clarke

School of Chemistry

The University of St Andrews, Jan 2008

Declaration

I, Gareth William Lamb, hereby certify that this thesis, which is approximately 38,244 words in length, has been written by me, that it is the record of work carried out by me and that it has not been submitted in any previous application for a higher degree.

Date Signature of candidate

I was admitted as a research student in October 2004 and as a candidate for the degree of Ph.D in October 2005; the higher study for which this is a record was carried out in the University of St. Andrews between 2004 and 2007.

Date Signature of candidate

I hereby certify that the candidate had fulfilled the conditions of the Resolution and Regulations appropriate for the degree of Doctor of Philosophy in the University of St. Andrews and that the candidate is qualified to submit this thesis in application for that degree.

Date Signature of supervisor

In submitting this thesis to the University of St. Andrews I wish access to it to be subject to the following conditions: for a period of 2 years from the date of submission, this thesis shall be withheld from use; I understand, however, that the title and abstract of the thesis will be published during this period of restricted access; and that after the expiry of this period the thesis will be made available for use in accordance with the regulations of the University Library for the time being in force, subject to any copyright in the work not being affected thereby, and a copy of the work may be made and supplied to any bona fide library or research worker, that my thesis will be electronically accessible for personal or research use, and that the library has the right to migrate my thesis into new electronic forms as required to ensure continued access to the thesis. I have obtained any third-party copyright permission that may be required in order to allow such access and migration.

Date Signature of candidate.

"*Some men spend a lifetime in an attempt to comprehend the complexities of women. Others preoccupy themselves with simpler tasks such as understanding the theory of relativity*"

Albert Einstein

Acknowledgements

I would like to start by thanking Dr. Matt Clarke for giving me the opportunity to work in his lab and do the project in the first place and for helping me to develop many of the skills that will hopefully hold me in good stead down in Bath. I am truly grateful.

I would also like to thank the whole of the Matt Clarke group past and present for all of their support during my PhD and for making the past three years so enjoyable. The usual suspects that owe most thanks include Dr. Jose Fuentes and Dr. Geoff Roff for all the invaluable help, Dr. Belen Diaz and Karen Damien for teaching me the 'vital' Spanish and Italian phrases, also Ed Milton and Charlotte Jones for putting a smile on my face even during some of the more testing days in the lab. A big thank you also goes to two of the newer members of the group, Gary Noonan and Scott Phillips. Tight lines Gary!

I also wish to express my gratitude to Dr. Bruce Williams, Andrew Miller, Dr. Dave Law, Dr. Glenn Sunley and all those from BP who have helped during my trips down to BP and taken time to listen to my research and contribute to so many fruitful discussions. A big thank you must also be given to the EPSRC and BP who have helped to fund my research and to all the people from the chemistry department at the University of St. Andrews who have assisted me over the last three years, in particular Alex Slawin, Melanja Smith and Tomas Lebl.

Finally, I would like to thank my parents and 'lil sis' Victoria for all their support, even braving the Scottish weather on their many trips. For some, mentioning no names, these trips were also a cultural learning experience where it was realised you don't need euros up here and there isn't a first, second or even a third road-bridge. Behind every man there is of course a fantastic woman, for me this has been Emma. Thank you so much for everything you've done to support me during the last three years you're the best, I couldn't have done it without you!

Abstract

The carbonylation of methanol to acetic acid is one of the most important applications in homogeneous catalysis. The first chapter comprises a review on the mechanistic studies into the catalytic cycle of the 'Monsanto process' and includes some of the most prominent studies into the use of phosphines in the rhodium-catalysed carbonylation of methanol.

The second chapter of this thesis reports on an investigation into the application of rhodium complexes containing several C_4 bridged diphosphines, namely BINAP, dppb, dppx and dcpb as catalysts for hydrogen tolerant methanol carbonylation. An investigation into the structure, reactivity and stability of pre-catalysts and catalyst resting states of these complexes has also been carried out. The origin of this hydrogen tolerance is explained based on the differing reactivities of the Rh acetyls with hydrogen gas, and by considering the structure of the complexes.

In the third chapter I report on an investigation into how electronic properties and coordination mode affect the elimination of phosphonium salts from rhodium complexes. The stability of a range of monodentate, bidentate and tridentate rhodium-phosphine complexes was tested. I also report on the formation of a novel bidentate complex containing a partially quaternised TRIPHOS ligand and investigate the mechanism of formation using $^{13}CH_3I$. Strong evidence is also presented supporting a dissociative mechanism as the means of phosphine loss from the rhodium centre.

In the final chapters I report an investigation into the stability of rhodium-aminophosphine ligand complexes and into increasing the solubility of potential rhodium pre-catalysts through the use of amine-containing phosphine ligands.

Abbreviations

%	percentage
δ	chemical-shift, in parts per million downfield of standard
Å	angström
Ac	acetyl
Ar	aromatic
atm	atmosphere
BDPP	(2*S/R*,4*S/R*)-bis(diphenylphosphino)pentane
BINAP	2, 2'-Bis(diphenylphosphino)-1, 1'-binaphthyl
BIPHEP	2, 2'-Bis(diphenylphosphino)-1, 1'-biphenyl
BP	British Petroleum PLC
br	broad (NMR)
Bu	butyl
ºC	degrees Celsius
ca.	circa
CI	chemical ionisation (mass spectroscopy)
cm	centimetre
cod	cylcooctadiene
d	doublet (NMR)
dcpb	1, 4-Bis(dicyclohexylphosphino)butane
dcpe	1, 2- Bis(dicyclohexylphosphino)ethane
DCM	dichloromethane
dd	doublet of doublets (NMR)
DIOP	4,5-bis(diphenylphosphinomethyl)-2,2-dimethyldioxolane
DMF	*N*, *N*-dimethylformamide
dppb	1, 4-Bis(diphenylphosphino)butane
dppe	1, 2- Bis(diphenylphosphino)ethane
dppm	1, 1-Bis(diphenylphosphino)methane
dppp	1, 3-Bis(diphenylphosphino)propane
dppx	1, 4-Bis(diphenylphosphino)xylene
dt	doublet of triplets (NMR)

e.g.	for example
EI	electron impact (mass spectroscopy)
eq.	equivalent
ES-	negative electrospray
ES+	positive electrospray
ESI	electrospay ionisation
Et	ethyl
FAB	fast atom bombardment (mass spectroscopy)
FT-IR	Fourier transform infrared
GC	gas chromatography
g	gram
HPIR	high pressure infrared
hr	hour
HRMS	high resolution mass spectroscopy
Hz	hertz
IR	infrared
J	coupling constant (NMR)
L	ligand
Lit	literature
LSIMS	liquid secondary ion mass spectroscopy
M	moles per litre
m	multiplet (NMR)
m/z	mass to charge ratio (mass spectroscopy)
M^+	molecular ion
Me	methyl
mg	milligram
MHz	megahertz
min	minute
ml	millilitre
mm	millimetre
mmol	millimole
mol	mole
MS	mass spectroscopy
NBD	noraboradiene

NMR	nuclear magnetic resonance
o	*ortho*
p	*para*
Ph	phenyl
ppm	parts per million
q	quartet (NMR)
quin	quintet (NMR)
rac	racemic
RT	room temperature
s	singlet (NMR)
S/C	substrate-catalyst ratio
T	temperature
t	triplet (NMR)
^{t}Bu	*tert*-butyl
Temp.	temperature
THF	tetrahydrofuran
TLC	thin layer chromatography
TOF	turn over frequency
TON	turn over number
v	wavenumbers (cm^{-1})
vol	volume

Table of contents

Chapter I
Part A: The carbonylation of methanol

1.1 The history of acetic acid production

Acetic acid, also known as ethanoic acid, is a major bulk chemical with a global demand of around 7 million tonnes per year.[1] Just under a quarter of this demand is met by recycling, with the remainder being manufactured from petrochemical feedstocks and biological sources.[2] The preferred method of manufacture is by the carbonylation of methanol and this accounts for approximately 60 % of the total world acetic acid manufacturing capacity.

Acetic acid is a valuable building block and has a number of commercial applications. The production of vinyl acetate accounts for between 40-45 % global consumption of acetic acid and once polymerised is used in paints and adhesives. The next largest consumer of acetic acid is the production of acetic anhydride, accounting for 25-30 % annual consumption of acetic acid, with its main application being the production of cellulose acetate for use in photographic film. Acetic anhydride is also used in the production of aspirin, heroin and other pharmaceuticals.

Other uses of acetic acid include the production of esters for use in inks, paints and coatings (15-20 %) as well as foodstuffs such as table vinegar and the acidity regulator E260. Glacial acetic acid can also be used directly as a solvent in organic synthesis; one such example is in the production of terephthalic acid (TPA), which is the raw material for the production of polyethylene terephthalate (PET), a recyclable plastic commonly used in packaging. Currently this only accounts for around 5-10 % of the global acetic acid consumption, however, there is increasing demand for PET, which may ultimately lead to a rise in this sector.

The production of acetic acid can be traced back as far as 10,000 BC.[3] In fact, any culture producing wine or beer will have inadvertently discovered that on exposure to air a souring occurs due to the production of vinegar by bacteria such as *Acetobacter*

and throughout antiquity this vinegar has been used in everything from foodstuffs to dyes. However, over the last 100 years, production of acetic acid has shifted away from the traditional fermentation of ethanol and evolved through a series of complex processes, taking advantage of the development of new technologies and the availability of raw materials.

At the start of the 20th century there were still a number of other non-catalysed processes in operation, one such example was the distillation of wood. This produced around 10,000 tonnes per annum, with *ca.* 30 % being used in the German manufacture of indigo dye.[4] However, in the early 1910's with the large-scale industrialisation of the coal mining industry, the first metal-catalysed route to acetic acid was developed.[5] This was a two-step process, which involved the mercury-catalysed hydrolysis of coal-derived acetylene to produce ethanal that was subsequently oxidised using a manganese ethanoate catalyst to form acetic acid.

In the late 1950's, the rapid expansion of the oil industry fuelled the development of two further processes. The first of these was the oxidation of paraffin hydrocarbons using manganese or cobalt salts.[6] This was commercialised by BP in Europe and Celanese in the US. The second of these processes was the palladium-copper catalysed oxidative hydration of oil-derived ethylene to ethanal.[7] Commercialised by Wacker Chemie in 1956, this was to become known as the Wacker process. The Wacker process at the time was hugely successful with *ca.* 90 % of the global demand for acetic acid/acetaldehyde being produced in this way. Today, although it still plays a role in this production of acetic acid, it has been marginalised by the development of carbonylation processes.

The first of these carbonylation processes was commercialised in 1960 by BASF,[8, 9] once again taking advantage of large amounts of newly available feedstock, CO and methanol, both of which can be derived from natural gas. BASF were able to benefit from significant cost advantages through the use of these cheap feedstocks. This process used an iodide-promoted cobalt catalyst and even though this was a vast improvement on existing technologies with selectivity towards methanol of *ca.* 90 %, it was severely disadvantaged by the use of very high pressures (600 atm) and high temperatures (230 ^{o}C) as well as the complex and expensive purification steps.

Although, the BASF process is considered to be the father of the modern day carbonylation process, very few plants were ever built as the 'Monsanto process' soon superseded the success of this breakthrough. In 1966, Paulik and Roth[10] of the Monsanto Company developed a rhodium-iodide catalysed system and within the space of four years put the process into commercial operation with the first plant being built in Texas City in 1970. The major advantage of the 'Monsanto process' over that of the BASF system was the use of significantly milder conditions (30-60 atm pressure and 150-200 ^{o}C) as well as a higher selectivity (~99 %) (Table 1.1). These advantages led to major cost reductions, with significant saving in construction costs and product purification. It should be noted however, that one disadvantage with all of the carbonylation processes is that the reaction medium is extremely corrosive (acetic acid/HI) and requires the use of expensive, exotic materials such as hastelloy for plant construction.

Process	Selectivity (% C per mol)	T/^{o}C	p/atm
Naphtha oxidation (BP)	65-70	185	48
Methanol carbonylation, cobalt catalyst (BASF)	90	230	600
Methanol carbonylation, rhodium catalyst (Monsanto)	>99	150-200	30-60
Methanol-Methyl acetate carbonylation, rhodium catalyst (BP)	'High'	150-200	30-50

Table 1.1. Comparison of reaction conditions and selectivity for commercial acetic acid processes

In 1986, BP Chemicals PLC acquired the rights to the Monsanto technology and rapidly licensed the technology around the world. Over the past 20 years they have continuously sought to optimise and improve upon the original Monsanto process with one such example being the co-production of acetic anhydride and acetic acid, by the carbonylation of methyl acetate and methanol in their A5 plant at Hull, UK. More recently, BP unveiled the Cativa process in 1996, which uses an iridium catalyst and a promoter system. Although based upon the rhodium catalysed system, the Cativa

process gives higher activity and operates under a much lower water concentration aiding in a more energy efficient purification.

Over the last three decades there has been a plethora of research published concerning the rhodium-catalysed carbonylation of methanol, including in-depth mechanistic studies and reported improvements to the system via the use of phosphine ligands. This review will address some of the most poignant examples.

1.2 The Monsanto process

Although the Monsanto Process came on-line in 1970, the actual mechanism of the catalytic reaction was not fully understood for a further 6 years. During this period several key papers were published on the preparation and properties of rhodium halocarbonyl complexes with Vallarino reporting the first halocarbonyl anions of rhodium.[11] Although, it should be noted that dimeric carbonyl halides, $[Rh_2(CO)_4X_2]$ (X = Cl, Br, I), had been known and extensively studied over the 20 years preceding this. One method that was developed by Valarino, and one that would prove useful in the characterisation of several key intermediates was the isolation of anionic rhodium species through counter ion exchange. Upon addition of a suitable organic cation such as tetrabutylammonium, $[(C_4H_9)_4N]^+$, and tetraphenylarsonium, $[(C_6H_5)_4As]^+$, the salts of the anion $[Rh(CO)_2X_2]^-$ (X = Cl, Br, I) could be isolated as crystalline solids in good yield. Through a series of electrical conductivity tests, the complex was shown to be similar to other compounds of Rh(I) d^8 configuration. The anion was therefore assigned a square planar geometry with the infrared spectrum indicating that the carbonyls lay in a *cis* configuration.

Soon, after this several others reported similar findings, including a study into the direct carbonylation of solutions containing rhodium salts.[12] This communication was developed and expanded upon by one Denis Forster, who would later contribute massively to the understanding of the catalytic cycle and its related mechanisms. Forster studied the carbonylation of Rh(III) halides in aqueous and aqueous-alcoholic media and supported the previous report by James and Rempel by showing the eventual formation of $[Rh(CO)_2X_2]^-$. [13] However, Forster also showed that the formation of this

anionic species was preceded by an intermediate and through the use of the techniques set out by Vallerino, Forster was able to isolate the intermediate as the salt, $[(C_4H_9)_4N]_2[Rh(CO)I_5]$.

In 1975 an article by Roth was published describing some of the chemistry involved in the production of acetic acid, with particular emphasis on the role played by rhodium complexes in the catalytic cycle.[14] This was the first publication to attempt to fully understand both the organic and organometallic cycles involved in this reaction. Through a series of known experimental properties Roth started to theorise on the composition of the carbonylation catalyst. It was believed that the catalytic species consisted of a coordination complex of rhodium with carbon monoxide and halogen ligands. He reported that a diverse range of rhodium and iodine compounds had been tested, and after an initial incubation period similar rates were observed, suggesting that they tend to form the same active catalytic species. Solvent effects, such as faster rates in more polar solvents, also indicated that the active species was ionic in nature.

The reported results of the kinetic studies of the rhodium-catalysed carbonylation of methanol showed several interesting features. Firstly the reaction order was found to be zero order with respect to methanol and carbon monoxide. As a consequence of zero order dependence on carbon monoxide, high reaction rates could be maintained at low reaction pressures. Another key observation was that concerning the fate of methyl iodide. During the reaction it was noted that methyl iodide concentrations reached a steady state very rapidly and that this was then maintained for the duration of the reaction with no decrease in rate. From these observations, Roth was able to come up with the basis of what we now know to be the acknowledged catalytic cycle for the rhodium-catalysed carbonylation of methanol even theorising that the oxidative addition of methyl iodide to the rhodium metal centre was the rate-determining step.

It was not until the mid-1970s that Forster and co-workers attempted to define the key intermediates in the catalytic cycle.[15, 16] From his previous work he knew that starting with Rh(III) halides the anionic species $[Rh(CO)_2X_2]^-$ could be generated through carbonylation in hydroxylic media. Using this as his starting point he proposed the following organometallic pathway (Scheme 1.1).

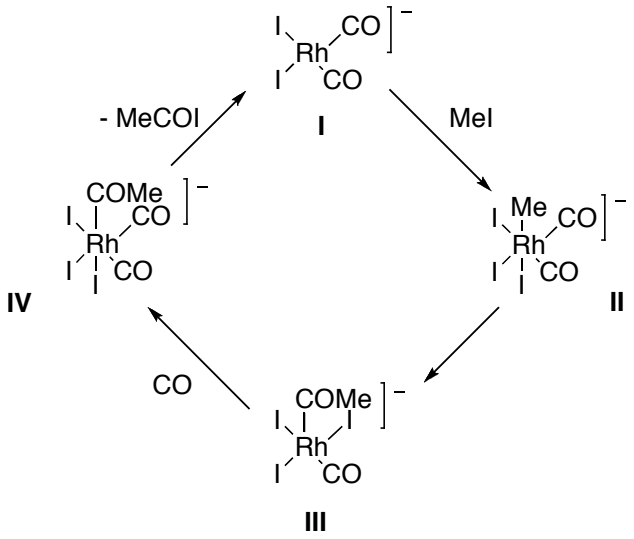

Scheme 1.1. Forster's original proposal for the rhodium catalysed carbonylation of methanol.

Through extensive research it was known that addition of an alkyl halide to a d^8 or d^{10} complex resulted in the formation of a metal-alkyl σ-bond. Using a specially designed high pressure infrared spectrometer, similar to those designed by Morris and Tinker,[17-19] it could be seen that the initial stretching modes at 2064 and 1989 cm^{-1} relating to $[Rh(CO)_2I_2]^-$ are replaced by bands at 2062 and 1711 cm^{-1} as the reaction proceeds. By heating $[Rh(CO)_2Cl]_2$ with $(CH_3)_3(C_6H_5)NI$ in the presence of nitromethane and methyl iodide, Forster was able to isolate the following complex, $[(CH_3)_3(C_6H_5)N][RhI_3(CO)(COCH_3)]$. The infrared spectrum of this material was identical to the previous species that had been observed in the reaction of $[Rh(CO)_2I_2]^-$ with MeI. As this proved the formation of the acetyl intermediate **III**, it was also reasonable to assume that compound **II** is also formed as an intermediate but that this species rapidly isomerises to **III**. Although Forster readily stated that he believed that the final step to complete the cycle was that of reductive elimination of acetyl iodide he was unable to support this with any spectral evidence. He also agreed with the previous views of Roth, in that the rate-determining step was that of oxidative addition of MeI, due to the observed catalytic resting state being that of $[Rh(CO)_2I_2]^-$.

After Forster's pioneering work in the 1970's very little else was contributed to the mechanistic understanding of the cycle until the late 80's/early 90's when a number of individuals from the University of Sheffield, in collaboration with BP, began to conduct state of the art spectroscopic and kinetic measurements. Adams *et al.* were the

first of these to publish their work.[20] It included a ^{1}H and ^{13}C NMR study into several ^{13}C labelled key intermediates. They went on to show that there must be at least two acetyl species present in solution that interconverted rapidly at room temperature, related to the dimeric structure solved by Forster and co-workers in earlier studies.[15] They also managed to obtain an X-ray crystal structure the monomeric pyridine species, $[Rh(COMe)(CO)(NC_5H_5)I_3]^-$. (Fig. 1.1)

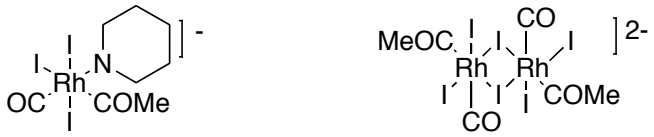

$[Rh(COMe)(CO)(NC_5H_5)I_3]^-$ $[NMe_3Ph]_2[Rh_2(COMe)_2(CO)_2I_6]^{2-}$

Figure. 1.1. The structures of the monomeric and dimeric rhodium acetyl complexes isolated independently by Mann et al. and Adamson et al.

Through these studies they were able to unambiguously prove several structures, one of which was the carbon monoxide adduct $[Rh(COMe)(CO)_2I_3]^-$. In the ^{13}C NMR spectra they observed a $^{2}J(^{13}C^{13}C)$ = *ca.* 60 Hz coupling for the two carbonyl ligands which was consistent with them being mutually *trans*, as it was well established that large coupling constants are found in Rh(III) complexes when the ligands are *trans* to one another, while smaller couplings tend to be found for mutually *cis* ligands. However, this is not the structure that commonly appears in mechanistic schemes, as it is necessary for the carbonyls to be *cis* to one another in order to facilitate reductive elimination of acetyl iodide, regenerating *cis*-$[Rh(CO)_2I_2]^-$. They therefore proposed that although several isomers existed, *trans*-$[Rh(COMe)(CO)_2I_3]^-$ was the only detectable isomer because it could not directly eliminate acetyl iodide, as this would give *trans*-$[Rh(CO)_2I_2]^-$, and as a result had a longer lifetime in solution (Scheme 1.2).

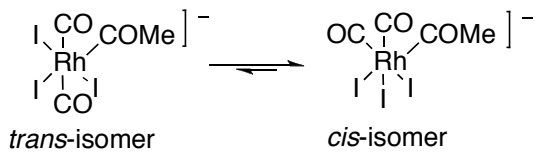

Scheme 1.2. The equilibrium between the *trans*- and *cis*-isomers of the CO adduct $[Rh(COMe)(CO)_2(I)_3]$.

They also noted that despite the facile formation of $[Rh(COMe)(CO)I_3]^-$, the rearrangement back to $[RhMe(CO)_2I_3]^-$, equilibrating the carbonyl groups does not

occur, a fact that we now know to be incorrect. From their observations they proposed a modified mechanism for the rhodium/iodide-catalysed carbonylation of methanol (Scheme 1.3).

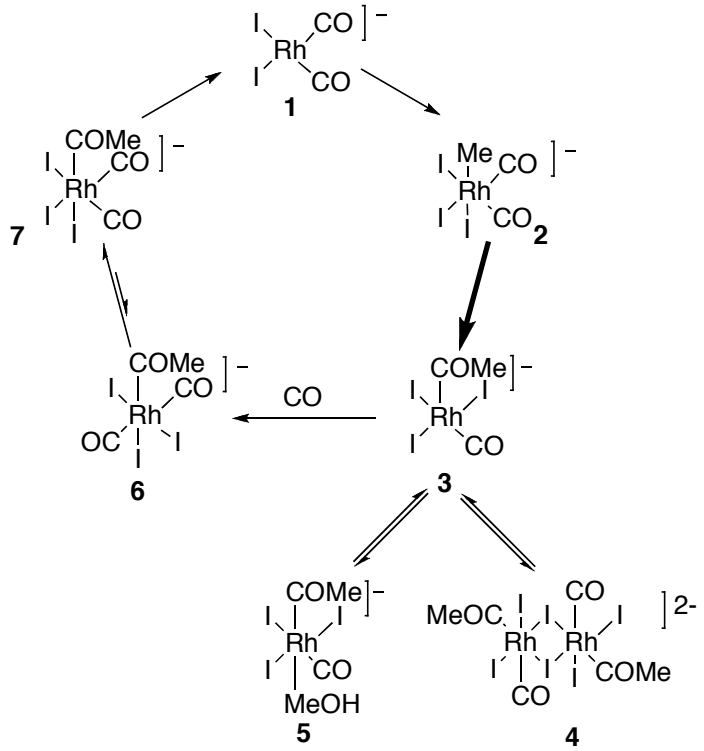

Scheme 1.3. The proposed catalytic cycle by Mann et al.

Interestingly, this modified cycle also proposes that in the presence of methanol a solvated species may form alongside that of the dynamic equilibrium between $[Rh(COMe)(CO)I_3]^-$ and $[Rh_2(COMe)_2(CO)_2I_6]^{2-}$.

It is surprising to think that by the early 90's, twenty years after Monsanto started its first plant in Texas City, the key intermediate to one of the world's most important industrial processes, utilizing homogeneous transition-metal catalysis, had not yet been detected. It wasn't until 1991 that Haynes, Mann and Maitlis *et al.* reported that the crucial intermediate, $[RhMe(CO)_2I_3]^-$, could be detected using FTIR and FTNMR spectroscopy.[21]

The observation of $[RhMe(CO)_2I_3]^-$ therefore allowed, for the first time, an estimation of the rate of methyl migration. Over the next few years, the collaboration at the University of Sheffield systematically investigated the kinetics of each of the key steps in the catalytic cycle and published their findings.[22, 23]

Through these studies, they proposed what is now considered to be the accepted dual catalytic cycle for the rhodium/iodide-catalysed carbonylation of methanol. They were able to expand on the work done by Forster and Mann by gathering crucial kinetic data and importantly observe all four key intermediates, vital to the understanding of the catalytic mechanism. The cycle and accompanying work has been broken down into the four key steps for ease of analysis and discussion.

1.3 The rhodium/iodide-catalysed cycle for the carbonylation of methanol

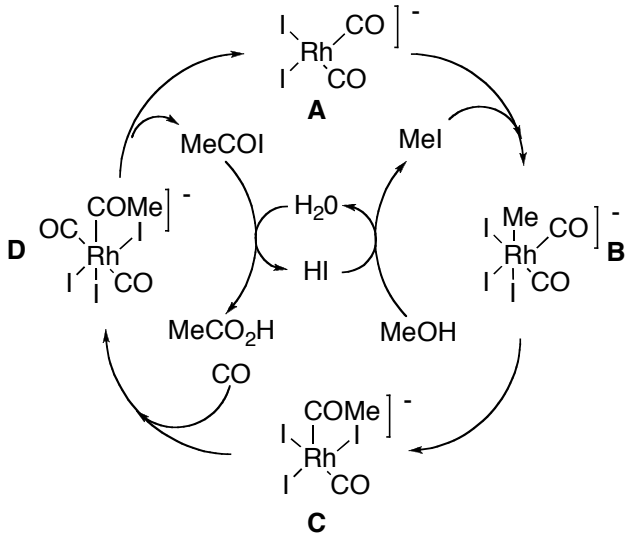

Scheme 1.4. The acknowledged rhodium/iodide dual catalysed cycle for the carbonylation of methanol

1.3.1 Oxidative addition of MeI to $[Rh(CO)_2I_2]^-$

Through the aforementioned kinetic studies, Haynes *et al.* were able to show that the oxidative addition of MeI to $[Rh(CO)_2I_2]^-$ obeyed second-order kinetics (first order with respect to [**A**] and [MeI]) with activation parameters being consistent with a S_N2 mechanism. Importantly the reaction rate was shown to have substantial dependencies upon solvent, added salts and counter ion. For example, kinetic data indicate that the reaction of methyl iodide with **A** to **C** precedes *ca*. 4 times as fast in methanol than in an aprotic solvent under comparable conditions (25 ^oC). These

observations would become crucial in the future development of this process and shall be discussed later in this section.

1.3.2 The key intermediate, $[MeRh(CO)_2I_3]^-$

Although in low concentrations, Haynes *et al.* were able to detect **B** by reacting $[Rh(CO)_2I_2]^-$ in a neat solution of MeI. The high concentration of MeI assisted by increasing the rate of the oxidative addition reaction forming **B**, whilst the rate of consumption of **B** via migratory insertion was slowed by the low polarity of the medium. Using scaled computer subtraction models two weak absorptions at 2104 and 2060 cm^{-1}could be assigned to the intermediate **B**. There are three possible structures for $[RhMe(CO)_2I_3]^-$ and these are shown in Fig. 1.2.

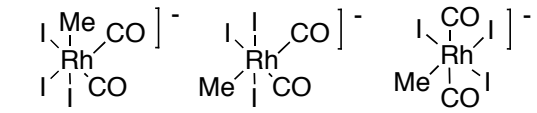

Figure 1.2. The three possible isomers of the oxidative addition product, $[RhMe(CO)_2I_3]^-$

Through the use of advanced spectroscopic methods, the collaboration at Sheffield was able to highlight the *fac*, *cis* isomer as the most feasible candidate. The presence of a single doublet in the Rh-CO region of the $^{13}C\{^1H\}$ NMR spectrum of **B** indicated that the complex contained equivalent carbonyl ligands being consistent with structures **1** and **3**, but not **2**. As well as this no coupling was reported between the methyl and the carbonyl carbons, which was also consistent with structure **1** or **3**, as a small $^2J_{(C\text{-}C)}$ value would otherwise be expected for **2**, where the methyl group is *cis* to the carbonyl. FTIR was then used to disseminate between **1** and **3**, with the observation of two ν(CO) bands of similar intensity being assigned solely to the *fac*, *cis*-$[RhMe(CO)_2I_3]^-$ isomer, **1**.

The detection of $[RhMe(CO)_2I_3]^-$ **B**, also allowed for the determination of reactivity data by monitoring its kinetic behaviour using FTIR spectroscopy. By using specifically labelled $[Rh(^{13}COMe)(CO)I_3]^-$ they were able to measure the first order rate constant of the reverse reaction between **C** and **B**. This showed that migratory insertion

is of an order of magnitude faster than the reductive elimination of MeI, proving that the low steady state concentration of **B** is due to rapid migratory insertion and not a fast back reaction. A low steady state concentration of the methyl species **B**, also goes some way to explaining the high selectivity of this cycle, especially towards the low rate of methane formation. Interestingly they also found that the equilibrium constant for the formation of **C** decreases with increasing temperature, meaning that its formation at higher temperatures is less favourable. It is therefore the trapping of **C** by CO, giving the dicarbonyl **D**, which restores the efficiency of this cycle.

1.3.3 Reductive elimination from $[Rh(COMe)(CO)_2I_3]^-$

The reductive elimination of acetyl iodide from the dicarbonyl species $[Rh(COMe)(CO)_2I_3]^-$ has received relatively little attention over the years. In 1995 the Du Pont Group showed the reversibility of the reaction (Scheme 1.5).

$$[Rh(COMe)(CO)_2I_3]^- \rightleftharpoons [Rh(CO)_2I_2]^- + MeCOI$$

Scheme 1.5. The reductive elimination of acetyl iodide from $[Rh(COMe)(CO)_2I_3]^-$

The rate of reductive elimination was shown to be slow at ambient temperatures (*ca.* 30 ^oC) having a rate almost equal to that of the rate-determining step of oxidative addition. At higher temperatures oxidative addition is rate determining, whilst below this temperature reductive elimination becomes rate determining. This demonstrates how changes in the reaction conditions may lead to dramatic changes in the rate-determining step of the catalytic cycle.

It is well known that it is possible to accelerate the rate of oxidative addition by increasing the nucleophilicity of the rhodium centre via the use of electron donating phosphine ligands. However, studies have also shown that phosphine ligands can also have a pronounced effect on the rate of reductive elimination. These shall be discussed in greater detail in Part C.

1.4 Water-gas shift reaction

The Monsanto process requires a substantial amount of water to achieve high catalyst activity and to maintain good catalyst stability. If this amount falls below ~8 wt. % then the rate determining step becomes the reductive elimination of the acetyl iodide from the dicarbonyl species $[Rh(COMe)(CO)_2I_3]^-$, **D**.[24] The main disadvantage of using such a high concentration of water is that rhodium also catalyses the water-gas shift reaction, leading to the production of CO_2 and H_2 (Scheme 1.6).

$$H_2O + CO \rightleftharpoons H_2 + CO_2$$

Scheme 1.6. A simplified equation for the water gas-shift reaction

The water-gas shift reaction itself has been known for over 100 years with its main application being in the large-scale production of hydrogen for ammonia synthesis. Other applications include increasing the H_2:CO ratio for methanation and Fischer-Tropsch synthesis, and also in the treatment of combustion exhaust gases through CO removal and H_2 generation for reducing nitrogen and sulphur oxides.

Mechanistic studies of the water-gas shift reaction by rhodium carbonyl iodide were carried out by Eisenberg *et al.* and they proposed a catalytic cycle (Scheme 1.7) that goes some way to explaining direct and indirect by-product formation during the rhodium catalysed carbonylation of methanol.[25, 26]

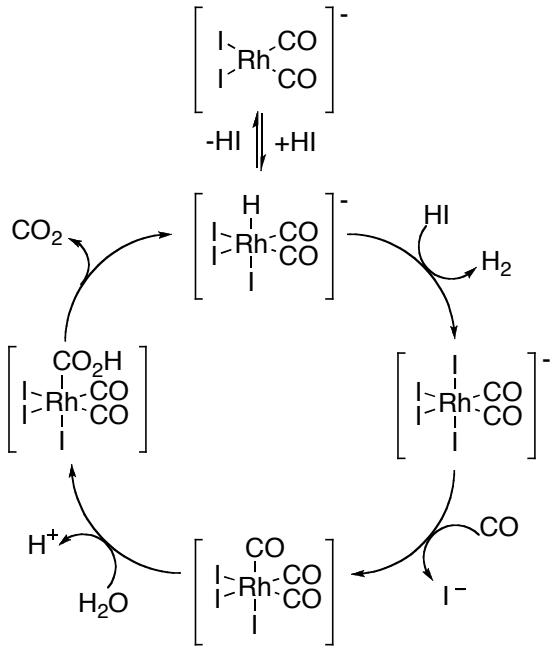

Scheme 1.7. The rhodium catalysed cycle for the water gas-shift reaction

The water-gas shift reaction represents a loss of selectivity with respect to the CO raw material. Due to the formation of gaseous by-products such as H_2 and CO_2, the CO present in the reactor is diluted down, lowering its partial pressure. To counter this, significant volumes of gas are vented leading to inefficiencies in the process. The yield on CO is however still good (*ca.* 85%) but with room for improvement.

One of the major liquid by-products of the Monsanto process is propionic acid. This is produced via the carbonylation of ethanol, which is often present as a minor impurity in the methanol feedstock. However, since more propionic acid is observed than can be accounted for from the ethanol source alone, other routes must be operating. One such suggestion is that rhodium catalyses the production of acetaldehyde, which then undergoes reduction by hydrogen, formed during the water-gas shift reaction, to give more ethanol that is in turn converted to propionic acid. The hydrogen produced via the water-gas shift reaction is also thought to be the source of methane production in these systems.

The rhodium-acetyl complex $[Rh(COMe)(CO)_2I_3]$, is one possible precursor for acetaldehyde formation as it reacts with HI to produce acetaldehyde and $[Rh(CO)I_4]^-$. This species is well known in this system, especially in CO deficient areas of the plant where it results in the loss of catalyst by precipitation of inactive rhodium triiodide.

In addition to propionic acid several others impurities exist, albeit on a much smaller scale. These mainly comprise of acetaldehyde condensation products, their derivatives and small amounts of iodide derivatives. However, under the full workings of the industrial plant the total liquid by-product production is less than 1 % and would therefore not be a problem except for the scale of acetic acid production and the purity required. The plants therefore have to employ 3 energy intensive distillation columns to produce high purity acetic acid.

1.5 Process scheme and removal of impurities

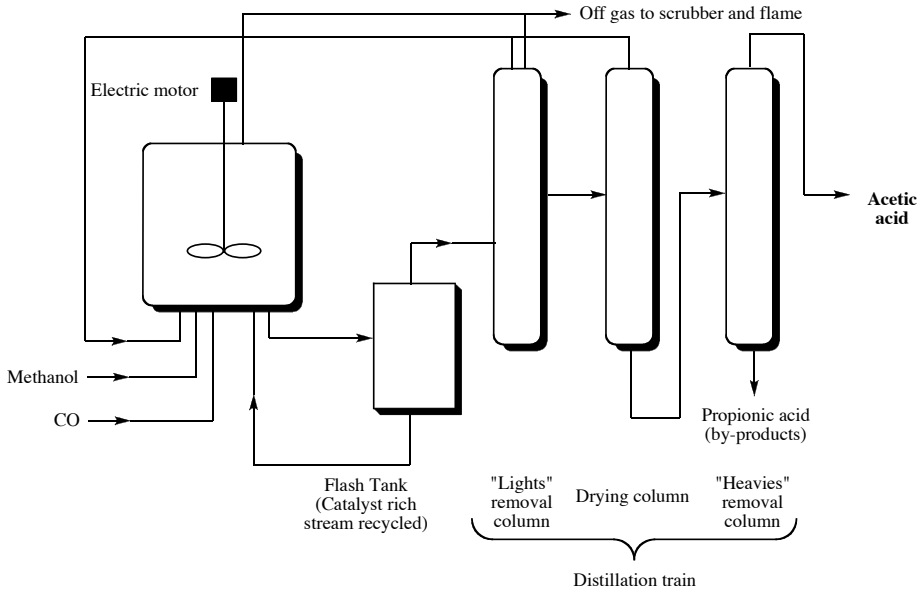

Figure 1.3. The major units comprising a commercial-scale Monsanto methanol operating plant.[24]

The industrial carbonylation of methanol is an example of a continuous process that operates in a stirred tank reactor. The simplified flow sheet in Fig. 1.3 shows that liquid is removed from the reactor through a pressure reduction value and enters an adiabatic flash tank. Here the lighter components such as methyl acetate, methyl iodide, some water and the product acetic acid are removed as vapour from the top of the vessel. The gaseous components are then collected and fed into a series of distillation columns for further purification. This process is known as ‘stripping’ and has the added advantage of retaining the catalyst in solution within the flash tank, which can then be recycled back into the reactor.

There are several limitations with the rhodium-catalysed carbonylation of methanol, as so far as the engineering is concerned. As previously mentioned, in order to maintain catalyst stability and to avoid precipitation of $[Rh(CO)I_4]^-$, a minimum partial pressure must be maintained along with a high water concentration. These restrictions reduce selectivity and increase production costs, especially as a significant amount of the water needs to be recycled to maintain a high standing concentration. Significant costs are also incurred by the operation of the large 'heavies' column that removes any of the liquid by-products previously discussed such as propionic acid.

1.6 Use of additives

In the early 80's Hoechst Celanese developed a major improvement to the Monsanto technology that involved the use of large quantities of LiI. This had the desirable effect of reducing the amount of water and HI used in the process. This increased the stability of the catalyst by solubilizing RhI_3, as this tended to precipitate out of solution. This had previously required some H_2 to reduce it back to the more soluble Rh(I) complex. The addition of LiI not only allowed a higher throughput and increased efficiency of the catalyst but also considerably reduced the side reactions, such as the water-gas shift reaction referred to earlier.

Several reasons have been postulated for the rate enhancement observed when iodide is added to a rhodium catalysed methanol carbonylation reaction. A paper by Hickey and Maitlis described the addition of a variety of salts, previously reported to improve the rate of reaction.[27] Addition of tetrabutylammonium iodide was seen to cause a maximum rate increase of *ca.* 2, attributed to a general salt effect. However, other quaternary salts such as tetraphenylarsonium, showed much larger increases in rate. Addition of bases such as meim (meim = 1-methyl imidazole) caused an even more pronounced affect by increasing the rate by a factor of 10. The presence of a species at low concentrations with two bands in the FTIR [ν(CO) 1980, 2055 cm^{-1}] led to Hickey and Maitlis proposing the formation of a five coordinate species (either $[Rh(CO)_2I_3]^{2-}$ or $[Rh(CO)_2LI_2]^-$) which they surmised may react more rapidly with MeI in an S_N2

mechanism than other species. Supporting the idea that mono-anionic species are much better nucleophiles towards MeI than their neutral counterparts.

Others have proposed that it is the role of metal salts such as LiOAc that has such a dramatic effect on the rate of product formation.[28] One can see they could be involved in the two possible reactions shown in Scheme 1.8.

$$MeOAc + MI \rightleftharpoons MeI + MOAc \quad \text{equation 1}$$

$$AcI + MOAc \rightleftharpoons Ac_2O + MI \quad \text{equation 2}$$

Scheme 1.8. Two equations showing the possible beneficial effect lithium salts may have upon the formation of acetic acid.

When M = H reaction 1 is slow, however the equilibrium may be shifted to the right by the use of a smaller cation, such as Li^+. In Reaction 2, the use of LiI once again has a positive effect on the equilibrium forcing it to the right, ensuring that acetyl iodide is converted to the product. These reactions may form what is known as the 'lithium cycle', which may be added as a third cycle in the catalytic reaction with the regeneration of MeI.

1.7 Iridium catalysed carbonylation of methanol: The Cativa™ process

The continued search for an improvement to the Monsanto process, coupled with a rising cost of rhodium, led BP to reinvestigate the early work done on the potential use of iridium instead of rhodium.[29] Although the initial work done by Forster showed that the reaction rate of rhodium was far superior to that of iridium, in 1996 BP disclosed that an improved iridium catalyst in combination with a promoter metal such as ruthenium could have a substantially improved activity and selectivity than reported in previous iridium systems.[24, 30, 31]

A distinctive feature of the Cativa™ process is its ability to operate at reduced water concentrations (less than 8 wt.% for the Cativa™ process versus 14-15 wt.% for the conventional Monsanto process). As the water concentration is reduced the rate of

reaction increases for both promoted and unpromoted systems. This therefore shares many of the advantages of the Celanese process discussed previously, including a lower by-product formation, an improved CO efficiency and decreased steam consumption. These improvements also result in several environmental benefits including an increased energy efficiency and greater than a 50 % reduction in total gaseous emissions.

Iridium was also found to offer a significant benefit in terms of increased stability compared with rhodium. The marked increase in the stability of the iridium system over that of the rhodium, even at very low water concentrations (0.5 %wt/wt), allowed for the use of much greater catalyst concentrations, making much higher reaction rates available. Investigations have also shown the iridium catalyst also remains stable under a wide range of conditions that would have previously seen the rhodium catalyst decompose to inactive and largely unrecoverable rhodium salts.

The anionic iridium cycle shown below in Scheme 1.9 is similar to that of the rhodium cycle but contains several differences responsible for the advantages of the Cativa™ over the Monsanto process.[32]

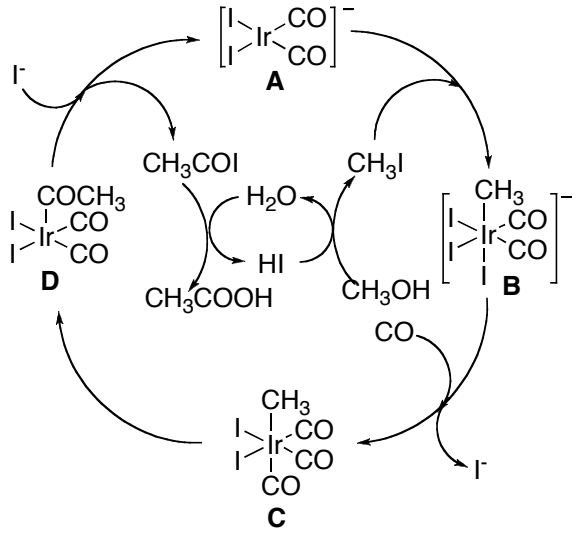

Scheme 1.9. The Iridium Cativa™ cycle

Detailed mechanistic studies by Maitlis, Haynes and co-workers[32] have shown that the oxidative addition of MeI to the iridium centre is no longer the rate-determining step and is approx. 150 times faster than the reaction with rhodium. For iridium it is the

subsequent migratory insertion of CO to form the iridium-acyl species **C**, which involves the elimination of ionic iodide and the coordination of an additional CO ligand that is the slowest step. This results in a dramatic improvement in the available reaction rates.

One of the key features of the Cativa™ process is the use of promoters. These fall into two distinct groups: simple iodide complexes of zinc, cadmium, mercury, gallium and indium, and carbonyl-iodo complexes of tungsten, rhenium, ruthenium and osmium. The promoters themselves show no activity towards the carbonylation themselves and instead appear to promote the lability of $[Ir(CO)_2I_3Me]^-$ towards migratory insertion. Studies also suggest a further role of the promoters is in preventing the formation and build-up of inactive iodide species such as $[Ir(CO)_3I_3]^-$ and $[Ir(CO)_2I_4]^-$.

1.8 Summary

The Monsanto process is one of the corner stones of modern homogeneous catalysis with a multi-million tonne annual turnover and is licensed to over ten companies worldwide. However, the development of the Cativa™ process has led to the successful improvement of what was already an established process for the commercial production of acetic acid. In the next part of this review we shall look as how phosphines may also play a role in future improvements to the rhodium-catalysed carbonylation of methanol.

Part B: The rational design of a catalyst for the carbonylation of methanol

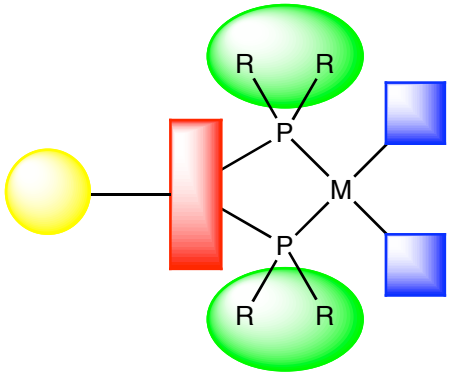

Figure 1.4. The rational design of a ligand

The rational design of a homogeneous catalyst is a complex procedure and one that often defies linear correlations due to our relatively basic knowledge of parameters and solution dynamics. However, by varying a certain range of parameters within a small set of catalytic candidates, a basic understanding of how this variation may alter activity can be achieved. These parameters may include varying the metal within a range of similar complexes such as $[Ni(CO)_4]$, $[HCo(CO)_4]$, $[Rh(CO)_2I_2]^-$, $[Ir(CO)_2I_2]^-$, or possibly varying the ligand, however this in itself is extremely complex, and can be broken down into several distinct areas (see Fig. 1.4). Each of these areas needs to be approached with caution, with each variation being measured independently of any other changes in the complex in order to understand their true effect. In this way a rational design of a catalyst can be a slow procedure with thousands of interchangeable parameters to be considered. Several groups have developed automated methods of preparing huge libraries of catalysts from just a handful of changeable parameters but these libraries tend in themselves to be focussed around a central design and therefore are only an expansion on the above theme.

The following part of this review will deal with the rationale behind the design of a catalyst with a preferential bias towards phosphine ligands and the carbonylation of methanol.

1.9 The use of phosphines as ligands in homogeneous catalysis

Many of the most important homogeneously catalysed reactions use phosphine ligands with their metal catalysts. The use of phosphines is widespread and features in both academic and industrial research involving homogeneous catalysis. There are several famous examples including the 'Wilkinson' catalyst $RhCl(PPh_3)_3$,[33] which catalyses the hydrogenation of olefins, Noyori's asymmetric hydrogenation catalyst which utilises BINAP,[34] Buchwald's series of phosphine containing ligands for C-N cross coupling[35] and literally thousands of other examples to choose from.

This interest generated by the use of phosphines is down to the way they behave as ligands. Phosphines have the ability to tune the steric, electronic, coordination and solubility properties of a complex and this makes them ideal candidates for research when designing a catalyst. They also promote the solubility of metal complexes in a wide range of organic media and although the majority of phosphines are insoluble in water, there are exceptions among the sulfonated phenylphosphines and pyridylphosphines. The ability of phosphines to stabilise both low and high oxidation states of metals is also a key feature in homogeneous catalysis.

This section will now give a brief introduction into the chemistry of phosphines in homogeneous catalysis and will seek to understand how different phosphines behave in catalytic reactions describing them in terms of their coordination mode, size, electronic character and in the case of bidentate ligands their bite angle.

1.9.1 Electronic parameters

The bonding involved in the coordination of a phosphine with a metal centre can be broken down into 2 components, the σ and the π-bond. The σ-bond is formed from the donation of a lone pair of electrons from the phosphine into an empty (hybrid)-orbital present on the metal, whereas, the π-bond is formed through backbonding between a filled metal d-orbital and an empty orbital on the phosphine ligand as can be seen in Fig. 1.5.

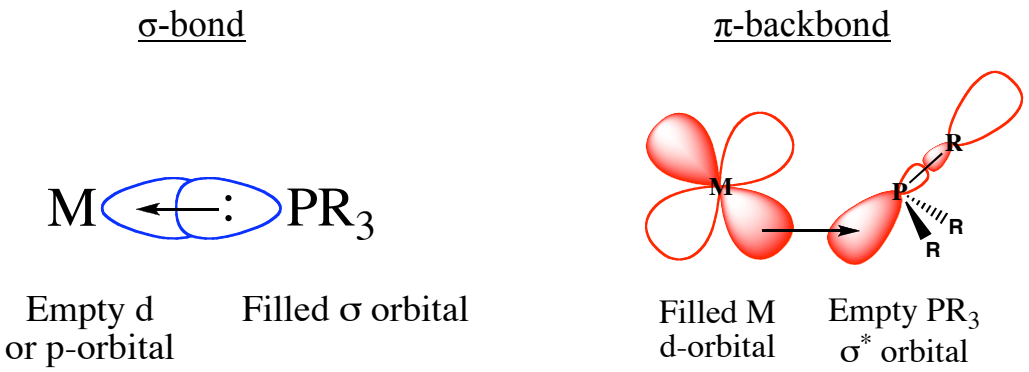

Figure 1.5. The orbital interactions of a phosphine ligands and a transition metal centre.

This empty phosphorus orbital has been described as being either a d-orbital or an antibonding σ-orbital; current consensus is that the latter is more appropriate, given the relatively high energy of a phosphorus d-orbital. The energy level diagram in Fig. 1.6 shows the σ-donor and π-acceptor properties of a phosphine-metal complex.

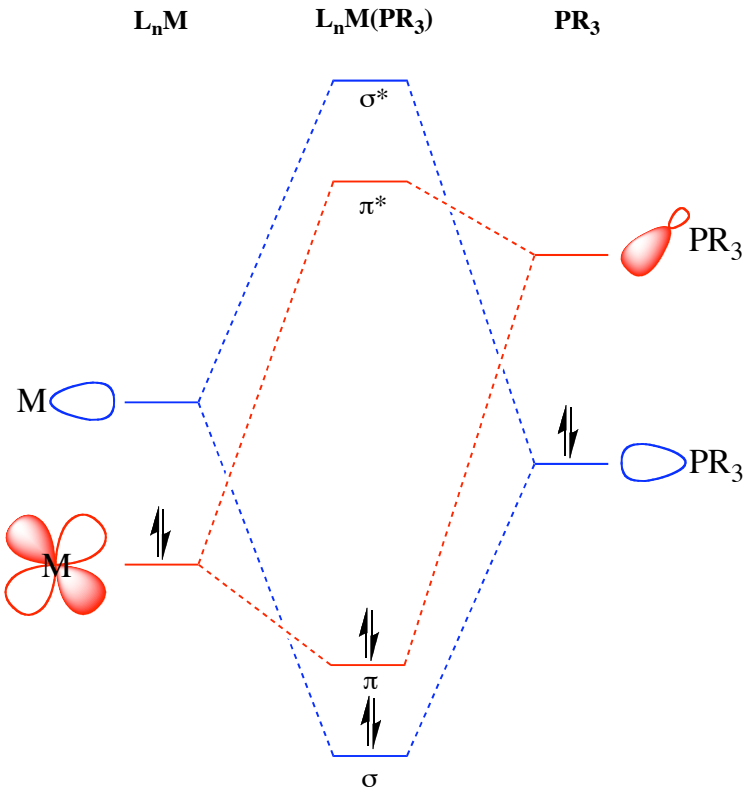

Figure 1.6. An energy level diagram showing the σ-donor and π-acceptor properties of a phosphine-metal complex.

Substituents on the phosphine can have an enormous effect on the σ-donating capability of the ligand. For example, placing an electronegative group on the phosphine lowers the electron density on the lone pair resulting in a decrease in the σ-bonding capability of the ligand. However, at the same time due to the lowering in energy of the π-acceptor (σ-*) on phosphorus, the ability for the metal centre to backbond is thought to be increased. Phosphines therefore can exhibit a range of σ-donor and π-acceptor capabilities and the electronic properties of the metal centre can be fine tuned by the substitution of electronically different phosphines.

In 1970 Tolman proposed that the CO infrared stretching frequency of a carbonyl group attached to a transition metal could be used to define the electron donor-acceptor properties of any given trivalent phosphorus ligand.[36] Tolman used complexes of the type $NiL(CO)_3$ as they form very rapidly on mixing $Ni(CO)_4$ with L in a 1:1 ratio at room temperature. More importantly spectroscopic determination of such compounds gives rise to a very sharp carbonyl band, in the infrared spectrum, the A_1 band. The σ-basicity and π-acidity of phosphorus ligands in complexes such as $NiL(CO)_3$ and $CrL(CO)_5$, in which L is the phosphorus ligand, can therefore be studied by noting the frequency of this A_1 band.

Strong back-donation, low C-O stretch

Weak back-donation, high C-O stretch

Figure 1.7. The electronic effect of phosphine ligands

Fig. 1.7 shows that strong σ-donor ligands give a high electron density around the metal centre resulting in a substantial back-donation to the CO ligands and lowered frequencies. Whereas strong π-acceptor ligands compete with CO for the electron back-donation and as a result the CO stretching frequencies will remain high.

The electronic parameters of phosphine ligands may differ slightly from metal to metal, in the case of Tolman who used $NiL(CO)_3$ the variability of the phosphines are reflected in Table 1.2.

Ligand PR_3, R=:	χ-value	IR frequency (A_1) of $NiL(CO)_3$ (cm^{-1})
t-Bu	0	2056
n-Bu	4	2060
4-$C_6H_4NMe_2$	5	2061
Ph	13	2069
4-C_6H_4F	16	2072
CH_3O	20	2076
PhO	29	2085
CF_3CH_2O	39	2095
Cl	41	2097
$(CF_3)_2CHO$	54	2110
F	55	2111
CF_3	59	2115

Table 1.2. Selected substituent contribution, χ, values together with corresponding A_1 band frequencies.[28]

χ is a substituent contribution appropriate to each group attached to the phosphorus. Carbon substituents give χ-values ranging from 0 to 20, phosphites are found in the range from 20 to 40, and halogen substituted compounds are found up to 59.

For rhodium carbonyl complexes, of which the entirety of this report will be based, the C-O stretching frequency of *trans*-$RhClL_2(CO)$ is most commonly used, examples of which are shown below in Table 1.3.

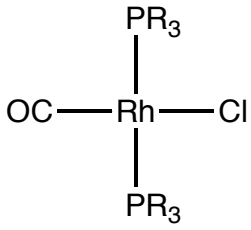

Phosphine Ligand	υ_{CO} [$L_2Rh(CO)Cl$] (cm^{-1})
$(PhO)_3P$	2016
$(p\text{-}CF_3C_6H_4)_3P$	1990
Ph_3P	1965
$PhMe_2P$	1965
Me_3P	1960
$P(N(CH_3)_2)_3$	1959
Et_3P	1956
Cy_3P	1943

Table 1.3. Selected examples of A_1 values for rhodium carbonyl complexes alongside the generic structure for $[Rh(L)_2CO(Cl)]$.[37]

1.9.2 Cone angle

To compliment his electronic parameter Tolman developed a steric parameter, θ, applicable to trivalent phosphorus ligands.[38, 39] Tolman constructed CPK molecular models (space filling models where the boundary of each atom is related to the actual volume it occupies in space, i.e. its van der Waals radius) and at a distance of 2.28 Å from the metal centre, a cone is constructed with all the substituents arranged as to occupy the minimum volume. The cone angle is then measured simply in degrees (see Table 1.4).

This method can be effective when measuring within a series of similar ligands, however for aryl phosphites some caution needs to be exercised in using the absolute values as not only are these based on the assumption of the metal-phosphine bond length being 2.28 Å, with the ligand retaining tetrahedral symmetry but also that the ligands form perfect cones. It has been seen in the example of $P(Cy)_3$ with a cone angle of 170 ^{o}, we would not expect $Pt\{P(Cy)_3\}_3$ to be particularly stable. However, crystal structure analysis shows that the ligands adopt an orientation so that the cyclohexyl groups mesh together and thus reduce steric crowding and stabilise the molecule. This point has been addressed by the use of the 'solid angle', which takes into account crystal structure data. The procedure involves the projection of all atoms of the ligand on the metal surface and the solid angle tells us how much of the surface is covered by

this projection. Several other methods exist utilising modern molecular mechanics and analysis of data taken from X-ray studies and data mining. One such method is the AMS method (AMS = the accessible molecular surface), which calculates the effective contours of the ligands and has been used extensively to calculate the pocket angle within the active site of enzymes.

Ligand PR_3, R=:	θ-value
H	87
CH_3	107
Me_3	118
PhO	128
n-Bu	132
Ph	145
i-Pr	160
C_6H_{11}	170
t-Bu	182
2-t-BuC_6H_4O	190
2-$(CH_3)C_6H_4$	194

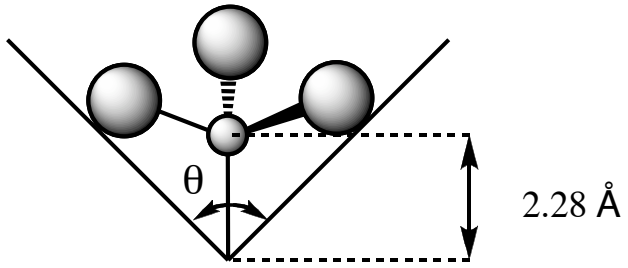

Table 1.4. Selected cone angles, θ, for trivalent phosphorus ligands alongside a representative diagram of Tolman's cone angle.[28]

1.9.3 Bite angle

Due to the chelate effect bidentate ligands can often help in stabilising certain complexes and thus reduce the number of possible different species present in solution. In this way, the use of bidentate ligands can offer a greater degree of control over stereo and regioselectivity in many catalytic reactions.

Extending the use of the Tolman angle to include bidentate ligands is not as straightforward as monodentates, due to variables such as the length and flexibility of the backbone. A standardised bite angle can be used as more convenient way of comparing bidentate ligands.[28] This 'bite angle' can be calculated either by molecular modelling or P-M-P angles determined from crystal structures. There is therefore a distinction between crystallographic bite angles that relate to specific measurements from a structure, and the natural bite angle,[40] a computationally calculated value that is

an extremely useful method to quantify the characteristics of diphosphine ligands. Molecular modelling techniques use a dummy rhodium atom and fixed Rh-P distances of 2.315 Å as a way of standardising the measurement so that a meaningful comparison between different ligands can be obtained.

In reality, the P-M-P angle found in transition metal complexes is a compromise between the preferred bite angle of the ligand and the preferred bite angle of the metal. The preference in bite angle of the ligand is mainly dictated by the steric hindrance of the substituent groups on the phosphorus arms as well as other constraints such as the flexibility of the backbone (see Table 1.5 for prime examples). The preferred bite angle of the metal, or 'electronic bite angle' as it is otherwise known, is associated with electronic structure at the metal centre. This bite angle determines the metal hybridisation and as a consequence metal orbital energies and reactivity and as a consequence may stabilise or destabilise certain transition states in the catalytic cycle.

Ligand	X-ray values (P-M-P)	Molecular modelling[a] (P…P)
dppm	71.7	
dpp-benzene	83.0	
dppe	85.0	78.1, 84.4 (70-95)
dppp	91.1	86.2
dppb	97.7	98.6
dppf	95.6	99.1
BINAP	92.4	
DIOP	97.6	102.2 (90-120)
Duphos(Me)	82.6	
BISBI	122.2	122.6 (101-148)[b]
		112.6 (92-155)
		123 (110-145)
NORPHOS		111.2
Transphos		107.6 (93-131)
DPEphos	102.5	102.2 (86-120)
Xantphos	107.1	111.7 (97-135)
DBFphos		131.1 (117-147)

Table 1.5. Diphosphines and their bite angle. [a] In brackets the flexibility range, i.e. accessible angles within 3 kcal/mol. [b] Two conformations of the backbone.[28]

There are many examples showing that the ligand bite angle is related to catalytic performance. Early examples include, platinum-diphosphine catalysed hydroformylation[41] and palladium catalysed cross-coupling reactions of Grignard reagents with organic halides.[42] More recent studies have included rhodium-catalysed hydroformylation,[43-54] nickel catalysed hydrocyanation[55, 56] and Diels-Alder reactions.[57]

1.9.4 Coordination mode

Monodentate ligands

These are the most commonly employed ligands in catalysis and organometallic chemistry. A massive variety of monodentate phosphine ligands exist with differing steric and electronic properties (see Tables 1.2 and 1.3 for prime examples).

Bidentate ligands

Bidentate phosphine ligands range from the simple symmetrical, with a minimum -CH_2- spacer group, to complex heterodentate unsymmetrical ligands containing a variety of cyclic and aromatic systems. The simplest bidentate phosphine ligand is dppm (bis(diphenylphosphino)methane), which contains a single CH_2 spacer. As the spacer group is increased in length through dppe (bis(diphenylphosphino)ethane) and dppp (bis(diphenylphosphino)propane) the properties of the ligands also begin to change. The increasing backbone gives a degree of flexibility to the ligand that may allow for a greater degree of stability with respect to conformational change within a catalytic cycle. The coordination of these ligands with transition metals such as rhodium is also affected and will be discussed in greater detail in the next chapter.

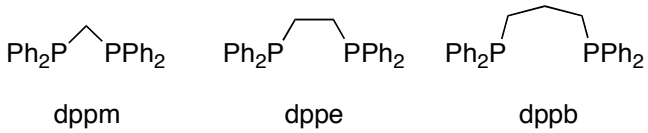

Figure 1.8. Simple bidentate ligands

Other more elaborate bidentate ligands have also been designed and these include unsymmetrical analogues of dppe, where Ar can be a range of aromatic substituents, Xantphos whose rigidity and bite angle are key to selectivity in certain hydroformylation reactions, and SPANphos whose novel spiro-backbone enables a fully *trans*-coordination to the metal centre.

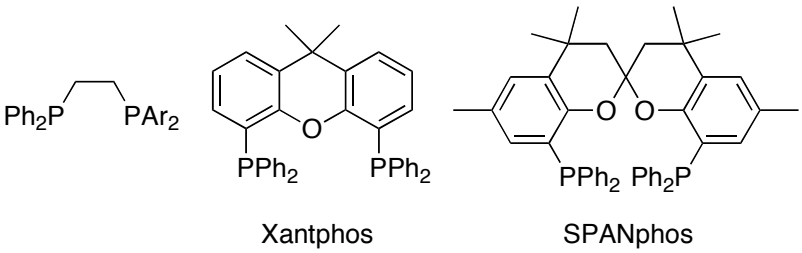

Figure 1.9. More complex bidentate ligands

Tridentate ligands

The most common examples of tridentate ligands include TRIPHOS, of which two versions exist, a *mer*-coordinating linear ligand and a facially coordinating tripodal ligand. Their use and coordination properties will be scrutinised fully in the coming chapters as they play a key role in understanding coordination and conformational change in the rhodium catalysed carbonylation of methanol.

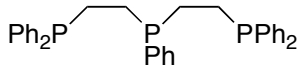

bis(diphenylphosphinoethyl)phenylphosphine

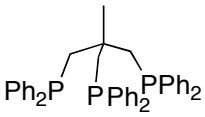

1, 1, 1-Tris((diphenylphosphino)methyl)ethane

Figure 10. Tridentate ligands

Hemilabile ligands

Hemilabile chelating ligands are defined as those that can adopt both mono- and bidentate co-ordination modes. Hemilabile ligands are chelating ligands that contain one substituent that is more weakly bound than the other. This means that the loosely bound ligand can be removed from the metal centre relatively easily to form an open chain structure.

A relevant example that illustrates this is the chelate complex *cis*-[Rh($Ph_2P(CH_2)_2$-P(O)Ph_2)(CO)Cl].[58] In the presence of CO, the Rh-O bond breaks with addition of CO. This results in the equilibrium shown below:

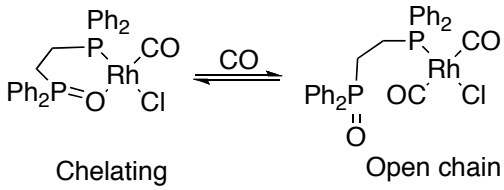

Scheme 10. Hemilabile ligand complexes

Part C: Phosphine-modified rhodium catalysts

This section summarises some of the most important work in the area of catalyst design for the rhodium-catalysed carbonylation. Since Forster in 1968, there have been many attempts to modify the industrial catalyst $[Rh(CO)_2I_2]^-$ by using a variety of different ligand types. This section will focus solely upon the research of phosphine modified rhodium complexes and demonstrate their ability to improve not only the rate of reaction but also catalyst stability and the selectivity towards acetic acid.

The oxidative addition of methyl iodide to the metal centre is the rate determining step of the rhodium based cycle and therefore a large section of catalyst design has focussed upon the improvement of this reaction. One way of increasing the rate of oxidative addition, and consequently the overall rate of reaction is the use of strong σ-donating ligands, creating an electron rich metal centre that will facilitate the oxidative addition of methyl iodide to the metal via an S_N2 mechanism. For this purpose other rhodium complexes have been synthesised over the last couple of decades, many of which utilise phosphine ligands, showing a dramatic effect in rate and performance compared to the Monsanto catalyst, $[Rh(CO)_2I_2]^-$.

The most important class of these rhodium catalysts are those containing simple trialkylphophine ligands such as PEt_3. Cole-Hamilton and co-workers at the University of St. Andrews have investigated the use of strongly electron donating trialkylphosphines as promoters for the rhodium catalysed carbonylation of methanol and were able to prepare the following complex, $[Rh(PEt_3)_2CO(Cl)]$, as an active catalyst precursor.[59, 60]

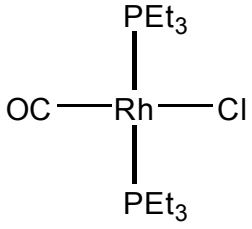

Figure 1.11. Structure of $[Rh(PEt_3)_2CO(Cl)]$

This precursor is a simple monodentate system, similar to those discussed in the previous section, with the two ligands *trans* to one another in a d^8 square planar geometry. The infrared spectrum of this precursor shows a strong absorption at 1960 cm^{-1}, suggesting a strong electron donating effect from the ligand, compared to the carbonyl stretching frequencies of other complexes of this nature (Table 1.3). The strong donating effect of the phosphine ligands also enabled the isolation of one of the key intermediates of the cycle, $[Rh(PEt_3)_2(Me)CO(I)_2]$, due to its increased lifetime in solution.

Studies done on this system have shown that $[Rh(PEt_3)_2CO(Cl)]$ is a highly active catalyst for the carbonylation of methanol, with a rate increase of 1½ times that of the industrial catalyst, $[Rh(CO)_2I_2]^-$. Detailed kinetic studies of the catalyst showed that the rate of oxidative addition of methyl iodide to the rhodium metal centre increases by a factor of 57 times at 25 °C. However, by creating an extremely electron rich metal centre a strong association with the CO ligand is also developed, retarding the subsequent migratory insertion into the Rh-C bond by a factor of 38 times. This retardation is the limiting factor behind the use of strong electron donating ligands.

Although overall there is an increase in the activity of the system the main disadvantage is the lack of stability of the catalyst. At the higher temperatures needed to achieve a good turnover (>150 °C) and achieve industrial significance, the catalyst had a very short lifetime and undergoes rapid decomposition.

At 150 °C using the modified precursor $[Rh(PEt_3)_2CO(Cl)]$, there is an initial increase in activity, however this rapidly drops off as the catalyst decomposes until after 20 minutes the rate is equivalent to that of the unmodified catalyst $[Rh(CO)_2(I)_2]^-$ showing that total loss of the phosphine has occurred.

The decomposition products were analysed and found to be a mixture of $Et_3P(O)$ and $[Et_3PMe]I$ with the deactivation of the catalyst proceeding via $[Rh(H)I_2(CO)(PEt_3)_2]$ and $[RhI_3(CO)(PEt_3)_2]$, even though a high water concentration was used to suppress ligand dissociation and decrease the formation of inactive Rh(III) species such as $[Rh(CO)_2I_4]^-$ or $[Rh(PEt_3)_2(CO)I_3]$. At higher temperatures any free

phosphine was rapidly quaternised by methyl iodide in solution, rendering any advantage redundant.

Recently, Dutta and Woollins *et al.* have developed an interesting alternative strategy to electron rich phosphine based carbonylation catalysts by using a carboxy ether group (-COOMe).[61] Almost counter intuitively the presence of this electron-withdrawing group resulted in an increased electron density at the rhodium through an interaction between the carbonyl and the metal centre. Both the mono and diphosphine complexes (Figure 1.12) reported an increase in the catalytic turnover number (TON) of around 1 ½ times that of $[Rh_2(CO)_4Cl_2]$ at 130 °C and 35 bar CO.

Although the electron density on the metal centre is substantially higher in the case of the bis(phosphine) complex it was noted that the partial association with carboxy ether groups contributed to a significant hindrance of the metal centre and reduced the rate of oxidative addition of methyl iodide.

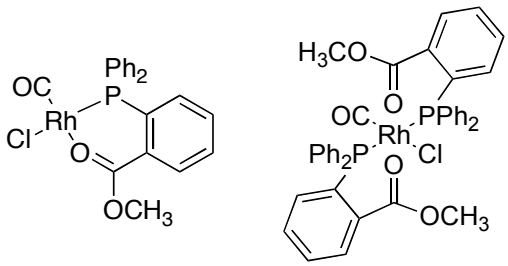

Figure 1.12. Mono and di-ligated rhodium complexes

These ligand systems show an important use of functional groups in controlling relative rates in the carbonylation of methanol away from the traditional approach of developing electron rich phosphines. However, the main disadvantage in the use of monodentate phosphine ligands still lies with their apparent lack of stability at temperatures approaching those required in an industrial setting. Therefore the bulk of research concerning phosphine modified systems for the rhodium-catalysed carbonylation of methanol is focused on the use of bidentate ligands as a way of increasing the stability of the catalyst and design of a system that is industrially viable.

Several simple bidentate diphosphine ligands such as dppe and dppp have shown promise in forming stable catalytic precursors. Although stable, these precursors lack

the catalytic activity needed to become viable replacements for the current rhodium technology. Therefore, there have been several key papers in the field of methanol carbonylation that have demonstrated improved rates using specifically designed analogues of the aforementioned ligands.

One such publication was by Carraz and Pringle in 2000.[62] They reported that unsymmetrical ethylene diphosphine ligands were more efficient catalysts than their symmetrical dppe counter-parts. As well as their increased activity they were also able to demonstrate a significant increase in stability at higher temperatures (185 ^{o}C) making them to be amongst the most stable ligand-modified systems reported to date.

Entry	Ligand	Rate[a]
1	1a	2.0
2	1b	5.0
3	1c	5.6
4	1d	8.5
5	1e	7.6
6	1f	2.9
7	1b + Ru[b]	13.7
8	2a	1.9
9	2b	2.0
10	2c	2.3
11	2d	1.7
12[c]	none	18.5

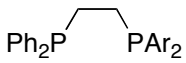

Unsymmetrical ligands
Ar =
C_6H_4OMe-4 1a,
C_6H_4F-3 1b,
$C_6H_4CF_3$-4 1c,
$C_6H_3F_2$-3, 5 1d,
$C_6H_2F_3$-3, 4, 5 1e,
$C_6H_3(CF_3)_2$-3, 5 1f.

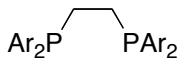

Symmetrical ligands
Ar =
C_6H_5 2a,
C_6H_4F-3 2b,
$C_6H_4CF_3$-4 2c,
C_6H_4OMe-4 2d.

Table 1.6. Kinetic data collected by Carraz et al. with the structures of the ligands used in the catalytic study alongside. [a] At 10% conversion, mol l^{-1} h^{-1} with estimated errors of 5-10%. [b] $[RuI_2(CO)_4]$ added to the catalyst mixture. [c] Catalyst is $[Rh(CO)_2I_2]^-$.

Carraz showed that rhodium catalysts containing unsymmetrical ethylene diphosphine ligands diplayed similar properties to iridium 'Cativa' type catalysts, with a rapid oxidative addition of methyl iodide and a greatly reduced rate in migratory insertion. It was also shown that as with the iridium 'Cativa' catalyst the rate was significantly increased by the use of iodide-abstracting Ru promoters.

Although the catalytic data in Table 1.6 show that ethylene diphosphine modified catalysts are markedly less active than $[Rh(CO)_2I_2]^-$, they do however show

that there is a dramatic increase in the rate of carbonylation when unsymmetrical ligands are used, compared to their symmetrical ethylene analogues. The reasoning behind this is complex and can be explained in terms of a balance between σ-donor and π-acceptor properties of the ligand.

Others have shown that mixed bidentate ligands can also give significant improvements in absolute rates over those obtained with $[Rh(CO)_2I_2]^-$. In 1987, Wegman et al. reported the carbonylation of methanol at unusually low temperature and pressure using $[Rh(Ph_2P(CH_2)_nP(O)Ph_2)CO(Cl)]$.[58] This unique precursor itself is not active in the carbonylation of methanol but on reaction with CO the ligand dissociates resulting in the hemilabile form shown in Scheme 1.11.

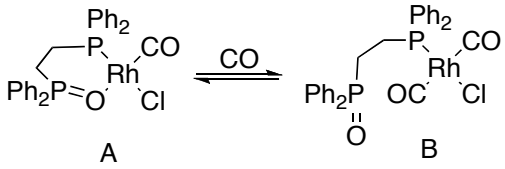

Scheme 1.11. Equilibrium of Wegman's complex under varying CO pressure.

Although they were unable to isolate a pure sample of the active catalyst B they demonstrated the hemilabile nature of the ligand using high-pressure infrared spectroscopy. At 22 ^oC and 1 bar CO the ratio η^2 to η^1 was determined to be 1:1. However, under reaction conditions of 80 °C and 3.5 bar CO, IR spectroscopic studies revealed only the presence of the η^1 species B (ν(CO) 2096 and 2012 cm^{-1}). No indication of any decomposition was observed, by the absence of the corresponding stretches at 1990 and 2060 cm^{-1} for $[Rh(CO)_2I_2]^-$. A catalytic turnover frequency (TOF) of 400 h^{-1} was reported under these conditions and contrasted against a typical TOF of 200-600 h^{-1} at 200 °C and 500 psig under normal operating conditions.

In 1995 Dilworth *et al.* described two very different classes of methanol carbonylation catalyst (Fig. 1.13) and more importantly reported significant improvements in the absolute rates over those of $[Rh(CO)_2(I)_2]^-$.[63]

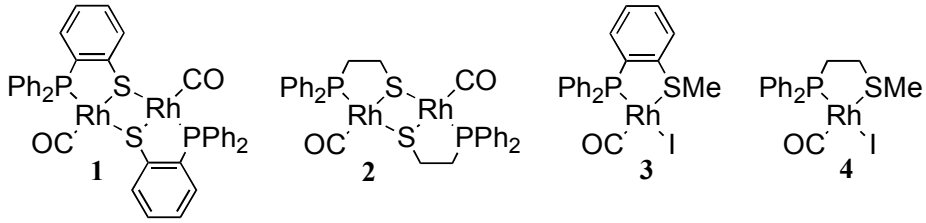

Figure 1.13. Structures of complexes described by Dilworth et al.

Catalyst	Max. Turnover h^{-1}
$[Rh(CO)_2I_2]^-$	450
1	1300
2	1800
3	1000
4	1500

Table 1.7. Kinetic data for ligands 1-4

As can be seen from Table 1.7 the use of these mixed donor ligands resulted in a greatly increased rate of reaction. Catalyst **2** shows the highest turnover with a maximum rate 4 times that of $[Rh(CO)_2I_2]^-$ under industrially significant conditions (185 °C, 70 bar CO).

Using infrared spectroscopic methods Dilworth *et al.* proposed that the catalytic mechanism for **3** and **4** was similar to that of the cycle for other diphosphine modified systems. The mechanism for **1** and **2** is, however, somewhat unclear but it seems likely that a cycle analogous to Scheme 1.4 (p 11) is also involved.

Baker *et al.* have also reported the synthesis and preparation of a new catalyst for the carbonylation of methanol containing a mixed bidentate ligand.[64] They found that the use of bis-(diphenylphosphino)monosulfide (dppms) allows for a substantial rate increase under industrially significant conditions.

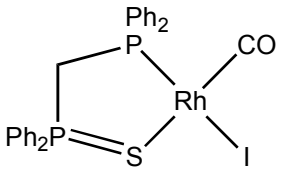

Figure 1.14. Structure of $[Rh(Ph_2PCH_2P(S)Ph_2)CO(I)]$

During the carbonylation of methanol at 185 °C and 70 bar CO, the reaction rate was reported to be over 8½ times greater than that of $[Rh(CO)_2I_2]^-$. HPIR data confirmed that the resting state was Rh(I) with $[Rh(Ph_2PCH_2P(S)Ph_2)CO(I)]$ (Fig. 1.14) being the only species observed and that the reaction rate was first order in [MeI]. In the studies carried out by Baker *et al.*, unlike the Wegman catalyst, there was no evidence of hemilable behaviour even though it had previously been postulated that this might be an important property for a ligand containing mixed donor atoms.

At the time the stability of $[Rh(Ph_2PCH_2P(S)Ph_2)CO(I)]$ at such high temperatures was not fully understood and Baker *et al.* were unable to assess the long-term stability of the catalytic system. However, in 1999 Haynes and co-workers published an important communication investigating the unique properties of this catalyst.[65] By studying the kinetics of the reaction they found that as with PEt_3 the rate of oxidative addition of MeI had been increased by ca. 50. However, unlike PEt_3 whose methyl intermediate may be isolated as a stable complex due to the slow rate of insertion, the methyl product $[Rh(dppms)Me(CO)I_2]$ prior to this paper had not been detected as the rate of insertion was so fast.

In 2002 Haynes and co-workers published the full paper comparing the steric and electronic effects of P-P, P-S and P-O donor ligands.[66] The paper included an in-depth study into the kinetics of the carbonylation of methanol and an interesting compartative study between the diphosphine ligands dppe, dppms and dppmo. The results were quite striking.

Reactant	Oxidative addition $10^3\ k_1$, $M^{-1}\ s^{-1}$	Migratory insertion $10^3\ k_2$, s^{-1}
dppe	1.41	0.4
dppms	1.19	620
$[Rh(CO)_2I_2]^-$	0.0293	54

Table 1.8. Rate constants (25 °C, CH_2Cl_2) for the oxidative addition and migratory insertion reactions of the modified and unmodified rhodium complexes.

Table 1.8 shows that at 25 °C, when using dppms, the rate of oxidative addition of methyl iodide to rhodium had increased by a factor *ca*. 41 times compared to the Monsanto catalyst $[Rh(CO)_2I_2]^-$. Very similar rates of oxidative addition were also seen for dppe and dppmo of 48 and 35 times respectively, relative to $[Rh(CO)_2I_2]^-$.

When looking at the kinetics of the insertion of CO there are some dramatic differences between the ligands. As with PEt_3, dppe has a slower rate of insertion compared to $[Rh(CO)_2I_2]^-$ (135 times slower) due to the increased donating effect of the ligand. However, dppms was shown to be >10 times faster than $[Rh(CO)_2I_2]^-$ and ca. 1500 times faster than dppe even though the donating properties of the two ligands are very similar. It was not until the X-ray crystallographic data was studied that the reasoning behind this became clear.

The main point of interest in all of the dppms structures was the steric crowding of one axial coordination site due to the orientation of the phenyl groups. When there is a vacant coordination site there is a π stacking interaction between the two phenyl groups, however, on addition of a methyl ligand to this site there is a disruption to the stacking and the phenyl groups are distorted out of position. Haynes and co-workers therefore proposed that migratory insertion is accelerated by relief of the steric tension created by the phenyl groups on the bidentate ligand. The reason why dppe does not undergo the same structural phenomenon is that there is much less preference for the phenyl groups to undergo π-stacking as the dppe system places much less constraint upon the conformation of the phenyl groups.

Unfortunately, although initially it had seemed a very promising catalyst, examination of the long-term stability of this catalytic system highlighted a serious flaw. For reaction times of over an hour at 185 °C the ligand was seen to breakdown, forming H_2S and a series of dppm complexes. For this reason the catalyst was never developed further.

The research that has been discussed in this chapter so far has shown that *trans*-coordinated systems such as $[Rh(PEt_3)_2CO(Cl)]$ are highly active yet unstable, whilst *cis*-chelating bidentate ligands such as dppe are stable but much less active catalysts. For these reasons Süss-Fink and co-workers decided to design a series of diphosphine

ligands with sizable enough spacer groups in order to promote a *trans*-coordinating system.[67-69] They theorised that ligands such as these would combine the high catalytic activity through *trans*-coordination with an increased stability due to the chelate effect of the diphosphine.

Süss-Fink and co-workers reported a series of *trans*-chelating diphosphine ligands containing ethylene-glycol and amino alcohol spacer groups. Not only were they highly active catalysts for the carbonylation of methanol but crucially robust and able to undergo successive recycling under the industrially significant conditions (170 °C and 22 bar CO).

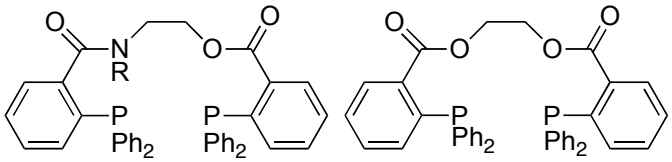

R = H (**1**), Ph (**2**) **3**

Figure 1.15. Structure of *trans*-chelating diphosphine ligands containing ethyl-eneglycol and amino alcohol spacer groups.

Entry	Precursor	Ligand	TON[a]
1	$[Rh_2(CO)_4Cl_2]$	-	381
2	$[Rh_2(CO)_4Cl_2]$	1	732
3	$[Rh_2(CO)_4Cl_2]$	2	803
4	$[Rh_2(CO)_4Cl_2]$	3	672
5	Residue from 3	-	781

Table 1.9. Methanol carbonylation data. Catalytic conditions: $[Rh_2(CO)_4Cl_2]$ (57 μmol), ligand (0.12 mmol, 2 eq.), CH_3OH (110.2 mmol), CH_3I (11.4 mmol), H_2O (81.9 mmol), 170 ^oC, 22 bar, 900 rpm, reaction time = 15 mins. [a] mol CH_3OH converted into CH_3COOH and CH_3COOCH_3 per mol catalyst precursor.

As can be seen from Table 1.9 all of the *trans*-chelating ligands tested were highly active, with activities more than twice that of the industrial standard. Entry 5 also shows that only a very limited amount of decomposition has occurred as the complex can be isolated and recycled whilst showing no dramatic decrease in activity.

The analysis of the residue from each of these runs showed a mixture of three complexes. Two of these have been isolated and fully characterised, the third minor species is yet to be identified. The two major species **1** and **2** are shown below in Scheme 1.12, **2** can also be prepared directly from **1**.

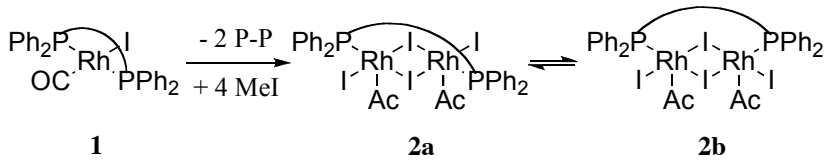

Scheme 1.12. Reaction of the monomeric complex with MeI and the formation of two isomeric dimers

X-ray crystal structures of both isomers, 2a and 2b, were obtained (Figure 1.16). These displayed two important interactions that may help to explain the increased stability of these systems. Firstly, there is a hydrogen bonding interaction between the acetyl oxygen and the hydrogen atom on the phenyl group and secondly the carbonyl oxygen from the ligand backbone clearly helps to stabilise the octahedral geometry around the rhodium centres.

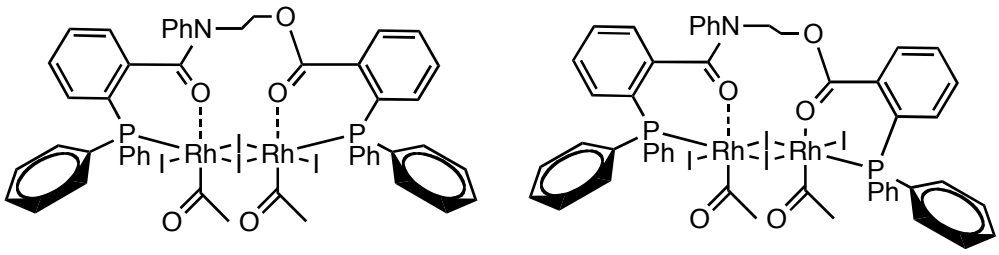

Figure 1.16. Isomers 2a and 2b showing the Rh-O interactions that complete the octahedral coordination geometry at the two Rhodium atoms.

This research is a prime example of a rational design of a catalyst. Süss-Fink has taken the best properties from individual catalytic systems and been able to combine these in order to create an asymmetric diphosphine ligand that has a series of interesting coordination properties and more importantly is a highly active and stable catalyst for the carbonylation of methanol.

Similarly, Van-Leeuwen and co-workers were also intrigued by the potential *trans*-coordination of a diphosphine ligand that had been formed accidentally whilst trying to prepare the bidentate ligand Xantphos.[70, 71]

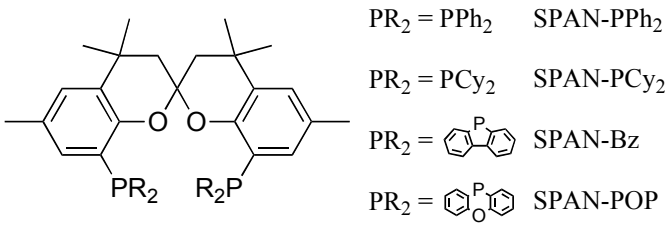

Figure 1.17. Structure of SPANphos ligand and possible R groups

The spiro-phosphine SPANphos (Figure 1.17) was shown to be a highly active catalyst in the carbonylation of methanol with reaction rates of up to 3 times that of $[Rh_2(CO)_4Cl_2]$. X-ray crystallography showed that both mono- and di-nuclear Rh species can be formed. However, it was discovered that the mono-nuclear precursor $[Rh(SPAN\text{-}PPh_2)CO(Cl)]$ did not react with methyl iodide and after prolonged exposure to MeI the only material recovered was that arising from halide metathesis. When comparing the catalytic activities of these complexes they reported a 4-fold rate increase in favour of the di-nuclear species.

A series of kinetic studies using HPIR and simultaneous NMR spectroscopy experiments appeared to suggest that only one of the two metal centres in this di-nuclear catalyst was active and throughout the run a strong signal at 1981 cm^{-1} referring to the inactive site is observed (Scheme 1.13). This suggests that the active catalyst or at least the resting state may be a Rh^{I}-Rh^{III} monoacetyl complex.

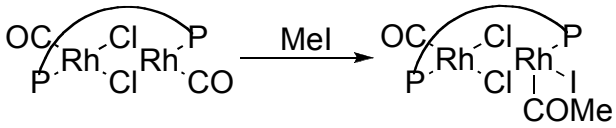

Scheme 1.13. Reaction with MeI and the proposed formation of the Rh^{I}-Rh^{III} monoacetyl complex

From these kinetic studies the rate of oxidative addition of MeI to the di-nuclear species was shown to be only ten times slower than that of the most active catalyst. The di-nuclear SPANphos system has therefore been described as the most active phosphine based catalyst reported to date.

One of the most recent publications in the field of rhodium-catalysed methanol carbonylation, published after our research was complete, was by Jimenez-Rodriguez *et*

al.[72] This paper reported on the use of the bidentate ligand bis(ditertiarybutylphosphinomethyl)benzene (dtbpmb) as it was known to form stable chelates and impart a very high electron density on the metal centre (Fig. 1.18). Thus one may see this as an expansion of the group's previous work using PEt_3 by creating an electron rich centre with a much greater degree of stability.

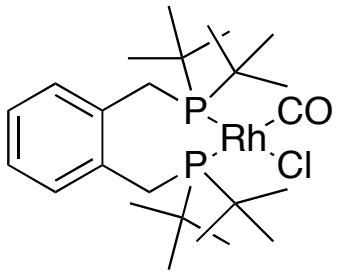

Figure 1.18. Structure of the catalytic precursor [Rh(dtbpmb)CO(Cl)]

Jimenez-Rodriguez *et al.* reported a series of catalytic studies at 150 ºC and 180 ºC in which high initial rates were observed. At 150 ºC the initial rate was 1.8 times that of $[Rh(CO)_2I_2]^-$, whilst an increase of 30 ºC in temperature cancelled out any advantage over that of $[Rh(CO)_2I_2]^-$. When these catalytic reactions were studied in greater detail using high pressure infrared spectroscopy (HPIR) and high pressure NMR spectroscopy it was possible to observe the formation of several of the key intermediates including the oxidative addition product $[Rh(dtbpmb)(Me)(CO)(I)_2]$ and the acetyl/CO adduct $[Rh(dtbpmb)(COMe)(CO)(I)_2]$.

Unfortunately, even at the relatively low temperatures of 120-125 ºC it was also possible to observe the decomposition of the catalyst through the growth of two bands at 2058 cm^{-1} and 1993 cm^{-1} characteristic of the formation of $[Rh(CO)_2I_2]^-$. Although they were unable to quantify the amount of decomposition that had occurred it was proposed that at higher temperatures (150-180 ºC) complete decomposition does occur with any rate increase being associated with the formation of the quaternary phosphonium salt $[(Me^tBu_2PCH_2)_2C_6H_4]^{2+}$.

In 1989 Moloy and Wegman reported on a related reaction, the rhodium-catalysed reductive carbonylation of methanol.[73, 74] This reaction was based on the conversion of synthesis gas to acetaldehyde and ethanol, the products of which can be

used as valuable precursors for the production of C_2 compounds such as ethylene and ethanol.

The catalytic cycle for the reductive carbonylation of methanol consists of two competing catalytic reactions, carbonylation and reductive carbonylation, and shall be discussed in detail in Chapter 2. The initial product formed from the reductive carbonylation of methanol is acetaldehyde and in the presence of a ruthenium co-catalyst is hydrogenated to ethanol. Moloy and Wegman investigated the use of diphosphine ligands in order to promote the hydrogenolysis of rhodium-acetyl species and the formation of acetaldehyde. The investigation led them to conclude that C_3 ligands, those having a three-carbon linker between the phosphorus atoms, were the most effective for this conversion. In particular dppp was reported to have a 82 % selectivity towards acetaldehyde/ethanol in comparison to a very low 7 % for dppb and 4 % for that of dcpe.

This paper and the following investigation also examined some of the key intermediates involved in the reaction. Of these, the rhodium-acetyl species $[Rh(dppp)C(O)Me(I)_2]$, was reacted directly with hydrogen forming a dimeric hydide species $[Rh(dppp)H(I)(\mu\text{-}I)]_2$, which was also characterised using X-ray crystallography. Crucially, Moloy and Wegman had shown that phosphine ligands have the potential to tune the selectivity of a reaction using subtle changes in the coordination properties of the ligand.

Following on from the work of Moloy and Wegman, BP began an investigation into the use of lower grade CO feedstock containing hydrogen as a way of improving the efficiency and cost effectiveness of the rhodium catalysed carbonylation of methanol. Using a similar experimental procedure as set out by Moloy and Wegman, BP highlighted several potential phosphine modified systems that may enable a greater selectivity towards acetic acid, as opposed to acetaldehyde for above, whilst under an atmosphere of 2:1 H_2:CO.[75, 76] In the large scale production of acetic acid, the use of synthesis gas is highly favourable as it would avoid the energy intensive distillation involved in the production of pure CO and potential optimisation under syn-gas conditions could lead to reduced propionic acids levels forming high grade acetic acid without the need for fractional distillation. If achieved, improvements such as these may

result in significant environmental benefits as well as creating a more cost effective process.

The initial investigation patented by BP[75] screened a large range of polydentate ligands, of which the Xantphos system showed the most promise with an extremely low selectivity towards hydrogenated products (0.3 %). However, the selectivity towards acetic acid was heavily impacted by the production of methane (61 %). Of those ligands tested, BINAP also showed a good selectivity towards acetic acid whilst producing comparatively little methane. A follow up investigation into Xantphos once again reported a low selectivity (3.1 %) towards acetaldehyde/ethanol in the presence of a ruthenium hydrogenation catalyst compared to a much greater 58.0 % selectivity for dppp under the same conditions.[76] The interest generated by Xantphos led BP to set up various collaborations aimed at understanding selectivity, stability and solubility of rhodium-phosphine catalysts for the carbonylation of methanol.

1.10 Aims

The Monsanto process is one of the most successful examples of a homogeneously catalysed industrial reaction and represents one of the major triumphs in modern homogeneous catalysis. Throughout this chapter it is illustrated how the activity and selectivity of this highly established process can be improved through the use of phosphine modified rhodium complexes. In this way phosphine modified systems may lend the rhodium-catalysed carbonylation of methanol many of the advantages so far only achieved in iridium systems. As well as improved rates and selectivity towards acetic acid, it is envisaged that these improvements may also include a greater catalyst stability at lower water concentrations leading to a much reduced distillation process and one that will not only be advantageous to the commercial operation of the plant but also to the environment.

In the initial stages of my PhD the mandate from the CASE sponsors BP was to investigate a number of problems that have hampered the development of an industrially viable catalyst for the rhodium-catalysed carbonylation of methanol. BP was primarily concerned with the long-term stability of rhodium-phosphine complexes under the harsh reaction conditions employed in this large-scale process (150-200ºC,

25-45 atm in MeOH/AcOH/MeI/H_2O). Under industrially significant conditions many phosphine modified rhodium catalysts decompose forming $[Rh(CO)_2I_2]^-$ and P(V) species, however several of the complexes discussed in Chapter 1 have shown that it is possible to prepare stable complexes containing phosphine ligands. Understanding why some complexes are more stable than others and the factors that determine this was therefore one of the main aims of this project.

Initial studies carried out by BP indicated that complexes containing the phosphine ligand Xantphos (Fig. 1.9) may be able to withstand the harsh industrial conditions, suggesting that this may be due to the rigid nature of the phosphine ligand or a possible tridentate co-ordination through the central oxygen atom. The stability and coordination chemistry of rhodium-Xantphos complexes was therefore be examined in greater detail in collaboration with the Haynes group at the University of Sheffield.

One disadvantage in the use of rhodium-Xantphos complexes is their relatively poor solubility in the reaction media at lower temperatures. At the lower operating temperatures found within the system outside of the reactor, the Rh-Xantphos catalyst is no longer soluble and precipitates out of solution. This precipitation would result in loss of catalyst from the system as well as several major engineering issues. Thus the future development of a catalyst with a greater degree of solubility was another key aim.

Although, little research has been carried out on preparing phosphine containing rhodium complexes possessing a greater degree of solubility in acidic media, an extensive literature precedent does exist for the synthesis of water-soluble phosphine based transition metal complexes. A further aim of our research will therefore examine the use of quaternised aminoalkyl and aminoaryl groups as a way of potentially increasing the solubility of the complex in a mixture of methanol, MeI, acetic acid and water.

Outside the main aims of the project, other interests lie in the further development of a hydrogen tolerant phosphine-modified rhodium catalysed process. Following the work by Moloy and Wegman and the screening of polydentate metal complexes by BP

our hope was to develop a rationale behind the use of phosphine ligands in hydrogen tolerant methanol carbonylation and how the properties of the ligand may affect the overall selectivity of the reaction.

Chapter II: Evaluation of C_4 diphosphine ligands in rhodium catalysed hydrogen-tolerant methanol carbonylation

2.1 Introduction

Current commercial processes for the carbonylation of methanol use pure CO which is purified from syngas (1:1 CO/H_2) and form propionic acid as the main liquid by-product which requires distillation to produce high-grade acetic acid. Both of these processes are expensive and extremely energy intensive. Therefore a step change in methanol carbonylation technology would be to reduce propionic acids levels such that fractional distillation was not required, and/or to develop catalysts able to utilise lower grade CO that contains hydrogen. Thus there are considerable cost and environmental advantages to be considered if a process could be designed that was tolerant of hydrogen impurities in the CO feed, whilst also eliminating by-products such as propionic acid and acetaldehyde altogether. Most of the possible variables have now been explored in the 'unmodified' catalyst systems, and phosphine modified catalysts may offer the best opportunity for fine-tuning the selectivity of the catalysts. The recent work by BP, as described in chapter 1, has demonstrated that several diphosphine ligands, most notably Xantphos, can retain high selectivity to acetic acid over acetaldehyde/ethanol/propanoic acid even in the presence of hydrogen.[75, 76]

An interesting paper by Moloy and Wegman in 1989 described reductive carbonylation of methanol with (2:1 H_2/CO) syngas to give ethanol and ethanal.[73, 74] Good selectivities towards reductive carbonylation products were observed with C_3 diphosphines such as dppp. These authors also studied key organometallic intermediates in the dppp-based system to shed light on the basic mechanism. This paper notes that the C_4 diphosphine, dppb, was particularly ineffective for reductive carbonylation, predominantly giving acetic acid derivatives as products. The poor selectivities observed with the dppb catalysts in this application suggested that this type of phosphine could offer opportunities in hydrogen tolerant methanol carbonylation. It

was therefore decided that this should be investigated further and in this chapter, the synthesis and characterisation of rhodium complexes of C_4 diphosphines and their application in methanol carbonylation using syngas is reported.

2.2 Coordination chemistry

The reaction of dppb with $[Rh(CO)_2Cl]_2$ has been reported to give the dimeric complex $[Rh(dppb)CO(Cl)]_2$, **1**.[77] **1** was prepared by the literature route, and our more extensive data agrees with the proposed formulation. In particular, FAB MS shows a M^+ 1184.1 peak as the highest mass ion and fragments assigned to $[M\text{-Cl}]^+$ (1149.1), and $[M\text{-2CO}]^+$ (1128.1), that would seem unlikely to arise from monomeric or polymeric complexes.

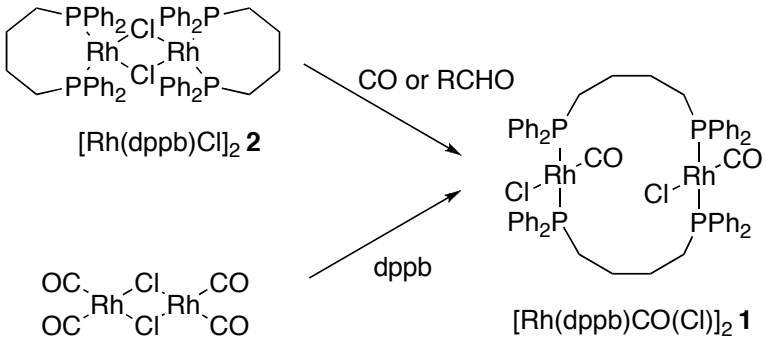

Scheme 2.1. Alternative methods for the formation of $[Rh(dppb)CO(Cl)]_2$

The original report on the synthesis of $[Rh(dppb)CO(Cl)]_2$ **1**, notes that it is not clear if this complex with bridging bidentate diphosphine ligands is a kinetic or thermodynamic product. To investigate this further, $[Rh(dppb)Cl]_2$ **2**,[78] in which dppb acts as a chelate ligand, was treated with CO. Quantitative formation of the bridging complex is observed: the fact that the dppb ligand rearranges from chelate to bridging ligand during the reaction with CO supports **1** being the thermodynamically preferred arrangement for this complex.

The carbonylation of $[Rh(dppb)Cl]_2$ **2** via the decarbonylation of aldehydes was also investigated as an alternative route to rhodium-diphosphine carbonyl complexes as it has been previously shown that formaldehyde may be used to prepare $[Rh(PPh_3)_2CO(Cl)]$ from a mixture of $RhCl_3.xH_2O$ and triphenylphosphine in ethanol.[79]

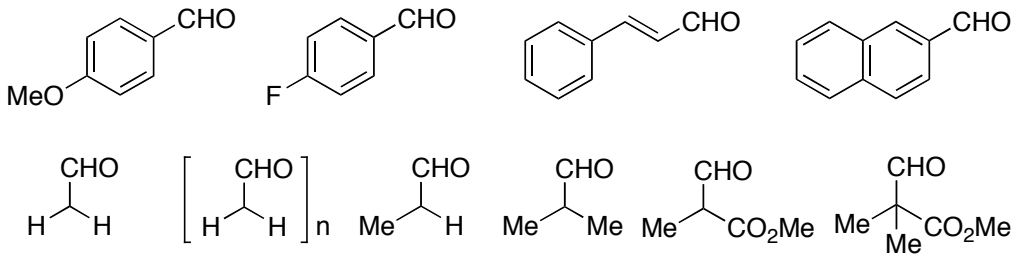

Figure 2.1. The range of alkyl and aryl aldehydes used in the preparation of $[Rh(dppb)(CO)Cl]_2$ **2**

All of the alkyl and aryl aldehydes of varying electronic properties (fluorobenzaldehyde, 4-methoxy benzaldehyde etc.) shown in Fig. 2.1 gave quantitative conversion of the rhodium starting material to $[Rh(dppb)CO(Cl)]_2$ **2** after 10 mins at 120 ºC. The bulky aldehyde, 2-carboxymethyl-2'-methyl propionaldehyde,[80] on the other hand gave a mixture of products that have not been characterised further.

Reactions of dcpb and dppx with $[Rh_2(CO)_4Cl_2]$ also gave sparingly soluble dimeric complexes, **3** and **4** respectively with bridging bidentate phosphine ligands. The infrared spectra of these complexes show a ν(CO) of 1949 cm^{-1} for $[Rh(dcpb)CO(Cl)]_2$ **4** and a ν(CO) of 1970 cm^{-1} for $[Rh(dppx)CO(Cl)]_2$ **3**. In comparison to $[Rh(PPh_3)_2CO(Cl)]$ (ν(CO)/cm^{-1}: 1965), one may observe $[Rh(dcpb)CO(Cl)]_2$ **4** has a much lower CO stretching frequency due to the strong electron donating effect of the cyclohexyl groups.

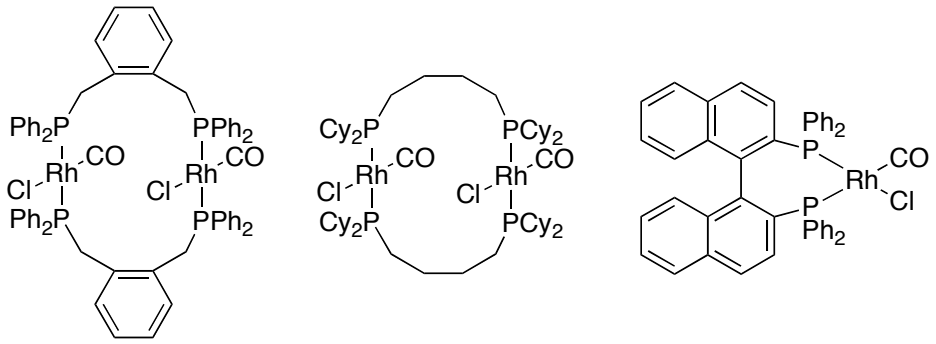

[Rh(dppx)CO(Cl)]$_2$ **3** [Rh(dcpb)CO(Cl)]$_2$ **4** [Rh(*rac*-BINAP)CO(Cl)] **5**

Figure 2.2. Rhodium/C_4-phosphine complexes

In contrast, reaction of $[Rh_2(CO)_4Cl_2]$ with *rac*-BINAP or reaction of [Rh(*rac*-BINAP)Cl]$_2$ [81] with CO gave the monomeric chelate complex, **5**.[82] This complex reacts

with NaI in acetone to give the iodo analogue, **6**. The structure of [Rh(BINAP)(CO)I] **6** was determined by X-ray crystallography.

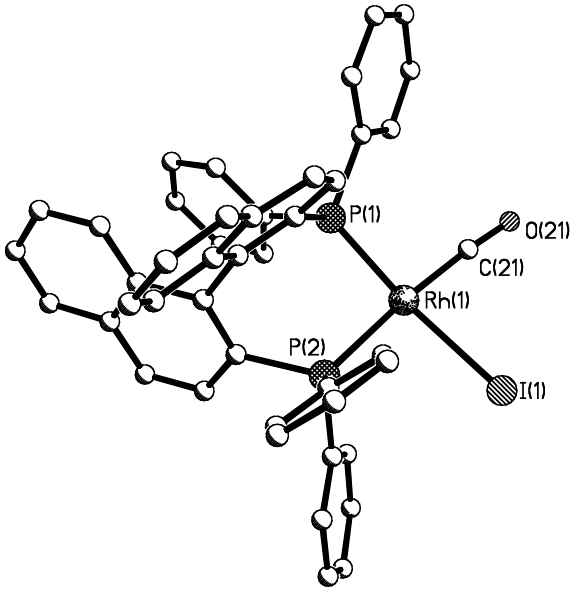

Figure 2.3. X-ray structure analysis of [Rh(BINAP)CO(I)] **6**.

Table 2.1. Comparison of crystallographic data for a range of Rh/BINAP complexes.

Complex	P-Rh-P	P(1)-Rh	P(2)-Rh
[Rh(BINAP)CO(I)] **6**	90.27(4)	2.237(12)	2.377(12)
[Rh(BINAP)CO(Cl)][81]	91.48(3)	2.250(1)	2.341(1)
$[Rh(BINAP)(NBD)]^{+}$ [83]	91.82(5)	2.305(1)	2.321(1)
$[\{Rh(BINAP)\}_3(OH)_2]^{+}$ [84]	88.60*	2.204*	2.210*

*Average bond length

Table 2.1 shows that structurally [Rh(BINAP)CO(I)] **6** is quite typical of other Rh/BINAP complexes with respect to bond lengths and angles. The expected *trans* effect of the CO is also observed in both the chloro- and iodo-complexes, with the P(2)-Rh bond length being significantly longer than that of the bond *trans* to the halide.

2.3 Investigating stability and reactivity of Rh(I) carbonyl complexes

The reactivity and stability of complexes **1** and **3-5** in the presence of methyl iodide was then examined. $[Rh(dppb)(CO)Cl]_2$ **1** was previously reported to be unreactive with methyl iodide.[85] However, in our hands, heating **1** with MeI at 140 ºC for 10 minutes in a glass pressure vessel in a microwave smoothly generates $[Rh(dppb)(C(O)CH_3)(I)_2]$ **7**, as the only phosphorus containing product. The stability and reactivity of other carbonyl complexes including $[Rh(PPh_3)_2(CO)Cl]$ **8** was then examined in greater detail. Stability was assessed by heating with a large excess of MeI (300 eq.) for an exact period of time (60 minutes) at a set temperature, followed by recording a $^{31}P\{^1H\}$ NMR spectrum of an accurately measured aliquot (0.50 cm^3) relative to a calibrated external standard of $^nBu_3P{=}O$ (solution in C_6D_6 in capillary tube). This study was complicated by the low solubility of some of the complexes, which precipitated from solution. The data reported in Table 2.2 therefore show both the concentration of Rh-phosphine species in solution relative to the standard and the % of the phosphorus species observed being Rh-phosphine species. The differences between the ligands are quite striking.

Table 2.2. Stability of Rh(I) carbonyl complexes in the absence of MeI.

Entry	Ligand	Temp. ºC	% in solution[(a)]	% Rh-P species[(b)]
1	dppb	140	44.3	94.4
2	dppb	150	58.3	33.5
3	dppx	140	19.5	>99
4	dppx	150	48.3	83.3
5	dcpb	140	0	0
6	BINAP	140	0	0
7	PPh_3	140	0	0

(a) % of complex in a solution of MeI/MeOAc relative to an external standard of tributylphosphine oxide (b) % of Rh-P complex present within the relative % that is soluble in solution.

The dppb and dppx carbonyl complexes react smoothly with MeI at 140 ºC, and after 60 minutes of reaction time, only very small traces of anything other than the Rh-acetyl complexes are detectable in solution (Entry 1 and 3). Rh(III) acetyls for dppb and dppx could be isolated by this preparative method in good yield. $[Rh(PPh_3)_2(CO)Cl]$ **8** reacts with MeI at 60 ºC, but after only 10 minutes at a temperature of 100 ºC or above, extensive decomposition to $Ph_3P(O)OH$ and $[Ph_3PMe]I$ takes place (Fig. 3.1). This is quantitative after 10 minutes at 140 ºC. For dppb and dppx complexes, a higher temperature of 150 ºC was needed to differentiate between their stability. At 150 ºC dppb complexes start to decompose more readily resulting in only 33.5 % stability whereas dppx complexes are able to maintain a greater stability even at this higher temperature.

The high stability of these complexes is somewhat surprising, since the dppb and dppx analogues have to rearrange from a bridging bidentate co-ordination mode to a monomeric chelate during the oxidative addition (or migratory insertion) process, and this presumably involves dissociation of one end of the diphosphine. This rearrangement must be fast relative to quaternisation of the phosphine. More surprising was the observation that despite many attempts, [Rh(BINAP)(CO)Cl] **6** reacts with MeI with severe decomposition: several phosphorus peaks without ^{31}P-Rh coupling are visible after 60 minutes at 140 ºC. Thus in this case, a Rh(I) chelate complex shows lower stability than a Rh(I) bridging bidentate complex.

Using the rhodium acetonitrile complex $[Rh(NCMe)CO(I)_2COMe]_2$ **9**[86] it was hoped that the BINAP and dcpb acetyls could be synthesised. However, both reactions did not go cleanly producing a mixture of products. In the case of *rac*-BINAP, the reaction most likely formed an acetyl species ($^{31}P\{^1H\}$ NMR (CD_2Cl_2): δ 32.6 (dd, $^1J_{Rh-P}$ 140.2 Hz), 21.5 (dd, $^1J_{Rh-P}$ 138.1 Hz); IR (KBr), ν(CO): 1706.9 cm^{-1}) and a set of minor signals ($^{31}P\{^1H\}$ NMR (CD_2Cl_2): δ 43.7 (dd, $^1J_{Rh-P}$ 161 Hz), 21.5 (dd, $^1J_{Rh-P}$ 125.1Hz); IR (KBr), ν(CO): 2001 cm-1) relating to the Rh(I) complex [Rh(*rac*-BINAP)CO(I)]. The formation of the latter product for *rac*-BINAP in the absence of CO, presumably, by a reverse process of migration and reductive elimination of MeI may imply lower stability for the Rh(III) acetyl. In any case, there seems to be a stark difference in stability and reactivity of these C_4 diphosphine complexes.

2.4 X-ray structures of Rh acetyls

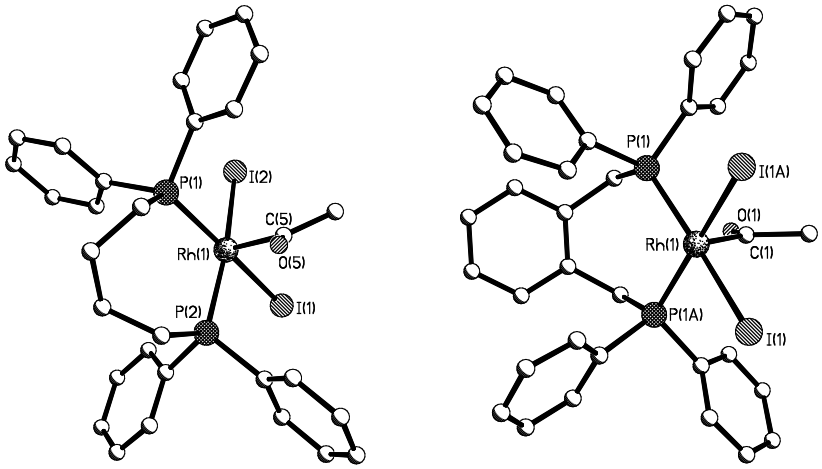

Figure 2.4. X-ray structure analysis of [Rh(dppb)(COMe)$(I)_2$] **7** and [Rh(dppx)(COMe)$(I)_2$] **10**

Crystals of [Rh(dppb)(C(O)CH_3)$(I)_2$] **7** and [Rh(dppx)(C(O)CH_3)$(I)_2$] **10** suitable for X-ray diffraction could be grown by slowly blowing nitrogen over the reaction mixture. The structures of these complexes were then determined by X-ray crystallography.

Table 2.3. Comparison of X-ray data for [Rh(L)COMe$(I)_2$] complexes for C_1, C_2, C_3 and C_4 diphosphines

	Rh-P[1]	Rh-P[2]	C-O	I-Rh-I	P-Rh-P
dppm[87]	2.267(6)	2.262(7)	1.160(3)	90.55(10)	73.30(2)
dppe[66]	2.267(2)	2.284(2)	1.178(9)	91.62(4)	84.74(7)
dppp[73]	2.299(1)	2.276(1)	1.182(7)	89.15(2)	90.49(5)
dppb **7**	2.320(9)	2.304(9)	1.196(4)	86.84(16)	99.13(3)
dppx **10**	2.308(2)	2.309(2)	1.210(13)	85.63(4)	103.31(11)

When comparing these crystallographic data with that of other rhodium-phosphine acetyl complexes available within the literature, one can see that going from a C_1 to a C_4 backbone both the Rh-P and C-O bond lengths steadily increase. Bond angles are also affected with a P-Rh-P angle increasing from 73 º to 103 º, coupled with a decreasing I-Rh-I angle. Although there is little difference between the bond lengths

of dppb and dppx complexes, the bond angles follow the previous trends of an increasing P-Rh-P and decreasing I-Rh-I angle.

With a greater understanding of Rh co-ordination chemistry of the C_4 ligands in hand, a series of catalytic studies in the carbonylation of methanol were undertaken using a range of CO/H_2 mixtures.

2.5 Methanol Carbonylation

Several carbonylation reactions were run under differing conditions. The main aim was to compare a range of C_4 ligands in a series of *in-situ* experiments and come up with a rational design for a hydrogen tolerant system for methanol carbonylation.

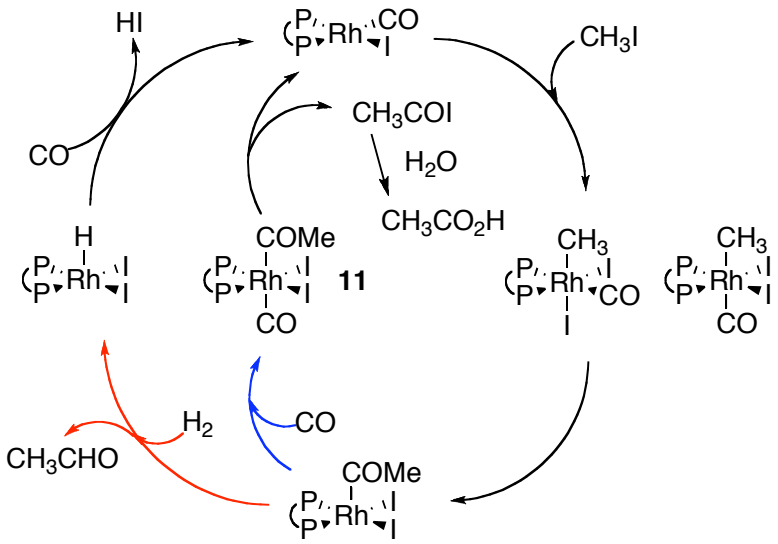

Scheme 2.2. Postulated mechanism for carbonylation versus reductive carbonylation in a rhodium-diphosphine-methyl iodide catalysed reaction.

The catalytic cycle in Scheme 2.2 shows the competing reactions. When hydrogen is present acetaldehyde may be formed via the red pathway on the left hand side of the cycle. However, this must compete with the blue carbonylation reaction forming the reactive intermediate **11** from which several carbonylated products are possible depending on the water concentration of the system.

Therefore several sets of carbonylation reactions were run using different gas mixtures and water concentrations. At 100 ºC, 22.6 g of MeI was charged into 100 g of methanol containing the precursor $Rh_2(CO)_4Cl_2$ and the phosphine ligand. The solution was then heated at 140 ºC for 40 minutes under a pressure of 26 bar of CO. The reaction was monitored using HPIR, although, the Rh-acetyl signals were obscured by MeOAc limiting the utility of the *in-situ* IR. After the reaction had run, both liquid and gas samples were taken for analysis, and any precipitated catalyst was recovered.

Table 2.4. Methanol carbonylation at 140 ºC using pure CO [(a)]

Ligand	none	dppb	dppx	dcpb	BINAP
TOF/h^{-1} [(b)]	**581**	**965**	**208**	**465**	**174**
Aldehyde/Acetyl ratio[(c)]	**0.085**	**0.046**	**0.080**	**0.031**	**<0.079**
Liquid analysis [(d)]	%mol/mol	%mol/mol	%mol/mol	%mol/mol	%mol/mol
Water	14.4	17.6	12.3	14.7	11.9
Methanol [(e)]	78.5	73.1	82.9	78.9	83.7
Methyl Iodide	3.0	2.8	3.3	3.2	3.2
Methyl Acetate	**3.9**	**6.2**	**1.4**	**3.1**	**1.2**
Acetic Acid	**0.2**	**0.4**	**0.1**	**0.1**	**0.1**
MeCHO (ppm)	**35**	**30**	**12**	**10**	**<10**
Gas Analysis [(f)]	%vol/vol	%vol/vol	%vol/vol	%vol/vol	%vol/vol
H_2	0.6	<0.1	<0.1	4.9	<0.1
CO	82.5	86.9	85.8	84.2	89.0
CO_2	0.2	0.09	<0.1	<0.02	0.04
CH_4	**0.4**	**0.08**	**<0.1**	**0.4**	**<0.05**

(a) Reaction conditions: $Rh_2(CO)_4Cl_2$ (0.386 mmol), Rh:ligand = 1:1, CO p = 26 bar, for 40 minutes at 140 ºC (b) TOF was calculated from the total conversion of methanol and methyl iodide to methyl acetate and acetic acid (c) Aldehyde/acetyl ratio was calculated from the ratio of acetaldehyde to carbonylated products (d) Calculated by calibrated GC analysis using an internal standard at BP, Hull (e) %mol/mol of methanol also comprises ~5-7 %mol/mol DME (f) Sampled at room temperature from headspace after cool down.

The results highlighted in bold comprise the most significant data. These being the amount of desired products formed i.e. acetic acid and methyl acetate, the amount of liquid and gaseous by-products formed as well as data regarding the activity and selectivity of the catalysts.

By looking at the amount of methyl acetate and acetic acid produced we can start to build up a picture of the activity of these systems and what affect the phosphine

ligand has upon this. The dppb system at 140 ºC appears to be the most active (965 TOF/h^{-1}) followed by $Rh_2(CO)_4Cl_2$ (581 TOF/h^{-1}). The least reactive under these conditions were the dppx and the BINAP systems.

The primary liquid by-product was acetaldehyde, under an atmosphere of CO as expected very little was observed. However, by running the reactions using syngas containing differing H_2:CO ratios, the hydrogen tolerance of these systems was evaluated.

Table 2.5. Methanol carbonylation at 140 ºC using 2:1 H_2:CO syngas [(a)]

Ligand	none	dppb	dppx	dcpb	BINAP
TOF/h^{-1} [(b)]	**144**	**232**	**176**	**259**	**109**
Aldehyde/Acetyl ratio[(c)]	**3.154**	**4.839**	**2.039**	**0.690**	**0.491**
Liquid analysis [(d)]	%mol/mol	%mol/mol	%mol/mol	%mol/mol	%mol/mol
Water	13.1	14.5	12.1	15.7	10.1
Methanol [(e)]	82.5	80.5	83.1	79.4	85.6
Methyl Iodide	3.4	3.3	3.5	3.1	3.6
Methyl Acetate	**1.0**	**1.6**	**1.2**	**1.7**	**0.8**
Acetic Acid	**<0.1**	**<0.1**	**<0.1**	**<0.1**	**<0.1**
MeCHO (ppm)	**335**	**830**	**265**	**125**	**40**
Gas Analysis [(f)]	%vol/vol	%vol/vol	%vol/vol	%vol/vol	%vol/vol
H_2	54.5	42.5	66.7	37	55.7
CO	19.9	21.2	16.3	25.0	31.2
CO_2	<0.1	<0.1	<0.1	<0.1	<0.1
CH_4[(g)]	**12.1**	**21.6**	**4.2**	**25.3**	**0.1**

(a) Reaction conditions: $Rh_2(CO)_4Cl_2$ (0.386 mmol), Rh:ligand = 1:1, 2: H_2:CO p = 26 bar, for 40 minutes at 140 ºC (b) TOF was calculated from the total conversion of methanol and methyl iodide to methyl acetate and acetic acid (c) Aldehyde/acetyl ratio was calculated from the ratio of acetaldehyde to carbonylated products (d) Calculated by calibrated GC analysis using an internal standard at BP, Hull (e) %mol/mol of methanol also comprises ~5-7 %mol/mol DME (f) Sampled at room temperature from headspace after cool down (g) %vol/vols of methane typically represent between 0.0001-0.6 %mol/mol converted from the initial %mol/mol of methanol and MeI.

Operating at 140 ºC under an atmosphere of 2:1 H_2:CO (26 bar) there was much less CO present in the autoclave than in our first experiment and as a result the quantity of liquid products formed was substantially reduced, as were the overall turn-over frequencies of the systems.

The most significant set of data within this table is the amount of acetaldehyde produced. Due to the increased amount of H_2 present, we observed a dramatic increase in the aldehyde/acetylated product ratio across all systems with those showing the greatest degree of hydrogen tolerance being dcpb and BINAP. It is also interesting to note that although all of the turn-over frequencies are low relative to the previous set of data run under an atmosphere of pure CO, the order of activity has changed with dcpb now being the most active whilst surprisingly $Rh_2(CO)_4Cl_2$ now records the 2nd least active system.

Within the gas analysis results the main point of interest is the formation of methane. From these reactions the structure of the ligand seems to have a large effect. These results suggest that a ligand containing a rigid backbone such as dppx or BINAP may reduce the amount of methane produced whereas systems containing ligands with a flexible backbone such as dppb and dcpb result in a large increase in the formation of methane irrespective of the steric bulk at the phosphorus or the bite angle. In order to confirm these trends, the experiment was repeated under a 3rd set of conditions (Table 2.6).

Table 2.6. Methanol carbonylation at 150 ºC using 1:5 H_2:CO syngas and an initial charge of 15 % H_2O [(a)]

Ligand	none	dppb	dppx	dcpb	BINAP
TOF/h^{-1} [(b)]	**740**	**857**	**387**	**690**	**426**
Aldehyde/Acetyl ratio[(c)]	**3.20**	**2.59**	**0.74**	**2.30**	**0.92**
Liquid analysis [(d)]	%mol/mol	%mol/mol	%mol/mol	%mol/mol	%mol/mol
Water	45.4	44.5	42.9	43.9	43.5
Methanol [(e)]	49.8	50.2	53.8	51.3	53.0
Methyl Iodide	1.5	1.4	1.5	1.6	1.6
Methyl Acetate	**2.7**	**3.2**	**1.5**	**2.6**	**1.7**
Acetic Acid	**0.6**	**0.7**	**0.3**	**0.6**	**0.3**
MeCHO (ppm)	**1100**	**1040**	**135**	**750**	**185**
Gas Analysis [(f)]	%vol/vol	%vol/vol	%vol/vol	%vol/vol	%vol/vol
H_2	37.2	27	27.0	31.4	20.2
CO	44.4	43.6	69.6	42.1	78.2
CO_2	2.3	1.8	0.5	1.1	0.3
CH_4[(g)]	**14.4**	**25.8**	**1.7**	**23.9**	**<0.1**

(a) Reaction conditions: $Rh_2(CO)_4Cl_2$ (0.386 mmol), Rh:ligand = 1:1, 1:5 H_2:CO p = 26 bar, for 40 minutes at 150 ºC, 15 %wt initial water concentration (b) TOF was calculated from the total conversion of methanol and methyl iodide to methyl acetate and acetic acid (c) Aldehyde/acetyl ratio was calculated from the ratio of acetaldehyde to carbonylated products (d) Calculated by calibrated GC analysis using an internal standard at BP, Hull (e) %mol/mol of methanol also comprises ~5-7 %mol/mol DME (f) Sampled at room temperature from headspace after cool down (g) %vol/vols of methane typically represent between 0.0001-0.6 %mol/mol.

In this third set of catalytic data the temperature and the partial pressure of CO was increased to 150 ºC under a 5:1 CO:H_2 atmosphere in order to increase the activity of the systems, and closer resemble industrial conditions. In a similar way the initial water concentration was also increased to 15 % in order to avoid the possible formation of inactive species and to maximise the possible activity of these systems.

The data contained within Table 2.6 clearly shows that the activity has increased significantly over that of the previous two sets of conditions with the order of reactivity for the catalysts being dppb> $Rh_2(CO)_4Cl_2$>dcpb>BINAP>dppx. The dppb system proved to be the most active with $Rh_2(CO)_4Cl_2$ and the dcpb systems also showing high activity, whereas the dppx and BINAP systems were approximately 50 % less active.

Although the overall formation of acetaldehyde produced has increased, when the acetaldehyde/acetylated product ratio is taken into account, one can see that there has been a slight fall that can be linked directly to the decrease in the amount of H_2 present in the system. From the acetaldehyde/acetylated product ratio one can see dppx and BINAP under these conditions is 4.5 times as hydrogen tolerant as $[Rh(CO)_2I_2]^-$ with as little as 0.74 % of the carbonylated products being the undesired by-product acetaldehyde. Under the previous set of conditions dcpb had been the most hydrogen tolerant system however with the increase in temperature there is a significant decrease in hydrogen tolerance with the acetaldehyde/acetylated product ratio going from 0.69 % to 2.30 %. It is proposed that this decrease in hydrogen tolerance is a direct result of the decomposition of the catalyst at higher temperature and shall be addressed in Section 2.6.

As well as acetaldehyde formation both the dppb and dcpb systems formed large amounts of methane, in the case of the dppb system >25 % of the autoclave headspace was methane, whereas dppx and BINAP systems gave very little methane as a gaseous by-product with BINAP giving <0.1 %v/v. These volumes of methane have been estimated to represent between 0.0001 (BINAP) and 0.6 %mol/mol (dppb). These values were taken from headspace calculations and the calculated total number of moles within the system post-run using recorded weights and %mol/mol of the individual constituents.

In conclusion, dppx and BINAP systems although suffering from comparably low activity are very hydrogen tolerant producing between 135-185 ppm of acetaldehyde at 150 ºC and almost negligible amounts of methane in all catalytic experiments. It should also be noted that to the best of our knowledge under the conditions set out in the third experiment the dppx system is the most hydrogen tolerant catalyst for the rhodium-catalysed carbonylation of methanol reported to date.

2.6 Catalyst resting states and catalyst stability

Table 2.7. % of catalyst recovered under different syngas conditions

	2:1 H_2:CO 140 ºC, 40 mins	1:5 H_2:CO 150 ºC, 40 mins
dppb	60.2	2.7
dppx	85	78.7
dcpb	27.8	5.9
BINAP	63.9	53.8

On cooling, the catalysts precipitated out of solution. It should be noted that in Table 2.7 the % recovery of precipitated catalyst does not completely decouple stability from solubility differences so these results must be interpreted cautiously. However, since all the Rh complexes involved show very limited solubility in the product mix, it is almost certain that these reflect catalyst stability. The precipitate collected from the BINAP systems was shown to be the Rh(I) carbonyl iodide species [Rh(BINAP)CO(I)] **6**. Although HPIR studies during the reaction were inconclusive, given that we also observed a lower stability of BINAP Rh(III) acetyls in the coordination chemistry studies, this is the proposed resting state. The higher stability of the BINAP catalyst under catalytic conditions can be ascribed to the presence of CO which enables the system to turnover and produce a Rh(I) resting state.

The Rh/dcpb catalyst that precipitated was only sparingly soluble with the $^{31}P\{^{1}H\}$ NMR showing the presence of a Rh(III) species with a typical P-Rh coupling of 138 Hz. However, FT-IR of the bulk sample showed the majority to be the Rh(I) species [Rh(dcpb)CO(I)] (1949 cm^{-1}) with a minor peak at 1710 cm^{-1} relating to the acetyl. Therefore, it is likely that the nature of the catalyst resting state is finely balanced. However, it is noted that the recovery of these sparingly soluble species was relatively low.

One may possibly expect the dcpb system to be much more active than dppb due to the strongly electron donating properties of the phosphines which may facilitate oxidative addition, with the bulky groups favouring reductive elimination. However, a reasonable explanation for similar performance is the increase in steric hindrance of the cyclohexyl groups and the considerable shielding these must give to the metal centre. Alternatively, given that we have been unable to isolate Rh species for dcpb in stoichiometric reactions and much lower recovery at the end of the catalytic runs had occurred, it is also possible that dcpb catalysts decompose under the reactions conditions. This is also supported by the dramatic rise in acetaldehyde being produced going from 140 ºC to 150 ºC which can be directly linked to decomposition of the catalyst and the formation of $[Rh(CO)_2I_2]^-$.

For dppx and dppb on the other hand it was possible to collect a substantial amount of precipitate formed at the end of each catalytic run. These precipitates were fully analysed and the resting state shown to be the Rh(III) species, $[Rh(L)(C(O)Me)(I)_2]$. The most stable catalyst system is dppx which manages 85 % recovery as a precipitate under catalytic conditions at 140 ºC, and was also seen to be the most stable in the previous study in hot MeI. In the runs carried out in aqueous methanol at 150 ºC, a similar crop of $[Rh(dppx)(C(O)Me)(I)_2]$ **10** was obtained (79 %) in comparison to the dppb catalyst that provided very little of the Rh acetyl precipitate. This is most likely due to decomposition of dppb complexes at higher temperatures.

2.7 Reaction of dppp, dppb and dppx complexes with hydrogen

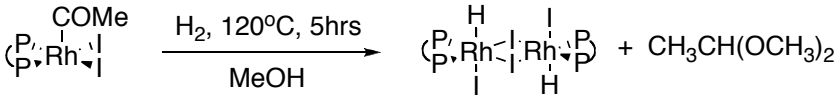

Scheme 2.3. Reaction of $[Rh(dppp)COMe(I)_2]$ with H_2 and the formation of the hydride dimer

The greater hydrogen tolerance of the dppx catalyst could reflect a more efficient reductive elimination for this ligand, or a reduced propensity for the complexes to undergo hydrogenolysis. According to Moloy and Wegman it is possible to generate the hydride dimer and acetaldehyde (as dimethyl acetal) by reacting $[Rh(dppp)(C(O)Me)(I)_2]$ **12** with hydrogen.[74] Ligand effects on this were investigated

by reacting the isolated acetyls [Rh(dppp)(C(O)Me)$(I)_2$] **12**, [Rh(dppb)(C(O)Me)$(I)_2$] **7** and [Rh(dppx)(C(O)Me)$(I)_2$] **10** with hydrogen under similar conditions set out above.

[Rh(dppp)(C(O)Me)$(I)_2$] **12** was heated in methanol at 120 ºC for 5 hours under 7 bar of H_2, this yielded a complex with the same spectroscopic data as previously described for the hydride dimer ($^{31}P\{^1H\}$ NMR d δ 27.3 $^1J_{Rh\text{-}P}$ = 125 Hz). Under these conditions we also observed the hydrogenolysis of [Rh(dppb)(C(O)Me)$(I)_2$] **7** and the formation of several new complexes that show hydride signals in the $^1H\{^{31}P\}$ NMR. Unfortunately we were unable to isolate any of these new complexes in pure form. Interestingly, when [Rh(dppx)(C(O)Me)$(I)_2$] **10** was reacted under the same forcing conditions no reaction occurred and the starting material was recovered in quantitative yield.

When this experiment was repeated at the lower temperature of 80 ºC the complexes containing dppp and dppb react to form hydrides. However, [Rh(dppx)(C(O)Me)$(I)_2$] **10** once again does not react with hydrogen and in fact at the lower temperature it starts to equilibrate back to the Rh(I) species [Rh(dppx)CO(I)]. This is backed up by the appearance of two sets of doublet of doublets in the $^{31}P\{^1H\}$ NMR data ($^{31}P\{^1H\}$ NMR dd δ 25.5 ppm ($^1J_{Rh\text{-}P}$ = 166 Hz, $^2J_{P\text{-}P}$ = 41 Hz), dd δ 9.11 ppm ($^1J_{Rh\text{-}P}$ = 122 Hz, $^2J_{P\text{-}P}$ = 40 Hz)) as well as FT-IR of the mixture, that clearly shows peaks for both the acetyl and the Rh(I) carbonyl (1710 cm^{-1} and 1968 cm^{-1} respectively). Interestingly, the [Rh(dppx)CO(I)] being formed by this reverse process is a monomeric chelate species as opposed to a dimeric bridging species formed from $Rh_2(CO)_4Cl_2$. There is therefore a clear difference in the reactivity of the Rh(III) acetyls with hydrogen that co-incides with the observations under catalytic conditions.

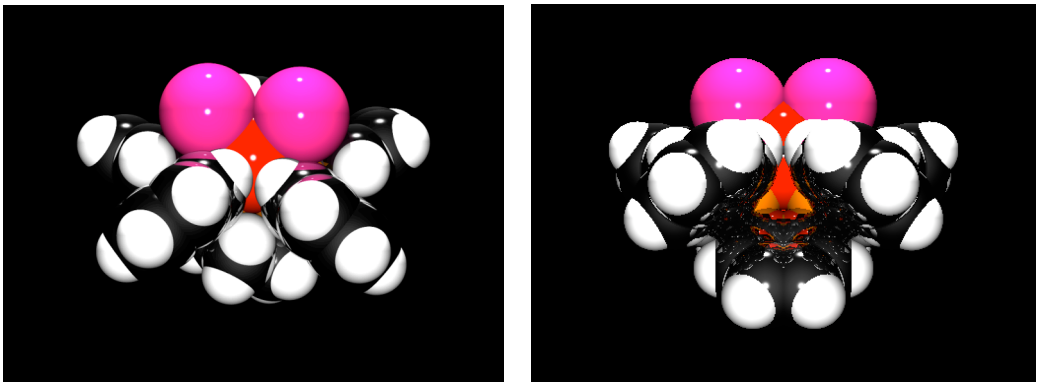

Figure 2.5. Molecular models of [Rh(dppb)(COMe)$(I)_2$] **7** and [Rh(dppx)(COMe)$(I)_2$] **10**.

One possible explanation for hydrogen tolerance can be seen when the crystal structures of the dppb and dppx acetyls are compared (Fig. 2.5). The more rigid dppx backbone forces the phenyl groups inwards, increasing the steric hindrance around Rh-acetyl bond. It seems reasonable that this more congested environment around metal centre coupled with the fact that dppx cannot easily change conformation to accommodate incoming reactants, accounts for the differences in catalytic products.

2.8 Conclusion

In summary, Rh(I) carbonyl complexes of the C_4 diphosphines dppb, BINAP, dcpb and dppx have been prepared and their reactivity studied. These studies reveal that only the dppb and dppx complexes smoothly give the expected Rh(III) acetyl complexes on reaction with a large excess of methyl iodide at 140 ºC. The complexes have been studied as catalysts for methanol carbonylation using CO that contains hydrogen. Examination of the insoluble catalyst residues from these reactions shows that dppx and dppb have Rh(III) acetyls as resting states and that the dppx complex is more stable with respect to elimination of P(V) by-products. In contrast, the dcpb system consisted of both Rh(I) carbonyl and Rh(III) acetyl species. By-product analysis of the organic carbonylation products reveals that the more rigid BINAP and dppx systems give much lower proportions of acetaldehyde and methane side products. An explanation for this comes from the relative reactivity of the Rh(III) acetyls with hydrogen: whereas dppb and dppp complexes react with hydrogen to give various

hydride species, there is no reaction for the dppx complex. Examination of the X-ray crystal structures of these two complexes suggest that the rigidity of the dppx backbone makes the diphenylphosphine group shield the acetyl from hydrogenolysis, which may be the ultimate origin of the greater hydrogen tolerance of the dppx carbonylation catalysts.

Chapter III: An investigation into the stability of mono, bi and tridentate rhodium-phosphine complexes

3.1 Introduction

Chapter 2 reported an investigation into the use of phosphine modified systems as a means to improving the selectivity towards acetic acid, whilst in the presence of hydrogen. However, before a suitable phosphine can be designed to deliver an improvement to selectivity and activity, the catalyst and ligand will need to show long-term stability under the forcing conditions required for industrial methanol carbonylation. Although it has been known for some time that rhodium complexes of monodentate phosphines are only stable for very short periods of time under industrially significant conditions, several diphosphine systems have been reported that seem to show significantly better stability.[62, 67, 70-72] However, there is still next to nothing known about how ligand co-ordination mode, electronic and steric effects impact on stability.

Therefore, this chapter will assess the stability of rhodium-phosphine complexes with a range of coordination modes and investigate the effect of varying the steric and electronic properties of the phosphine ligand. Evidence will also be presented that supports a dissociative mechanism as the means of phosphine loss from a tridentate complex.

3.2 Assessing the stability of rhodium-phosphine complexes in MeI

3.2.1 Methodology

An accurately measured amount of complex was dissolved up into a 3:1 mixture of methyl acetate and methyl iodide. This solution was then heated to the desired

temperature for a set amount of time; the use of a microwave was employed to control the accuracy of the temperature and due to the instantaneous nature of microwave heating, the reaction time is also very accurate relative to conventional heating. A carefully measured aliquot of solution was then sampled and added to a tube containing a referencing standard. This was then analysed using $^{31}P\{^{1}H\}$ NMR spectroscopy allowing the stability to be quantified in terms of the percentage of rhodium-phosphine species in solution.

The aforementioned standard was tributylphosphine oxide, which was made up to an accurate molarity in a solution of deuterated benzene. This solution was then contained within a sealed capillary tube making it possible to reuse the standard, thus guaranteeing that the exact same amount was used in each experiment. During assessment as a standard, tributylphosphine oxide showed a linear relative response to variations in the concentration of [Rh(dppe)CO(Cl)], making it an ideal candidate to accurately quantify any decomposition that may occur during the following stability tests. The only assumption made was that all the rhodium complexes produced, in the presence of MeI for any given phosphine, show similar response ratios to the Rh(I) starting material, that was calibrated in each case against $^{n}Bu_3P{=}O$. One potential complication is that some complexes could show good stability but poor solubility. Thus, the composition of the ^{31}P containing species is also discussed.

3.2.2 The model system: $[Rh(PPh_3)_2CO(Cl)]$

$[Rh(PPh_3)_2CO(Cl)]$ **8** was used as a model system in order to assess the accuracy and effectiveness of the above methodology. Solutions containing accurately measured amounts of complex were heated at different temperatures ranging from 60 ºC to 140 ºC. Using the $^{31}P\{^{1}H\}$ NMR spectra taken from each sample the stability of the complex was calculated (Fig. 3.1). One can see that the percentage of complex in solution decreases with increasing temperature, and that this is in direct correlation with the growth of the peak at 24 ppm in the $^{31}P\{^{1}H\}$ NMR spectra, corresponding to the formation of the P(V) species $PPh_3Me^{+}I^{-}$. The formation of P(V) species such as $PPh_3Me^{+}I^{-}$ and $PPh_3(O)$ is a direct result of the decomposition of the complex.

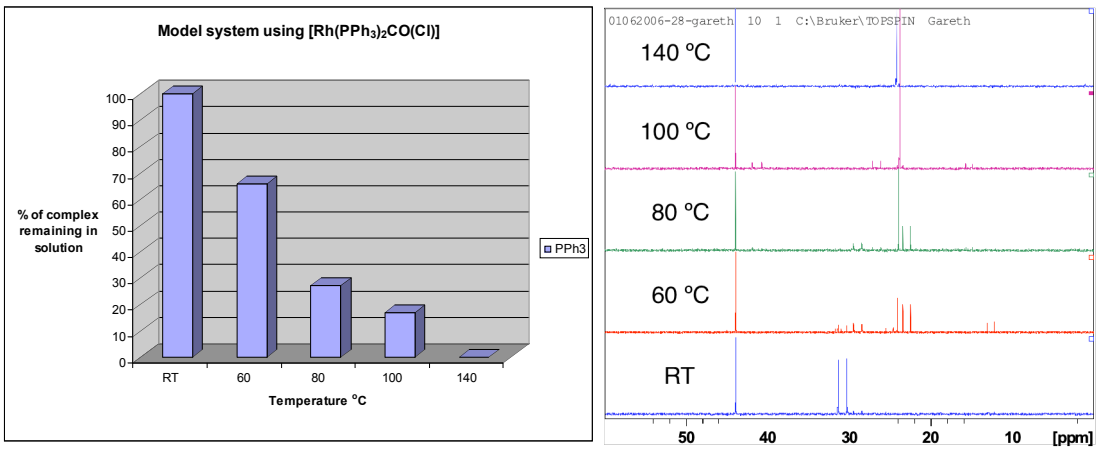

Figure 3.1. The stability of $[Rh(PPh_3)_2CO(Cl)]$ **8** at a range of temperatures alongside $^{31}P\{^1H\}$ NMR spectra.

Whilst these results were used as a benchmark against which other monodentate ligands were compared, this approach was also extended to measure the stability of other rhodium carbonyl complexes containing bi and tridentate ligands.

3.3 Studying monodentate ligand systems

Monodentate ligand complexes were used to investigate how steric and electronic properties may affect stability. In Chapter 1, we discussed how complexes containing monodentate ligands have a significantly lower stability compared to their bidentate counterparts, and therefore as with the model system the following tests were performed under milder conditions (60-100 ºC). Although less stable, they can be prepared with relative ease using a large selection of monodentate ligands, with varying steric and electronic properties, which are either commercially available or easily accessible via synthetic methods. The rhodium complexes of these ligands conform to the generic *trans* configuration (Chapter 1, Part B), which makes them an ideal choice to assess how changes in the steric and electronic properties affect the overall stability of the complex, without the complication of variations in the coordination mode. With this in mind the following complexes were prepared.

3.3.1 Stability of sterically hindered monodentate phosphine complexes

The complexes in Fig. 3.2 were used to investigate how steric constraints imposed by the ligand, upon the rhodium centre, may affect the stability of the complex. The results of which are shown in Fig. 3.3.

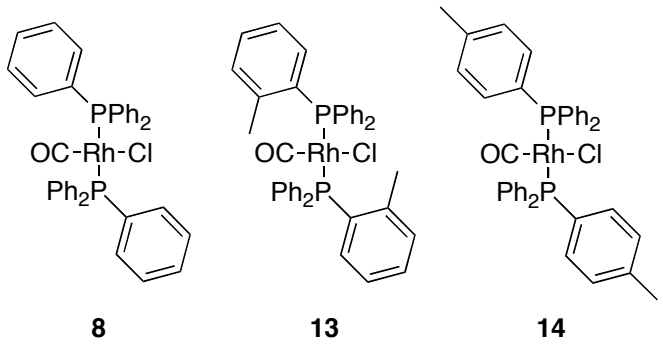

8 **13** **14**

Figure 3.2. A series of complexes with varying steric properties

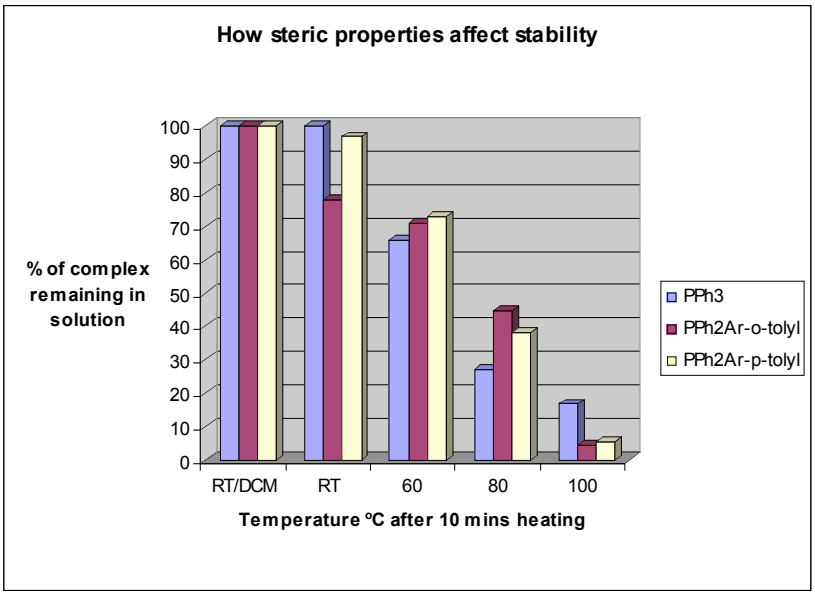

Figure 3.3. A comparison in the stability of *o*- and *p*-tolyl complexes against that of $[Rh(PPh_3)_2CO(Cl)]$ **8**.

The results in Fig. 3.3 suggest that relatively small changes to the cone angle and steric properties of the ligand have very little effect on the overall stability of the complex. However, it may still be conceivable that the use of very bulky phosphines could show significant stability differences.

Another observation that resulted from this study was that the complex containing the *o*-tolyl diphenyl phosphine ligands undergoes oxidative addition at a much slower rate. After 10 minutes at 60 ºC, a large amount of unreacted Rh(I) starting material still remained in comparison to the other complexes. This is supported by the research of Dutta et al. who have also shown that the oxidative addition of methyl iodide may be hindered by the use of *ortho*-substituents on the phosphine ligand.[61]

3.3.2 Stability of electron poor monodentate phosphine complexes

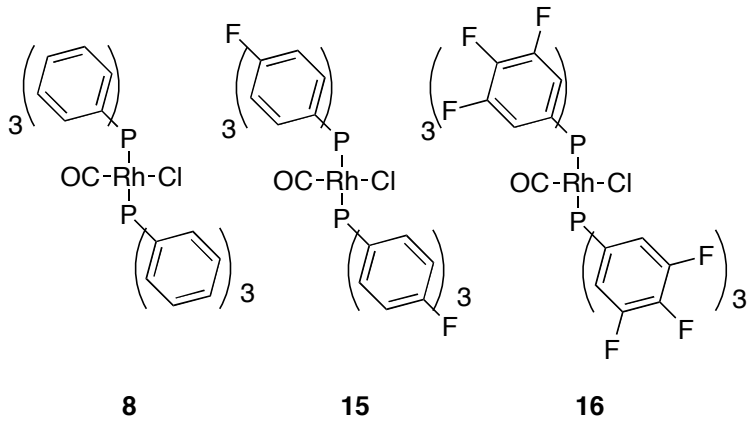

Figure 3.4. A series of complexes with increasingly electon poor donor ligands.

A series of complexes were prepared containing increasingly fluorinated phosphines in order to study how changes in the electronic properties of the ligand may affect the stability of the complex, while also avoiding any large variation in the steric bulk of the ligand. The infrared spectra of these complexes show that the ν(CO) increases from 1965 cm^{-1} for **8** to 1985 cm^{-1} for the most heavily fluorinated complex **16**, this is evidence of a gradual decrease in electron density around the metal centre (Section 1.19).

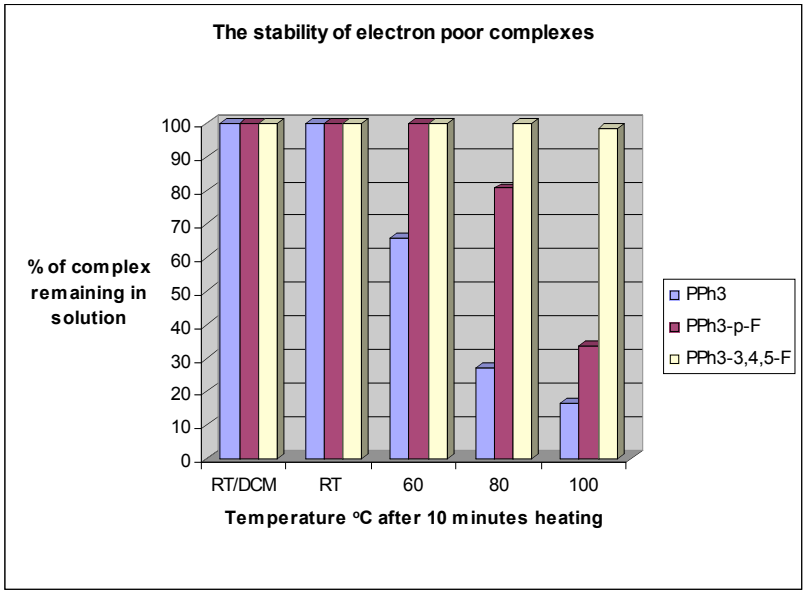

Figure 3.5. A comparison in the stability of electronically poor rhodium complexes.

The results of the stability tests (Fig. 3.5) were quite striking and at first glance seem to suggest that electron withdrawing substituents may be advantageous towards the overall stability of the complex. However, the experimental $^{31}P\{^{1}H\}$ NMR data show that as the number of electron withdrawing substituents are increased so does the amount of unreacted starting material. This may in part be due to the stabilisation of the Rh(I) oxidation state of the complex by poor electron donating ligands and has no added advantage to the cycle as a whole. Once a certain activation energy has been surpassed, enabling the reaction with methyl iodide to occur, the complex rapidly decomposes. In my opinion, it is likely that phosphine loss is predominantly from Rh(III) species. However, a further experiment in which the highly fluorinated phosphine was reacted with MeI at room temperature demonstrated that this phosphine did not completely quaternise. Thus, it is also possible that the longer lifetime of the dissociated fluorinated phosphines is the key to higher stability.

3.3.3 Stability of electron rich monodentate phosphine complexes

It has previously been proposed by Rankin *et al.* that the stability of rhodium-phosphine complexes may be enhanced by the use of electron rich phosphine ligands.[59, 60, 72] It was theorised that strong electron donating ligands would strengthen the

rhodium-phosphine bond and reduce the likelihood of phosphine loss via a dissociative mechanism.

To test this theory a number of complexes containing electron rich phosphine ligands were prepared (Fig. 3.6). Once again these complexes were compared against our model system, $[Rh(PPh_3)_2CO(Cl)]$ **8** and the infrared reflect an increase in donor strength of the phosphine with the ν(CO) decreasing from 1965 cm^{-1} to 1959 cm^{-1}, moving from left to right.

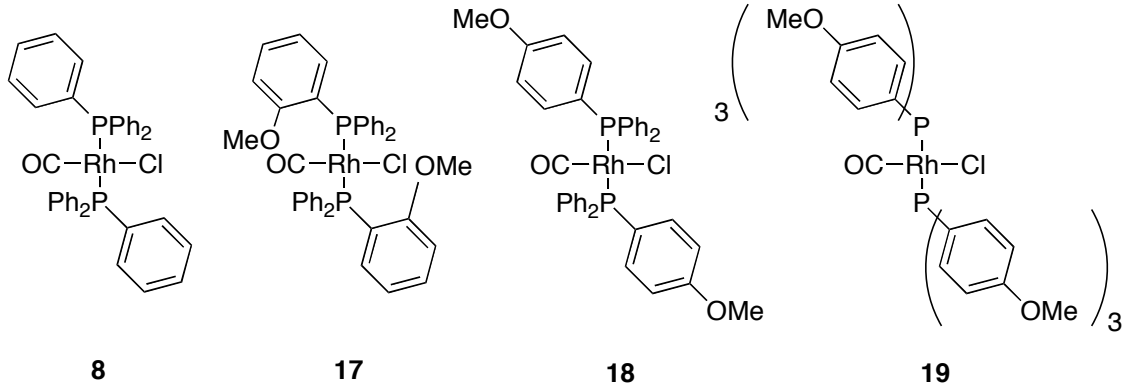

Figure 3.6. A series of rhodium phosphine complexes containing electron donating anisole groups in *ortho* and *para* positions.

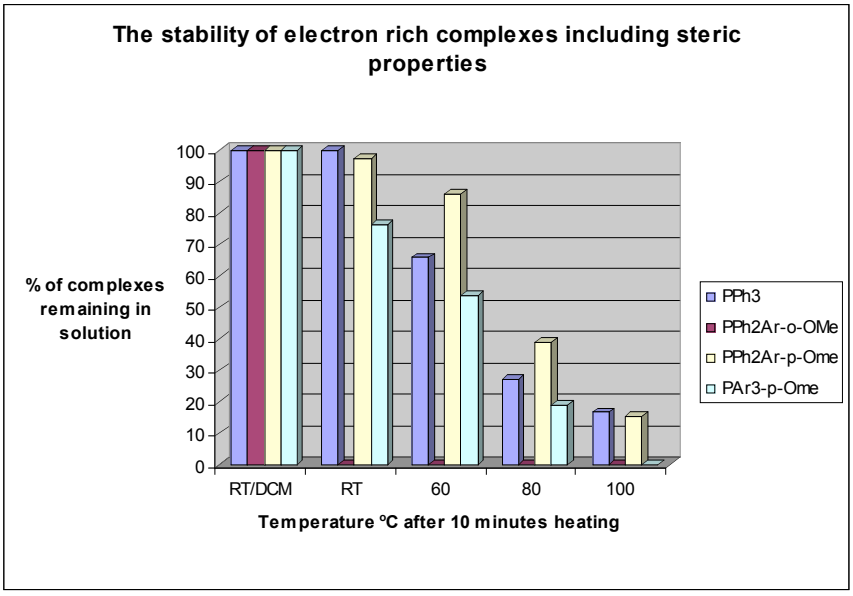

Figure 3.7. The stability profiles of electron rich anisole complexes

The results in the Fig. 3.7 above show that the use of strong electron donating ligands gave no added benefit to the stability of the complex. At best, one could say that

the results of the complex containing the mono anisole ligand, $PPh_2(C_6H_4$-*p*OMe) are moderately improved at lower temperatures. However, realistically no improvement has occurred, with all of these complexes unable to survive at temperatures greater than 100 ºC.

The incompatibility of the *ortho*-substituted ligand was also a surprise, as it was initially hoped that the positioning of the methoxy group *ortho* to the phosphorus may help to stabilise the complex, in a similar way to the catalysts designed by Dutta *et al.* (Section 1.11).[61] However the opposite seems to be the case, with the addition of MeI causing the complex to rapidly decompose even at room temperature. It is postulated that this may be due to the methoxy group interacting with the rhodium in a way that destabilises the bond between the metal and the phosphorus and causes loss of the ligand in the presence of MeI.

3.3.4 Summary of the monodentate study

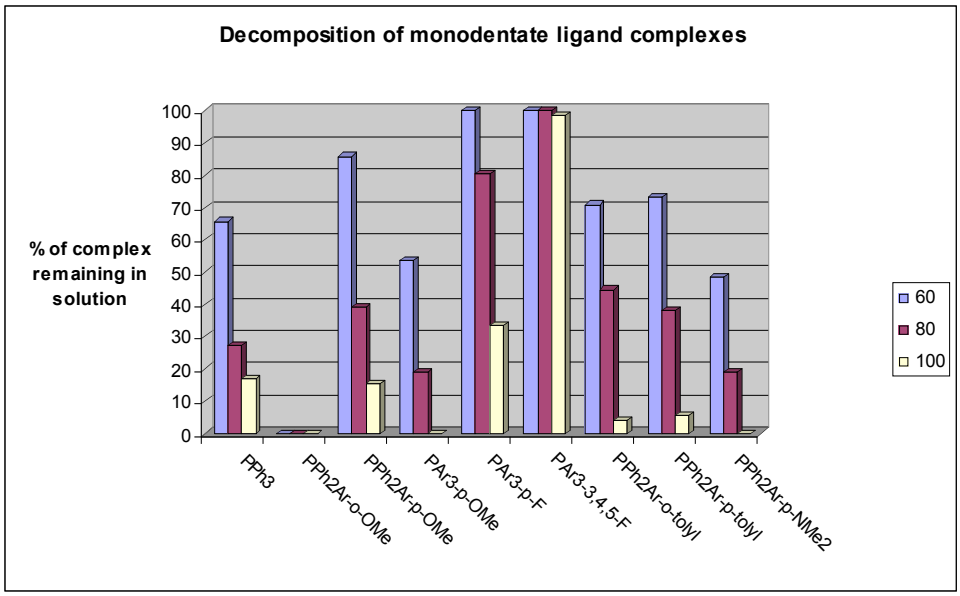

Figure 3.8. Summary of results for the monodentate complexes.

On the whole small variations in the electronic and steric properties of a ligand seem to make little difference on the stability of the complex. However, this study provides two important observations, the first is the apparent incompatibility of the

ortho-methoxy group with this type of system and the second is the stabilising effect of poor electron donating ligands upon Rh(I) complexes.

Given that oxidative addition is a key step in methanol carbonylation and the catalyst spends some time period as a Rh(III) species, increasing stability by completely preventing the formation of Rh(III) species is not a viable option. From these observations, it is proposed that if a catalytic turnover was allowed to occur the resting state for complexes of the type $[Rh(L)_2CO(Cl)]$, where L is a monodentate phosphine ligand similar to those discussed, would be Rh(I) due to a rate determining oxidative addition. This proposal is also supported by a reported Rh(I) resting state for $[Rh(PEt_3)_2CO(Cl)]$.[59]

3.4 Studying bidentate ligand systems

Unlike monodentate systems bidentates are potentially more complex in terms of steric and electronic properties. In this section we have examined a series of bidentate ligands ranging from the relatively simple dppe to the more rigid and complex Xantphos ligand. Within this range we see a variety of different coordination modes and examine how changes in conformation play an important role in catalyst stability.

The method used to test the stability of these bidentate complexes was similar to that of the monodentates with respect to the use of the standard. However, due to the increased stability of the bidentate systems a higher temperature of 140 ºC was employed. It was hoped that a temperature of 140 ºC would allow for some differentiation in the stability of the complexes, as previous work had shown that at lower temperatures many of the complexes were too stable to really draw any comparisons. While at temperatures greater than 140 ºC the formation of hot spots in the microwave vessel resulted in the premature decomposition of the rhodium complex. This is in part due to the high concentration of rhodium complex in solution compared to the industrial methanol carbonylation conditions, and is thought to be a process that occurs independently of the phosphine ligand. A different experimental setup and analysis method was required to test stability at higher temperatures and lower concentrations and shall be described in Section 3.5.

3.4.1 A comparison of monomeric *cis*-chelated complexes with dimeric bridging systems

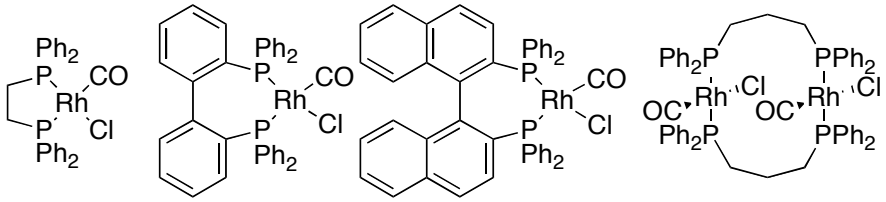

20 **21** **5** **22**

Figure 3.9. The structures of the three *cis*-chelated complexes, (left to right) [Rh(dppe)CO(Cl)] **20**, [Rh(BIPHEP)CO(Cl)] **21**, [Rh(BINAP)CO(Cl)] **5** and $[Rh(dppp)CO(Cl)]_2$ **22**.

There are several key differences between the complexes shown in Fig. 3.9, the most obvious being the coordination mode between the *cis*-chelated complexes **20**, **21**, **5** and the dimeric bridging complex $[Rh(dppp)CO(Cl)]_2$ **22**. Amongst the *cis*-chelates there are considerable differences in the steric bulk and rigidity of the backbone when moving from dppe to BINAP. Other differences within all four complexes include the length of the backbone between the two phosphorus atoms: dppe (C_2), dppp (C_3) and the other two ligands (C_4). It is foreseeable that these structural observations may play a crucial role in the overall stability of the complex.

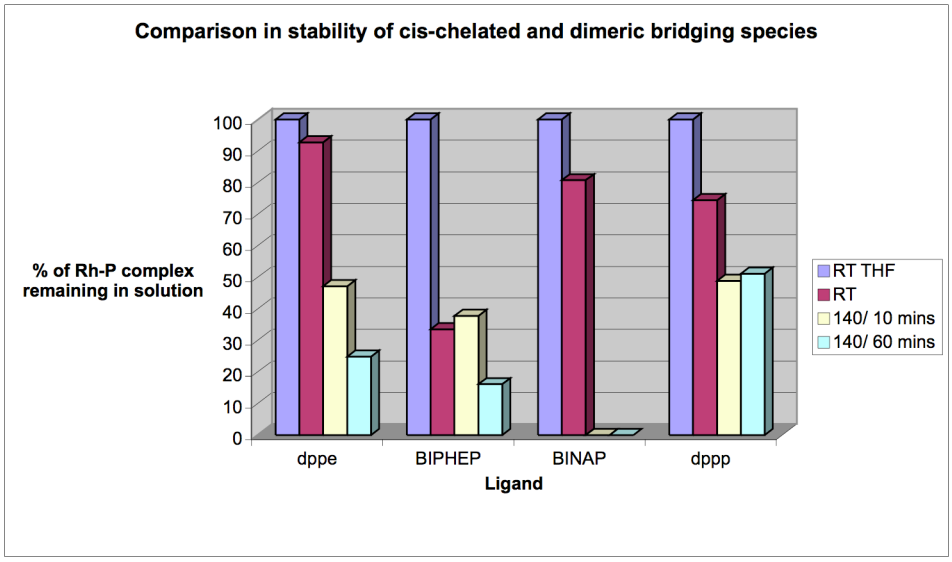

Figure 3.10. Studying the stability of *cis*-chelated and dimeric bridging complexes containing dppe, BIPHEP, BINAP and dppp.

The results displayed in Fig. 3.10 show some noticeable differences between the four complexes. The least stable complex is that containing BINAP, whose instability at higher temperatures under catalytic conditions has previously been mentioned in section 2.6. During this set of experiments [Rh(BINAP)CO(Cl)] **5** shows complete decomposition after only ten minutes at 140 ºC, whereas dppe, dppp and BIPHEP all show a much higher degree of stability. These results however can only be fully understood in conjunction with the experimental $^{31}P\{^{1}H\}$ NMR data shown below.

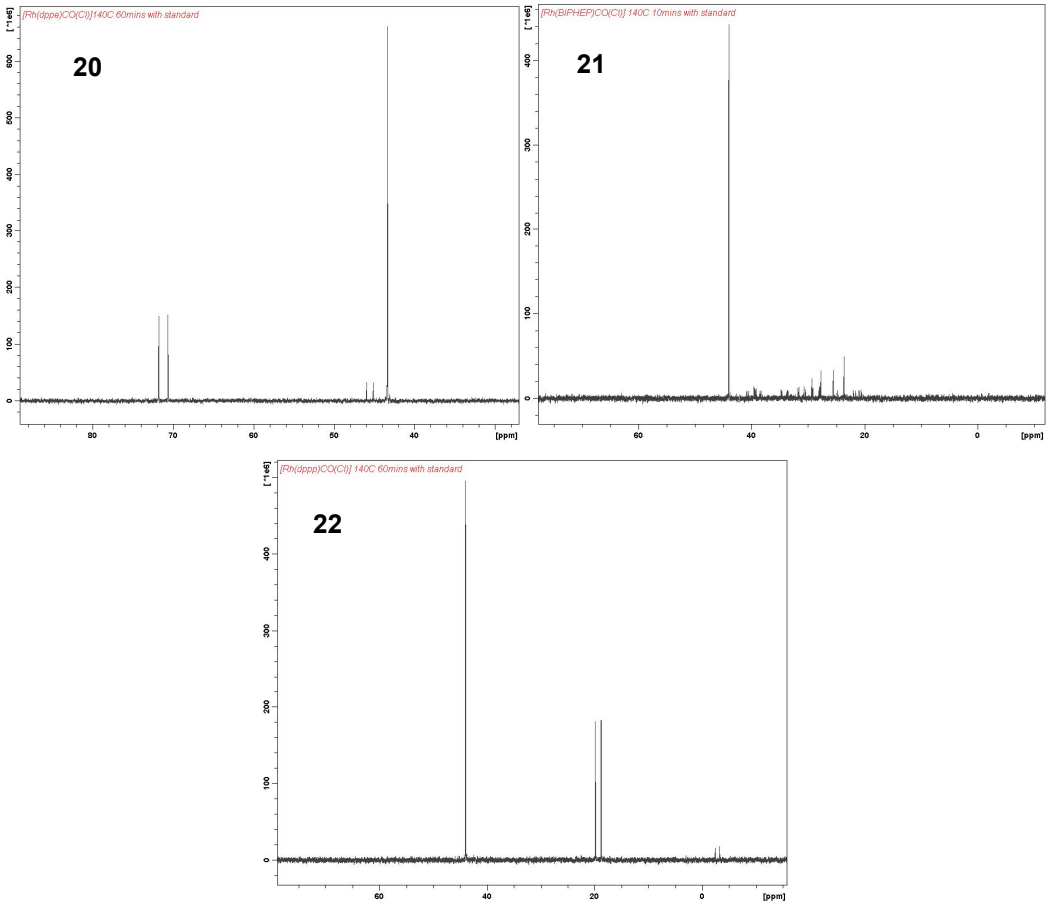

Figure 3.11. Post run $^{31}P\{^{1}H\}$ NMR spectra after the preformed complexes [Rh(dppe)CO(Cl)] **20**, [Rh(BIPHEP)CO(Cl)] **21** and [Rh(dppp)CO(Cl)]$_2$ **22** were independently heated to 140 ºC for 60 mins in the presence of MeI.

Although the data suggest that only ca. 25 % of complexed dppe remains in solution, the $^{31}P\{^{1}H\}$ NMR spectrum clearly shows that this is simply down to the poor solubility of the complex formed as opposed to decomposition of the complex. The $^{31}P\{^{1}H\}$ NMR spectrum of the dppp system also only displays peaks with Rh-P couplings with no P(V) species being observed. This is supported by the visual

observation of large amounts of precipitate being formed within the heating vial for both the dppe and dppp runs. These precipitates were characterised and as expected found to be the acetyl species [Rh(dppe)COMe(I)$_2$] **23** and [Rh(dppp)COMe(I)$_2$] **12**. These complexes have previously been reported by Sanger,[77] with the X-ray crystallographic data being presented by Haynes and co-workers.[66] At lower temperatures it is also possible to observe the formation of both isomers resulting from the oxidative addition of methyl iodide. This is due to the retardation of migratory insertion caused by the strong electron donating effect of the ligand resulting in a higher concentration of oxidative addition intermediate being present in solution.

The $^{31}P\{^1H\}$ NMR spectrum from the reaction with [Rh(BIPHEP)CO(Cl)] **21** on the other hand, shows clear signs of decomposition and the formation of several P(V) species. Unlike dppe and dppp, [Rh(BIPHEP)CO(Cl)] **21** and its intermediates were fully soluble in solution with no precipitates being formed, that may otherwise have led to complications in quantifying the stability of the complex. Other signs of decomposition included blackening of the vial caused by the formation of rhodium black as a result of ligand dissociation.

As with [Rh(dppb)CO(Cl)]$_2$ **1** and [Rh(dppx)CO(Cl)]$_2$ **3**, we have seen that in the case of [Rh(dppp)CO(Cl)]$_2$ **22** the coordination mode of the precursor complex does not impact upon the overall stability of the system. In fact as a dimeric bridging species [Rh(dppp)CO(Cl)]$_2$ **22** was free to rearrange and form monomeric *cis*-chelates such as [Rh(dppp)COMe(I)$_2$] **12** without loss of stability. Surprising it was the *cis*-chelated complexes of BINAP and BIPHEP that resulted in the least stable systems. One reason for the stark contrast in stability between these complexes and in particular the *cis*-chelates is the difference in rigidity of their backbone. It is theorised that the ability to undergo conformational change during the catalytic cycle is essential for the stability of the catalyst and in the case of BINAP, and to a lesser extent BIPHEP, the rigidity and bulk of their backbone prevents this from occurring. In section 2.6 we also discussed the potential role of resting states and the stability of the key Rh(I) and Rh(III) intermediates under CO and N_2 atmospheres.

3.4.4 The stability of rhodium-Xantphos complexes

A series of Xantphos and Nixantphos complexes was prepared via literature methods and the structures of which can be seen below (Fig. 3.15).

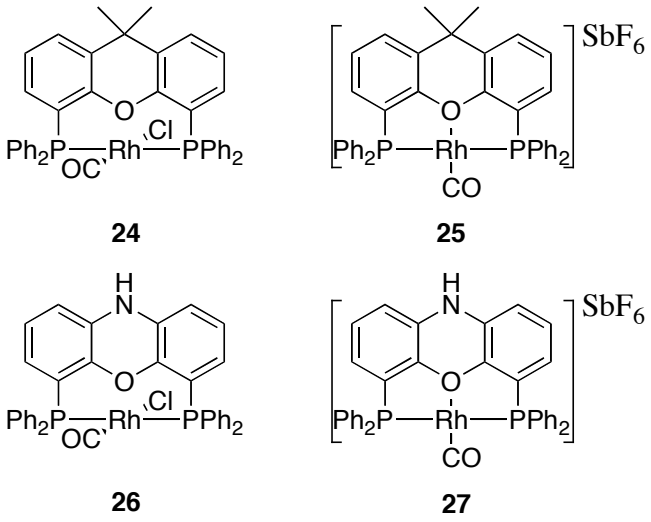

Figure 3.15. Structures of Xantphos and Nixantphos complexes containing bi and tridentate coordination modes.

Similar to the problems encountered previously the solubility of some of these complexes in a solution of MeOAc and MeI was quite poor. [Rh(Xantphos)CO(Cl)] **24** was the only complex in this set to be fully soluble in this solvent mixture with the results showing that it is also remarkably stable with little to no decomposition at 140 ºC even after 60 minutes (Fig. 3.16).

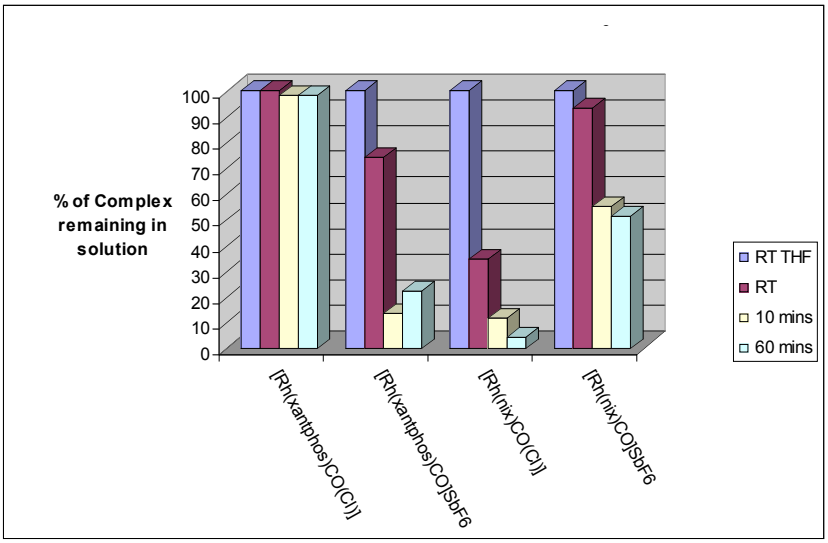

Fig. 3.16. Stability of Xantphos complexes at 140 ºC

The solubility the salt [Rh(Xantphos)CO]SbF_6 **25** was significantly decreased at room temperature. However, upon heating full solubility was observed.

Although, it was hoped that the nitrogen containing backbone of the Nixantphos ligand may help to increase the solubility of the complex in the presence of MeI, the rhodium complexes formed were very insoluble in methyl acetate/methyl iodide and suffered from a significantly reduced level of stability as a result.

3.5 Low concentration, high temperature autoclave studies

In order to fully test some of the most stable complexes that have been highlighted throughout this chapter a series of high temperature, low concentration catalytic runs were carried out in Hastelloy autoclaves. At low catalyst loadings, complexes containing the ligands dppe, dppp, dppx, Xantphos and TRIPHOS were heated to 175 ºC under 5 bar CO, in a solution of methanol and methyl iodide for 1 hr to simulate the industrially significant conditions of this reaction. Due to the nature of the products a biphasic system resulted rendering the quantitative analysis of the results using an external standard invalid, as a homogeneous catalyst concentration throughout the system no longer existed. Therefore the following observations are of a qualitative manner.

The complexes were made at low concentration in a solution of methanol and analysed using $^{31}P\{^{1}H\}$ NMR to ensure complete formation of the complex had occurred before the addition of methyl iodide was made. The solution was then added to the autoclave and heated to 175 ºC under 5 bar CO for 1 hr. After 1 hr the resulting catalytic solutions were reduced to dryness and the solids were analysed using $^{31}P\{^{1}H\}$ NMR. The data collected showed some interesting and starkly contrasting results for the stability of these complexes under catalytic conditions at such high temperatures.

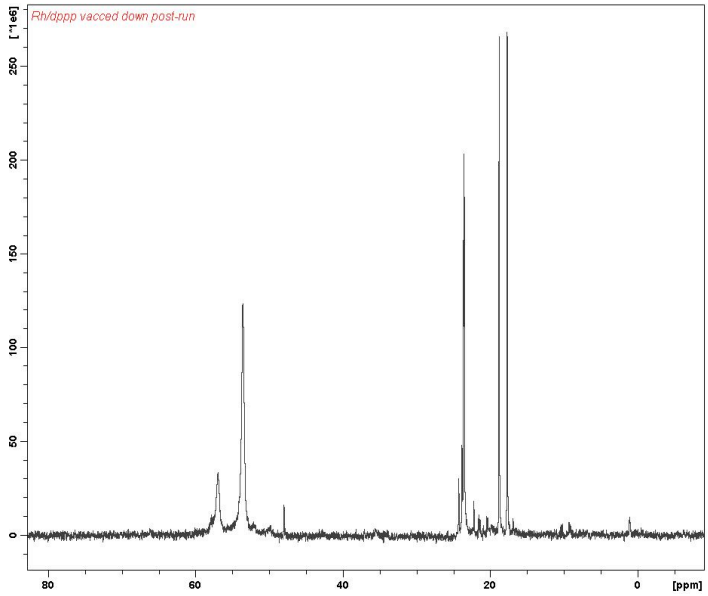

Figure 3.17. $^{31}P\{^{1}H\}$ NMR spectrum ($CDCl_3$) after $[Rh(dppp)CO(Cl)]_2$ **22** was heated at 175 ºC for 1hr under 5 bar CO in a MeOH/MeI mix.

Fig. 3.17 shows that $[Rh(dppp)CO(Cl)]_2$ **23** displayed a low level of stability at the higher temperature of 175 ºC with a substantial amount of P(V) species being detected. The solid that was recovered at the end of the run did however still contain a strong rhodium-phosphine signal in the $^{31}P\{^{1}H\}$ NMR at 18.25 ppm with a $^{1}J_{Rh\text{-}P}$ of 131.7 Hz. This is evidence of the formation of the acetyl complex $[Rh(dppp)COMe(I)_2]$ **12** and is supported by the previous work of Moloy and Wegman.[73, 74]

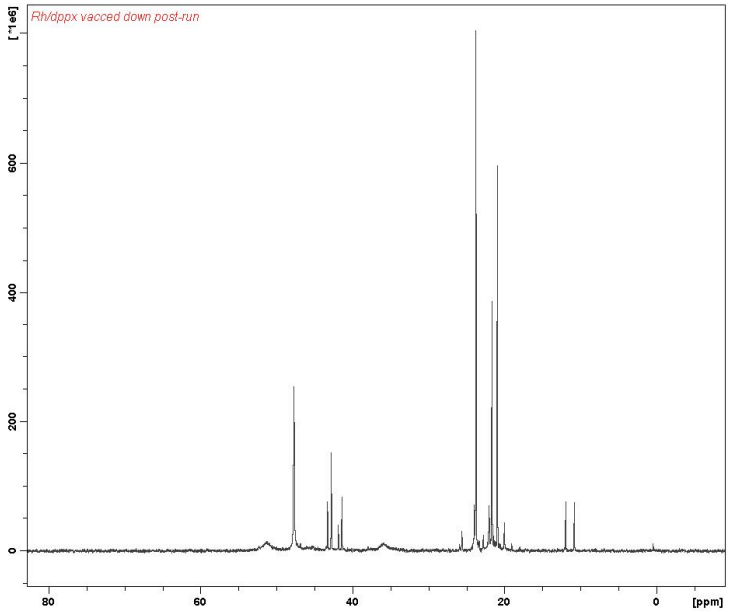

Figure 3.18. $^{31}P\{^{1}H\}$ NMR spectrum ($CDCl_3$) after $[Rh(dppx)CO(Cl)]_2$ **3** was heated at 175 ºC for 1hr under 5 bar CO in a MeOH/MeI mix.

It was decided that $[Rh(dppx)CO(Cl)]_2$ **3** should be tested as it had already been shown in previous studies (Section 2.6) that this complex had an added degree of stability over that of $[Rh(dppb)CO(Cl)]_2$ **1** which undergoes substantial decomposition at 150 ºC. However, Fig. 3.18 shows that at 175 ºC even $[Rh(dppx)CO(Cl)]_2$ **3** rapidly decomposes resulting in several dominant P(V) species and only a very minor rhodium-phosphorus in the $^{31}P\{^{1}H\}$ NMR at 11.4 ppm with a $^{1}J_{Rh-P}$ of 139.6 Hz signal corresponding to the acetyl $[Rh(dppx)COMe(I)_2]$ **10**.

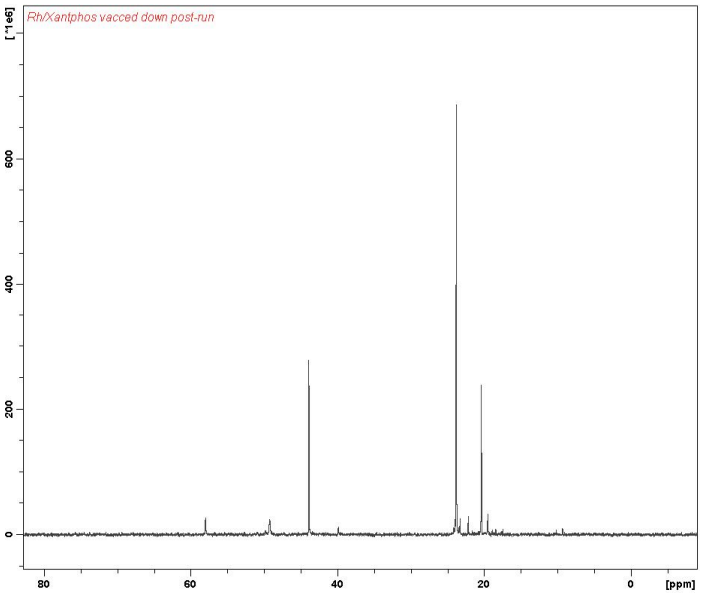

Figure 3.19. $^{31}P\{^{1}H\}$ NMR spectrum ($CDCl_3$) after [Rh(Xantphos)CO(Cl)] **24** was heated at 175 ºC for 1hr under 5 bar CO in a MeOH/MeI mix.

Previous studies into complexes containing Xanthphos ligands have resulted in a high degree of stability with [Rh(Xantphos)CO(Cl)] **24** in particular being one of the most stable complexes under the previous set of conditions (N_2, MeOAc/MeI) even when tested at temperatures above 170 ºC. Therefore it was surprising to find that under catalytic conditions [Rh(Xantphos)CO(Cl)] **24** decomposes completely resulting in only P(V) species (Fig. 3.19). Although these experiments are less quantitative than the MeI assay, they are closer to catalytic conditions and thus highly significant.

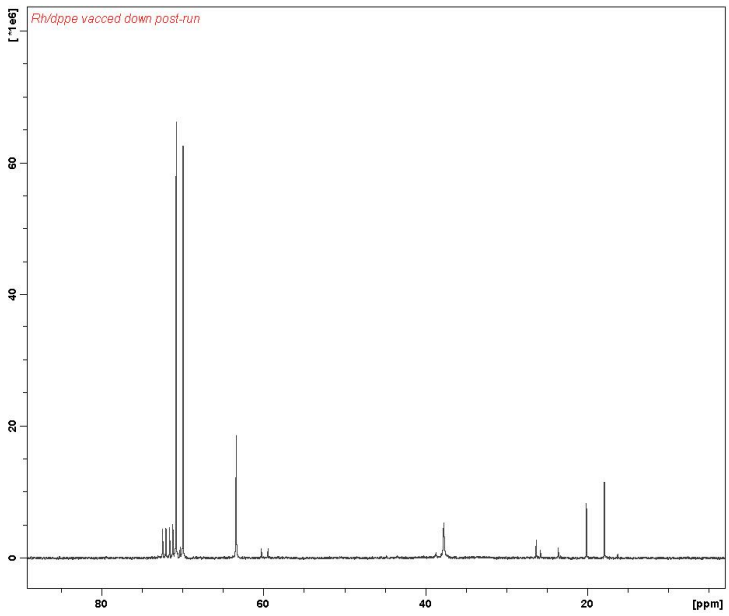

Figure 3.20. $^{31}P\{^{1}H\}$ NMR spectrum ($CDCl_3$) after [Rh(dppe)CO(Cl)] **20** was heated at 175 ºC for 1hr under 5 bar CO in a MeOH/MeI mix.

The most stable catalyst and one that also performed extremely well in the previous tests at 140 ºC was that containing the ligand dppe. To avoid the formation of $[Rh(dppe)_2]Cl$ as this was not a direct comparison with the other complexes within this section, [Rh(dppe)CO(Cl)] **20** was preformed and isolated prior to use in the catalytic reaction. At 175 ºC and under 5 bar CO formation of $[Rh(dppe)COMe(I)_2]$ **22** occurs with a strong signal in the $^{31}P\{^{1}H\}$ NMR at 71.0 ppm with a $^{1}J_{Rh\text{-}P}$ of 139.3 Hz (Fig. 3.20). This supports the high stability of dppe complexes.

Another observation one is drawn to, is the fact that there seems to be a strong correlation between the bite angle of the ligand and instability within this series of complexes. With P-Rh-P bite angles of less than 90 º complexes have a much greater degree of stability over those with bites angles of over 99 º such as dppb and xantphos.

It is however still unclear how ligand flexibilty affects the overall stability of the catalyst in the case of dppx there is strong evidence that the added rigidity of the xylene backbone helps to increase the stability of the complex. Whereas the lack of flexibility in the BINAP ligand may hinder formation the key Rh(III) intermediate leading to a much less stable system. As is often the case, the key to a successful catalyst is the ability to balance the requirements of the system in order to establish the optimum efficiency/design.

3.6 An investigation into the elimination of phosphonium salts from rhodium complexes under methanol carbonylation conditions

There are two plausible mechanisms by which phosphines can be lost from Rh complexes during catalysis:

1. Dissociation of phosphine from the metal centre followed by quaternisation by the methyl iodide to give a phosphonium salt, or
2. Direct elimination of a phosphonium salt from a Rh(III) complex of type $[Rh(L)_n(Me)(I)(CO)]$.

Cole-Hamilton et al. have previously reported highly active rhodium catalysts containing electron rich phosphine PEt_3 ligands.[59, 60] At temperatures exceeding 120 ^oC the catalyst rapidly decomposes forming the phosphonium salt $[Et_3PMe]^+I^-$. Cole-Hamilton et al. proposed that $[Et_3PMe]^+I^-$ may be formed directly from $[Rh(PEt_3)_2(Me)(I)(CO)]$ presenting the possibility that direct elimination of the phosphonium salt could be responsible for phosphine loss in other systems. I have therefore studied this dissociation for a Rh/TRIPHOS system and provide evidence that supports a dissociative mechanism as the means of phosphine loss.

One interesting observation already discussed was the increased stability of the bridging bidentate complex, $[Rh(dppb)(CO)(Cl)]_2$ **1** over that of chelate complex, [Rh(BINAP)(CO)(Cl)] **5** in hot methyl iodide. This observation does not easily fit with a dissociative model for phosphine loss in these complexes, since on reaction of Rh/dppb dimer with methyl iodide, the only species present is the crystallographically

characterised acetyl species, with chelating dppb ligand, [Rh(dppb)(COMe)$(I)_2$] **7**. Interestingly no quaternisation occurs during this transition from a bridging to a chelating co-ordination mode, even though dissociation of one or more phosphorus atoms from the metal centre must occur in order to achieve this rearrangement.

The TRIPHOS complex [Rh(TRIPHOS)$(CO)_2$]Cl **28** however, quantitatively forms a new species (Fig. 3.21) that contains two co-ordinated phosphines and one quaternised phosphine, and therefore is less stable than either of the bidentate systems. However, the quaternised chelate complex was itself highly stable with no sign of other 'free' P(V) products.

Similar results were obtained under methanol carbonylation conditions with the only detectable TRIPHOS complex being **29a**, containing a mixture of quaternised and coordinated phosphines. The structure of the novel TRIPHOS complex was elucidated by spectroscopic and crystallographic methods.

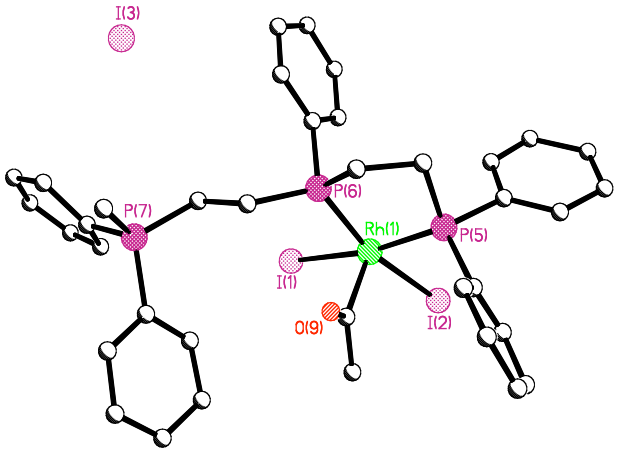

Figure 3.21. X-ray structure analysis of [Rh(PPh$(CH_2)_2$($PPh_2(CH_2)_2$)(PPh_2CH_3)$^+I^-$))$COCH_3(I)_2$] **29a**.

Table 3.2. Comparison of X-ray data for $[Rh(L)COMe(I)_2]$ complexes (bond lengths are in angstroms and bond angles are in degrees).

	Rh-P[(a)]	C-O	I-Rh-I	P-Rh-P
dppm[87]	2.265	1.160(3)	90.55(10)	73.30(2)
dppe[66]	2.276	1.178(9)	91.62(4)	84.74(7)
TRIPHOS	2.261	1.222(18)	91.79(4)	85.46(13)
dppp[73]	2.288	1.182(7)	89.15(2)	90.49(5)

(a) Average bond length of $Rh\text{-}P^1$ and $Rh\text{-}P^2$

Table 3.2 compares the key bond lengths and angles in a range of bidentate rhodium-phosphine acetyl complexes. From the crystallographic data contained within Table 3.2 one can see that the bond lengths and angles are similar to the dppe complex. One may also observe that **29a** has a longer C-O bond length compared to the other complexes in this series.

The $^{31}P\{^1H\}$ NMR spectrum of **29a** contains three different phosphorus environments, two of which are related by a $^3J_{P\text{-}P}$ coupling of 47.2 Hz. These relate to the dissociated, quaternised phosphine P(7) (Fig. 3.16) showing a signal at 26.5 ppm and to phosphine P(6) at 79.5 ppm that shows a coupling to the quaternised phosphine and a large $^1J_{Rh\text{-}P}$ of 143.7 Hz which confirms its coordination to Rh(III) in this novel 'bidentate' system. Phosphorus (5) is assigned to a peak at 70.7 ppm with $^1J_{Rh\text{-}P}$ of 134.1 Hz and a $^2J_{P\text{-}P}$ of 2 Hz.

It was hoped that by examining the mechanism behind the formation of this complex, we may gain a greater understanding of phosphine loss in these systems, which may in turn lead to the future design of more stable catalysts. A number of $^{13}CH_3I$ labelled experiments were carried out in order to assess whether quaternisation of the phosphine occurs via direct elimination from the rhodium centre or via dissociation of the phosphine. The doubly labelled complex $[Rh(PPh(CH_2)_2(PPh(CH_2)_2)((PPh_2{}^{13}CH_3)^+I^-))CO^{13}CH_3(I)_2]$ **29b**, was prepared to aid in the characterisation of complexes **29a-29d**. The ^{13}C NMR ($CDCl_3$) spectrum of **29b** contained a singlet at 45 ppm associated with the $CO^{13}CH_3$ group (a) and a doublet at 9

ppm with a $^{1}J_{P\text{-}C}$ coupling of 54 Hz characteristic of the $^{13}CH_3$ group (b) present on the quaternised phosphine. This one step reaction gave a single phosphorus containing species that was fully characterised (Scheme 3.1).

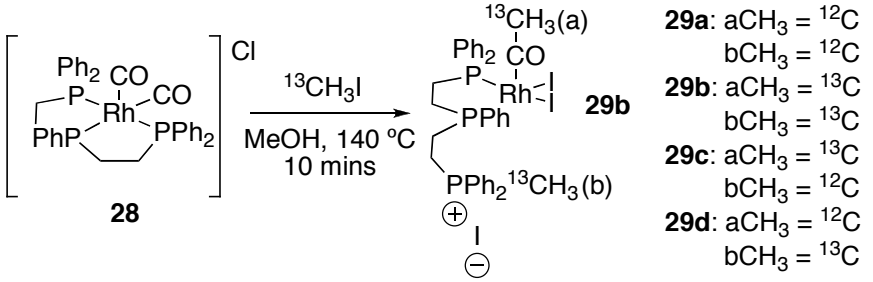

Scheme 3.1. Direct formation of complex **29** and index of $^{13}C/^{12}C$ analogues

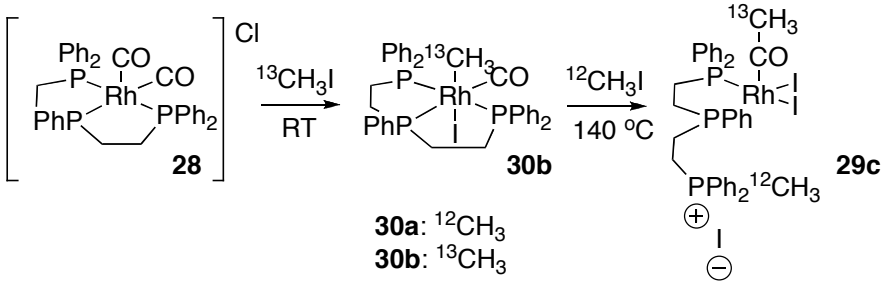

Scheme 3.2. Labelled studies using $^{13}CH_3I$

On reaction with $^{13}CH_3I$ (Scheme 3.2), the precursor [Rh(TRIPHOS)$(CO)_2$]Cl **28**, forms [Rh(TRIPHOS)(^{13}Me)(CO)I] **30b** which may be isolated in good yield with the $^{13}C\{^{1}H\}$ NMR spectrum showing a clearly defined doublet of quartets relating to the labelled methyl group. When complex **30b** was then dissolved in methanol and heated to 140 ^{o}C in the presence of $^{12}CH_3I$, formation of labelled **29c** took place, alongside an unidentified product. The $^{13}C\{^{1}H\}$ NMR ($CDCl_3$) spectra of the resulting solution, including the unidentified compound, contained a single peak at 41 ppm relating to the labelled $^{13}CH_3$ now located as part of the acetyl group and shows no evidence of the $^{13}CH_3$ label in the part of the ^{13}C spectrum characteristic of the $(RPPh_2{}^{13}CH_3)^{+}$ group. The opposite of above was also examined by heating a sample of unlabelled [Rh(TRIPHOS)(^{12}Me)(CO)I] **30a** to 140 ^{o}C in the presence of $^{13}CH_3I$. Once again, this two-step reaction produced a side product but the $^{13}C\{^{1}H\}$ NMR of this mixture clearly shows two doublets at 9.19 ppm and 8.13 ppm with $^{1}J_{P\text{-}C}$ couplings of 54.8 and 56.6 Hz respectively, characteristic of the $^{13}CH_3$ now being present as part of the quaternised

phosphine. These results therefore point towards a dissociative mechanism in the quaternisation of this ligand.

In order to investigate this further, the direct preparation of the rhodium acetyl complex was attempted by reacting the rhodium acetonitrile dimer **9**,[86] with the TRIPHOS ligand (Scheme 3.3).

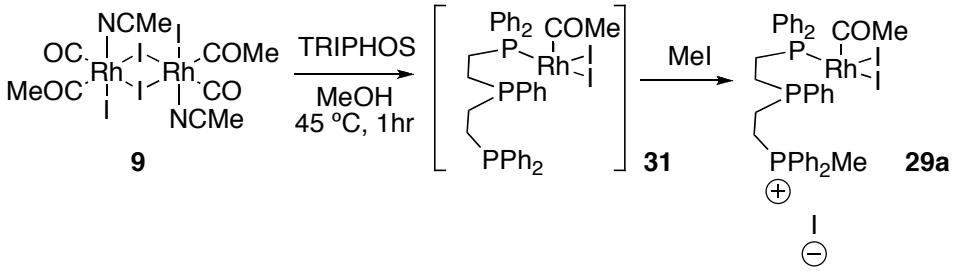

Scheme 3.3. Reaction of $[Rh(CO)(MeCN)(COMe)I_2]_2$ **9** with TRIPHOS and the subsequent quaternisation of the free phosphine with MeI.

Although, it was not possible to isolate a pure complex from the reaction of $[Rh(CO)(MeCN)(COMe)I_2]_2$ **9** with TRIPHOS, the $^{31}P\{^1H\}$ NMR spectrum is consistent with the formation of complexes containing one free arm of the TRIPHOS ligand, since a signal at δ_P = -10.49 ppm is observed (c.f. δ_P = 83.31 ppm and 52.42 ppm for the coordinated phosphines). The spectroscopic data and reactivity observed suggest an acetyl complex of type **31** as the major species. Moreover this product mixture reacts *cleanly* with MeI to give only complex **29a**. This latter experiment suggests that the TRIPHOS ligand does not form a stable tridentate acetyl species thus making dissociation a favourable pathway.

3.6.2 Conclusions

In summary, Rh(I) complexes containing monodentate, bidentate and tridentate phosphine ligands have been prepared and their reactivity studied. From the monodentate studies we have shown that subtle changes in the electronic and steric properties on the whole have very little effect on the stability of rhodium-phosphine complexes under methanol carbonylation conditions. These studies have also shown that coordination mode can have a large impact on the stability of rhodium-phosphine

complexes, with monodentate complexes being inherently unstable whilst complexes containing the bidentate ligands dppe, dppp and dppb react smoothly with MeI at 140 ^{o}C to give their respective Rh(III) acetyl complexes. Other bidentate ligand complexes such as [Rh(BINAP)CO(Cl)] **5** and [Rh(Xantphos)CO(Cl)] **24** however, have been shown to be inherently unstable at higher temperatures. The use of the tridentate ligand TRIPHOS results in the dissociation of one of the phosphines and favours the formation of a bidentate intermediate **29a** containing a quaternised phosphine no longer associated with the metal centre.

A series of $^{13}CH_3I$ labelled studies has provided strong evidence that, for the TRIPHOS system, the loss of the phosphine occurs via a simple dissociative mechanism and not through direct elimination. This does not however, rule out the possibility that for other ligands phosphine loss could occur via direct elimination from the metal centre. However, these studies along with our previous observation on the Rh-BINAP system suggest that the stability of Rh-phosphine complexes to MeI is related to the stability of the Rh-acetyl species. Further studies aimed towards increasing the stability of phosphine modified rhodium carbonylation catalysts are required.

Chapter IV: The reactivity and stability of rhodium(I) aminophosphine carbonyl complexes under methanol carbonylation conditions

4.1 Introduction

The use of amino/imino phosphine ligands is wide ranging, being incorporated into everything from ethylene polymerisation[88-91] to the hydrogenation of ketones, enamines and esters.[92-94] This chapter reports an investigation into the use of aminophosphine ligands as a means to accessing a range of coordination modes in rhodium carbonyl complexes. The potential hemilabile nature of some tridentate aminophosphine ligands could mean that unlike TRIPHOS (Section 3.6) the third donor group may be able to dissociate and re-associate with the metal centre without quaternisation and loss of the tridentate coordination capability.

It has been proposed that a tridentate coordination mode may help to stabilise certain intermediates in the catalytic cycle for the carbonylation of methanol. Recently and subsequent to our studies in this chapter, evidence for this has been described by Best *et al*.[95] They have shown that a methoxy group may be used as a third donating site and help to stabilise Rh(III) acetyl species through the interaction of the lone pair with the metal centre. They reported a ν(CO) shift of ca. 12 cm^{-1} in the infrared spectrum consistent with a greater electron density at the metal centre resulting from electron donation by the methoxy group. This Rh-O interaction was also confirmed by X-ray crystallography with a distorted octahedral geometry around the Rh centre (Scheme 4.1).

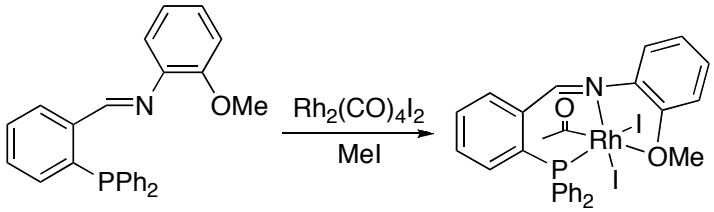

32 **33**

Scheme 4.1. Formation of the Rh(III) acetyl species.

We have investigated the ability of aminophosphine ligands to stabilise complexes during the carbonylation of methanol and in particular how certain donor atoms may be used to adjust the donating properties of the ligand and affect the balance between bidentate and tridentate coordination modes.

4.2 Preparation of aminophosphine ligands

A series of novel aminophosphine ligands were synthesised by the adaptation of a literature procedure (Scheme 4.2).[92] These ligands were prepared by reacting diphenylphosphino benzaldehyde with the respective amine via a condensation reaction with a subsequent reduction of the imine using $NaBH_4$. In some instances an acid catalyst was required to force the reaction to completion. In the case of the diamines **35** and **37** (Fig. 4.1) it was necessary to add the diphenylphosphino benzaldehyde drop wise over the course of several hours to an excess of amine at 0 ^{o}C in order to prevent the formation of the di-imino compound. It was also common to observe two singlets in the $^{31}P\{^{1}H\}$ NMR for the formation of the mono-imine, the first at ca. -13 ppm and the other at ca. -16 ppm. These refer to the E/Z isomers and once reduced to the amine using $NaBH_4$ form a single peak in the $^{31}P\{^{1}H\}$ NMR spectrum.

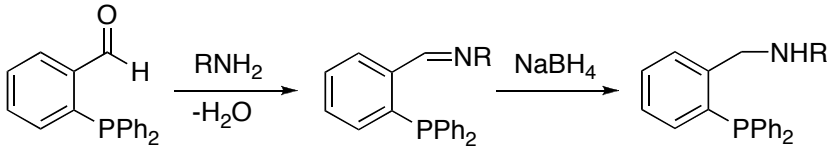

Scheme 4.2. The preparation of aminophosphine ligands.

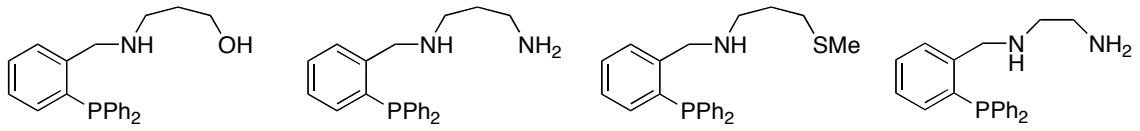

PNO-C_3 34 **PNN-C_3 35** **PNS-C_3 36** **PNN-C_2 37**

Figure 4.1. The aminophosphine ligands prepared for the study.

The aminophosphine ligands **34-37** (Fig. 4.1) were prepared, and with the exception of **37** contain a three-carbon linker between the middle nitrogen and the terminal heteroatom. This was done in order to effectively assess the impact individual donor atoms would have upon coordination mode, away from the complications of varying steric and electronic properties. **37** was prepared as a direct comparison to **35** as it was also proposed that a shorter linker may aid the chelation of the third atom and also promote stability.

4.3 Preparation of the Rh(I) complex: Reaction with $Rh_2(CO)_4Cl_2$

Upon isolation, the aminophosphine ligand was complexed with ½ eq. of $Rh_2(CO)_4Cl_2$ in a solution of methanol. This solution was stirred for 30 mins before a crude sample was taken and analysed using $^{31}P\{^1H\}$ NMR spectroscopy. The $^{31}P\{^1H\}$ NMR spectrum showed that the reaction had gone to completion forming a new rhodium-phosphorus complex. This complex was then isolated and fully characterised allowing for the determination of the coordination mode between the aminophosphine ligand and the rhodium centre (Scheme 4.3).

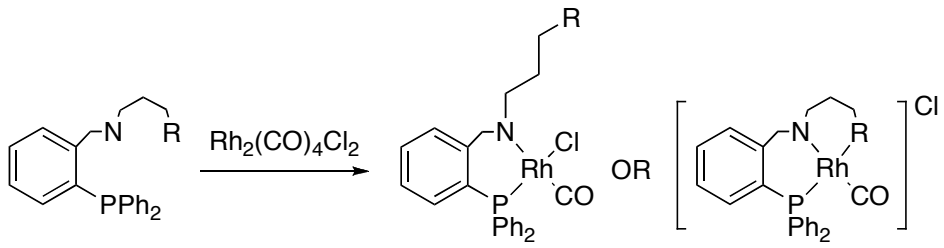

Scheme 4.3. Synthesis of the Rh(I) complex in either a bi or tridentate coordination mode.

In the following section strong evidence is presented for the coordination mode for each of the novel complexes.

4.3.1 Rh/PNO-C_3: Bidentate

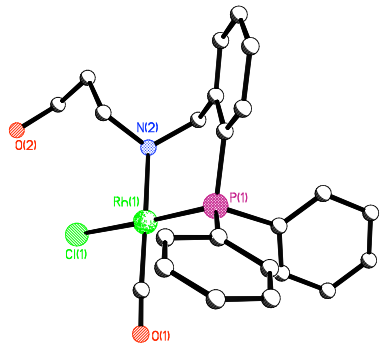

Figure 4.2. X-ray structure analysis of [Rh(PNO)CO(Cl)], **38**.

The $^{31}P\{^{1}H\}$ NMR spectrum of the complex formed from the reaction of **34** with $Rh_2(CO)_4Cl_2$ showed a strong doublet at 47.68 ppm with a $^{1}J_{Rh\text{-}P}$ of 179. 98 Hz. This is in good agreement with data presented by Best *et al.* for the bidentate complex [RhI(CO)(PNAr)] (Ar = 2-$MeOC_6H_4$)[95] whose $^{31}P\{^{1}H\}$ NMR also contains a doublet at 44.5 ppm with a $^{1}J_{Rh\text{-}P}$ coupling of 171 Hz.

The $^{13}C\{^{1}H\}$ NMR spectrum confirms the presence of a carbonyl with a doublet of doublets at δ 187.9 ppm with a $^{1}J_{Rh\text{-}C}$ of 70.21 Hz and a $^{1}J_{P\text{-}C}$ of 18.80 Hz. This is supported by a carbonyl stretch within the infrared spectrum at 1981 cm^{-1}. Although this is strong evidence for the formation of a single carbonyl species with a Rh-P coordination, the true nature of the coordination mode could not be fully resolved without further evidence.

The alkyl region of the $^{13}C\{^{1}H\}$ NMR spectrum shows an upfield shift of 3 ppm in all four *C*H_2 signals with no rearrangement occurring. If coordination of the hydroxyl group had occurred a significant downfield shift in the signal of the CH_2 closest to the OH would be expected due to the deshielding of the oxygen atom by the metal centre. The fact that this shift is seemingly absent suggests that the Rh(I) complex is bidentate. Further evidence of a bidentate coordination mode can be seen from the $^{1}H\{^{31}P\}$ NMR spectrum, which contains a free -OH signal. Finally, the structure could also be confirmed by growth of crystals in d_4-MeOH, from which a bidentate coordination mode could be determined using X-ray crystallography (Fig. 4.2).

4.3.2 Rh/PNN-C_3: Tridentate

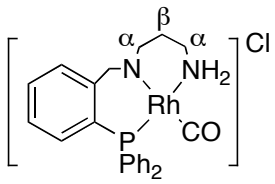

Figure 4.3. The rhodium/aminophosphine complex [Rh(PNN-C_3)CO]Cl, **39**.

The $^{31}P\{^{1}H\}$ NMR spectrum of complex **39** shows a doublet at 40.85 ppm with a $^{1}J_{Rh\text{-}P}$ of 151.47 Hz. This coupling is in stark contrast with the $^{1}J_{Rh\text{-}P}$ coupling of 180 Hz of the bidentate PNO complex **38** and with that of other bidentate complexes, with P *trans* to Cl, found within the literature.[95] If this PNN complex was of a bidentate nature then a similar coupling would be expected, as the labile amino group would have little influence upon the metal centre. The evidence from the $^{31}P\{^{1}H\}$ NMR spectrum therefore seemingly points towards a tridentate coordination mode.

The $^{13}C\{^{1}H\}$ NMR spectrum of complex **39** contains a carbonyl signal at δ 188.54 (Rh*C*O, dd, $^{1}J_{Rh\text{-}C}$ 71.85 Hz, $^{1}J_{P\text{-}C}$ 20.61 Hz) with the infrared spectrum also showing a carbonyl stretch at 1986 cm^{-1}. One can also observe within the $^{13}C\{^{1}H\}$ NMR spectrum a downfield shift of 3-5 ppm in three of the four *C*H_2 signals, the β carbon (Fig. 3) however shows a 3.46 ppm shift upfield. This pattern of upfield and downfield shifts, caused by a possible anisotropic effect within the α and β carbons, is consistent with a deshielding of the amine and is thus evidence of a tridentate coordination with rhodium. This is in contrast to the shifts observed within the $^{13}C\{^{1}H\}$ NMR spectrum of the bidentate complexes previously discussed.

Evidence of a tridentate coordination mode is also apparent within the $^{1}H\{^{31}P\}$ NMR spectrum. The $^{1}H\{^{31}P\}$ NMR spectrum of the free ligand contains a singlet at 3.99 ppm assigned to the N*H*$_2$ group, after complexation with the rhodium precursor [$Rh_2(CO)_4Cl_2$], this singlet is replaced by a multiplet at 3.73 ppm showing that tridentate coordination has occurred.

4.3.3 Rh/PNS-C_3: Tridentate

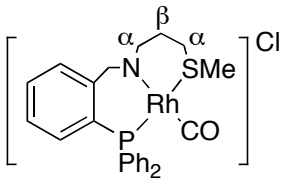

Figure 4.4. The rhodium/aminophosphine complex [Rh(PNS-C_3)CO]Cl, **40**.

The $^{31}P\{^1H\}$ NMR spectrum of complex **40** shows a strong, clean doublet at 33.45 ppm with a $^1J_{Rh\text{-}P}$ of 153.37 Hz. This is in direct contrast to the bidentate complexes previously described and therefore suggests that similar to complex **39** this compound is also tridentate in nature. (Fig. 4.4)

Other evidence of a tridentate coordination mode can be seen in the $^{13}C\{^1H\}$ NMR spectrum which shows a downfield shift of between 4.43 and 3.67 in three of the four *C*H_2 carbons, the exception to this shift is that in the β position which shows an upfield shift of 2 ppm. As explained for the previous PNN-C_3 complex, this anisotropic effect is consistent with a deshielding of the sulphur atom through coordination with rhodium and in contrast to the behaviour of the carbon atoms in the bidentate PNO-C_3 complex, **38**. The $^{13}C\{^1H\}$ NMR also shows a large downfield shift for the S*C*H_3 supporting the proposed tridentate mode.

The $^1H\{^{31}P\}$ NMR spectrum of the ligand contains a singlet at 2.04 ppm for SMe, on coordination with rhodium this singlet is replaced by a strong doublet at 2.79 ppm with a coupling of $^3J_{Rh\text{-}H}$ = 1.79 Hz. This is not only consistent with a tridentate coordination mode but also with the Rh-SC*H*$_3$ data found in the literature and related unpublished work.[96]

4.3.4 Rh/PNN-C_2: Tridentate

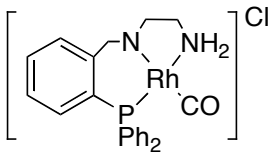

Figure 4.5. The rhodium/aminophosphine complex [Rh(PNN-C_2)CO]Cl, **41**.

Once again the $^{31}P\{^{1}H\}$ NMR spectrum of complex **41** shows a doublet at 42.09 ppm with a $^{1}J_{Rh-P}$ of 152.27 Hz. This is characteristic of a tridentate coordination as described in the previous complexes and as opposed to the bidentate PNO complex **38**.

Downfield shifts of 2.1-4.4 ppm in the CH_2 region of the $^{13}C\{^{1}H\}$ NMR spectrum compare to that of the free ligand also shows that unlike the bidentate complexes discussed in Section 4.3.1. This downfield shift is a direct result of the deshielding by the rhodium centre and therefore provides us with strong evidence that a Rh(I) tridentate system is present (Fig. 4.5).

Further evidence for a tridentate coordination mode can be seen when comparing the $^{1}H\{^{31}P\}$ NMR spectrum of the free ligand with that of the complex. The $^{1}H\{^{31}P\}$ NMR spectrum of the free ligand contains a singlet at 4.00 ppm for the NH_2, however when complexed the singlet is replaced with a complicated multiplet at 3.89 ppm.

4.4 Formation of rhodium-aminophosphine trichloride complexes

On standing in chlorinated solvents, complexes **38** and **39** form rhodium trichloride complexes. The complexes were not prepared in significant quantities, and were therefore primarily characterised by X-ray crystallography.

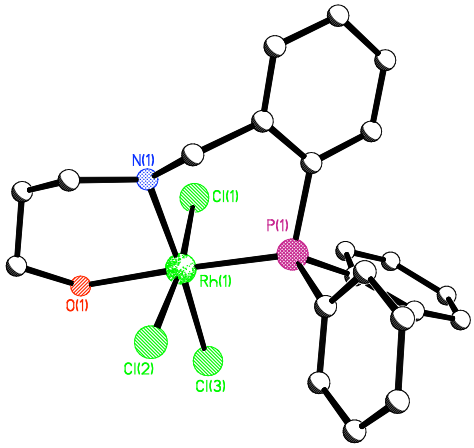

Figure 4.6. X-ray structure analysis of $[Rh(PNO)Cl_3]$ **42**.

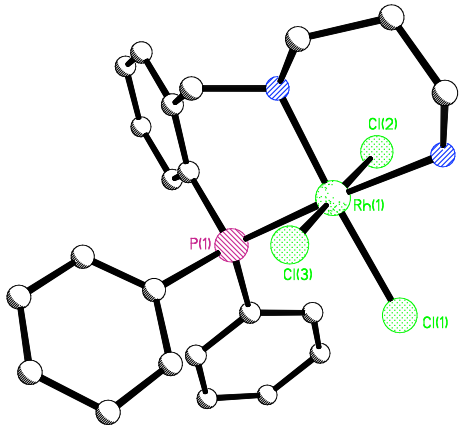

Figure 4.6. X-ray structure analysis of [Rh(PNN-C_3)Cl_3] **43**.

In the case of [Rh(PNO)Cl_3] **42**, it was not possible to isolate or detect the PNO trichloride complex **42** in sufficient quantity to assign a signal in the $^{31}P\{^1H\}$ NMR spectrum, possibly due to its poor solubility, but a LSIMS on the X-ray crystals was obtained with good agreement with the proposed formulation. In particular, FAB MS shows fragments assigned to 522.0 $[M\text{-}Cl]^+$ and 487.0 $[M\text{-}2Cl]^+$.

Similarly crystals of **43** were formed and were also analysed by X-ray crystallography. Evidence for the formation of [Rh(PNN-C_3)Cl_3] **43** could also be seen by removing the solvent from the glass vessel in which the crystals had formed and dissolving the remaining solid in THF. The $^{31}P\{^1H\}$ NMR spectrum contained two doublets, the first was at 40.68 ppm with a $^1J_{Rh\text{-}P}$ of 153.0 Hz assigned to the carbonyl complex **39**, the second doublet relating to the formation of complex **43** was at 22.73 ppm with a $^1J_{Rh\text{-}P}$ coupling of 110.9 Hz. LSIMS (FAB) of the mixture also supports the proposed formation of trichloride species with a signal at 521.1 $[M\text{-}Cl]^+$.

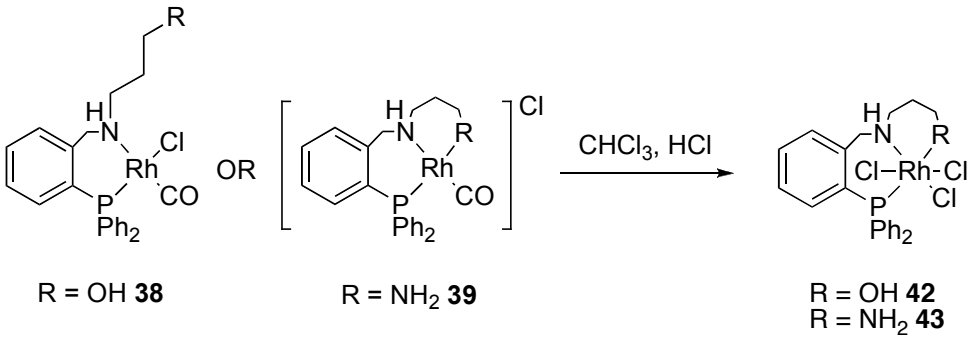

Scheme 4.4. Attempted preparation of rhodium trichloride species from either bi or tridentate carbonyl complexes.

Having shown the affinity rhodium-aminophosphine complexes have for the formation of trichloride species, we attempted to synthesise complex **43** directly by heating the carbonyl complex **39** in chloroform (Scheme 4.4) with the addition of HCl (500 eq.). However, the $^{31}P\{^{1}H\}$ NMR spectrum of the resulting solution showed that once again a mixture of complexes had formed with signals assigned to the carbonyl complex **39** and the trichloride complex **43**.

Table 4.1. Comparison of X-ray data for $[Rh(L)Cl_3]$ aminophosphine complexes **42** and **43**

Key bond lengths	PNO	PNN
Rh-N/O	2.177(3)	2.099(14)
Rh(1)-N(8)	2.101(3)	2.130(13)
Rh(1)-P(1)	2.249(13)	2.279(4)
Rh(1)-Cl(1)	2.356(17)	2.364(4)
Rh(1)-Cl(2)	2.312(11)	2.314(4)
Rh(1)-Cl(3)	2.343(10)	2.359(4)

Table 4.1 comprises the key bond lengths for the trichloride complexes **42** and **43**, from these one can see a significantly shorter bond length between the rhodium and the hetero-atom for the PNN complex indicating that the N atom is a much stronger donor in comparison to O.

4.5 Reaction under methanol carbonylation conditions

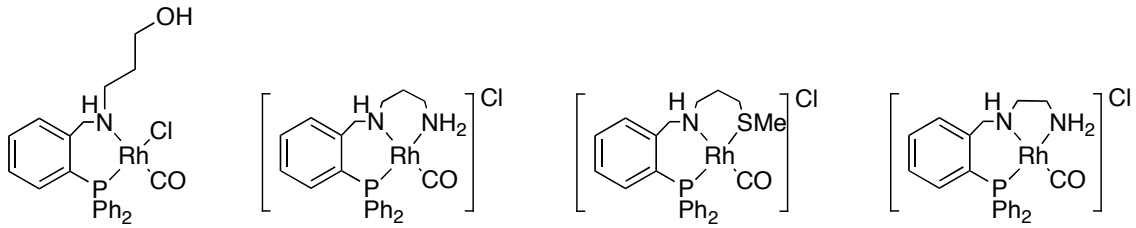

38 **39** **40** **41**

Figure 4.6. Summary of the rhodium phosphine complexes prepared.

Once the complexes **38-41** (Fig. 4.6) had been isolated and fully characterised their stability was tested under the methanol carbonylation conditions of 140 ^{o}C and 26 bar CO for a period of 30 mins. Most of the complexes were highly soluble in a mixture

of methanol and methyl iodide, which would lend itself well to the industrial requirements of the process. Pre-run and post-run samples of the catalytic mixtures were taken, and a summary of the resulting $^{31}P\{^{1}H\}$ NMR spectra now follows.

All of the aminophosphine rhodium complexes, whether they displayed a bi or tridentate coordination with respect to the Rh(I) carbonyl complex, showed a low degree of stability at 140 ºC under simulated catalytic conditions. All except the PNS complex showed complete decomposition with only P(V) species remaining in the $^{31}P\{^{1}H\}$ NMR spectra after 30 mins. Although, the catalytic run using complex **40** also resulted in large amount of complex decomposition, it was the only complex in this series whose post run $^{31}P\{^{1}H\}$ NMR spectrum contained a doublet at 30.52 ppm with a $^{1}J_{Rh-P}$ coupling of 119.6 Hz showing at least partial stability. Although the rhodium-PNS system is the most stable in this series, it's stability falls far short of other bidentate ligand complexes discussed in previous chapters.

Several attempts were made to isolate the PNS complexes that remained stable at the end of the catalytic run. This included heating at a lower temperature of 120 ºC in an attempt to isolate the complex before decomposition had occurred. This however resulted in a mixture of several complexes, although very little decomposition was observed. A lack of gas uptake was also noted even after heating for 1 hr at 120 ºC, leading us to believe that as well as being unstable at higher temperatures, complexes such as those described in this chapter are at best very inactive, at worst not active at all for the carbonylation of methanol. This may be due to the formation of a co-ordinately saturated Rh(III) acetyl species that can no longer undergo addition of CO required for the reductive elimination of acetyl iodide. Evidence of co-ordinately saturated rhodium complexes containing tridentate aminophosphine ligands is supported by the formation of complex **33** described in section 4.1.

We finally found it was possible to separate and isolate two different rhodium-PNS complexes using a chromatatron from a reaction mixture formed by heating complex **40** at 140 ºC for 10 mins under N_2 (Fig. 4.7). A chromatatron employs a silica disc that is rotated at high speed, on which compounds may be separated into circular

bands that are collected in Schlenk glassware. The entire process was done under an atmosphere of N_2 and the following complexes were tentatively identified.

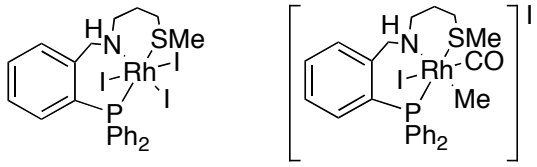

44 **45**

Figure 4.7. The structures of the two isolated rhodium-aminophosphine complexes.

The $^{31}P\{^{1}H\}$ NMR spectrum of complex **44** showed a doublet at 21.52 ppm with a $^{1}J_{Rh-P}$ coupling of 109.9 Hz similar to that of the PNN trichloride complex **43**. Crystals of complex **44** were grown by slow evaporation of the eluent, the structure of which was then shown to be the triiodide complex (Fig. 4.8). This shows once again the tendency of these compounds to form trihalide complexes.

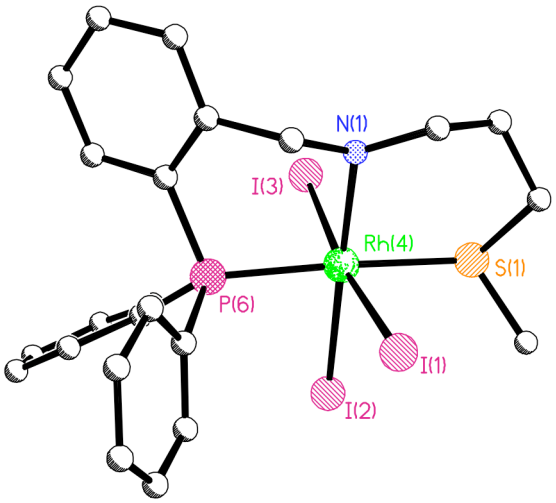

Figure 4.8. X-ray structure analysis of [Rh(PNS)I_3] **44**

The $^{31}P\{^{1}H\}$ NMR of complex **45** showed a doublet at 29.80 ppm with a $^{1}J_{Rh-P}$ coupling of 119 Hz. Unlike **44** the infrared spectrum of complex **45** contained a C-O stretch at 2053 cm^{-1}, which is characteristic of the intermediate formed from the oxidative addition of methyl iodide. As a comparison the tridentate complex [Rh(TRIPHOS)CO(Me)I]I has a carbonyl stretch at 2075 cm^{-1} and the bidentate complex [Rh(dppe)CO(Me)I_2] has a carbonyl stretch of 2065 cm^{-1}.[74] As well as infrared

spectroscopy, this proposed formulation is also supported by HRMS (Found 651.9815 [M^+]; $C_{25}H_{29}NOPSRhI$ requires 651.9807 [M^+]).

Unfortunately, it was only possible to isolate complexes **44** and **45** on a minute scale. Although some evidence was obtained towards the identification of the proposed species it was not possible to remove trace (non Rh-phosphine) impurities in order to carry out a more thorough analysis.

4.6 Conclusions

In conclusion, a series of rhodium aminophosphine complexes have been prepared and their stability and reactivity towards methyl iodide under CO and N_2 atmospheres investigated. Complexes **38-41** have been shown to be highly unstable at 140 ºC, with the PNS system being the only one out of the series to show any degree of stability. It was also possible to tentatively assign the structures of two Rh-PNS intermediates (**44** and **45**).

One can also observe a trend in donor atom properties, the weakest donor out of the C_3 series was the PNO ligand as this was the only one not to form a Rh(I) tridentate carbonyl complex. The next strongest donor was the PNN ligand, although a tridentate coordination was observed within the Rh(I) carbonyl complex this system suffered from a much greater degree of instability compared to that of PNS, making the sulphur containing ligand the strongest donating heteroatom in the series.

Although the complexes discussed in this chapter are seemingly redundant for use in the rhodium-catalysed carbonylation of methanol, these systems may be potentially useful within other reaction such as hydrogenation or the polymerisation of ethylene, however such reactions are outside of the scope of this thesis.

Chapter V: The design of highly soluble catalysts for the rhodium catalysed carbonylation of methanol

5.1 Introduction

The design of highly soluble phosphine-modified catalysts for the carbonylation of methanol may result in significant developments for the future of the process. Research carried out in collaboration with BP has highlighted several complexes as potential Rh-phosphine catalysts for the carbonylation of methanol. However, one of the major problems faced in the further development of these systems is the poor solubility of the catalyst at lower temperatures. A greater level of solubility at lower operating temperatures is required during the 'stripping' process under flash tank conditions (described in Chapter 1.5). Deposition of the catalyst during this procedure results in a poor catalyst recovery and several engineering problems as the tank and piping are slowly coated with precipitated complex, therefore a soluble catalyst is crucial to the running of this process.

Rhone-Poulenc Industries were among the first to develop water-soluble catalysts in the late 70's and early 80's for several large-scale processes including the biphasic hydroformylation of propene and other olefins.[97] Interest in water-soluble catalysts was driven by a desire to achieve the high activities and selectivities observed in the analogous homogeneous reactions but with an improved method of catalyst recovery. There are a variety of other methods for catalyst separation being developed, but water-soluble catalysts for the reaction of partially water soluble, but preferentially organic soluble substrates, is one of the most attractive.[98, 99]

Water solubility of organometallic complexes is generally achieved via the use of ligands containing highly polar groups such as amino, carboxylic acid, hydroxide and sulfonate. Unfortunately, those containing hydroxyl groups often show little water

solubility while ligands containing carboxylic or amino groups are only soluble in basic or acidic media respectively. Those containing sulfonated groups, however, have been extensively studied and were among the first of the water-soluble catalysts to be commercialised by Rhone-Poulenc.

Sulfonated triphenylphosphine (TPPTS) was reported by Kuntz in 1976, with further work being conducted on rhodium and ruthenium complexes containing sulfonated ligands by Wilkinson and co-workers.[100] Direct sulfonation of the phenyl groups using H_2SO_4/SO_3 results in the functional group being placed in the meta-position. Direct sulfonation using H_2SO_4/SO_3 may also be disadvantageous when using ligands containing sensitive functional groups such as DIOP and in some cases catalysis may be retarded by sulfonate coordination. A novel approach to these problems was the preparation of cationic water-soluble phosphines such as amphos (Figure 5.1) reported by Baird and co-workers.[101, 102]

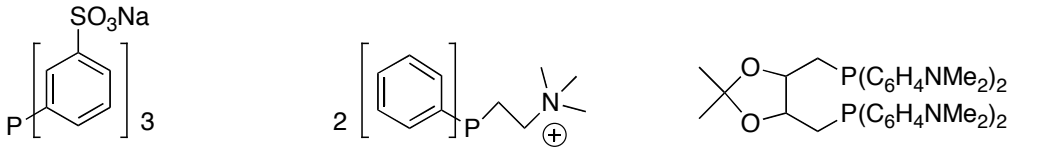

TPPTS
Kuntz/Rhone-Poulenc 1976
Cornils/Ruhrchemie 1987

amphos
Baird 1981

dimethylamino derivative of DIOP
Toth 1990

Figure 5.1. A selection of water-soluble ligands for use in homogeneous catalysis

The development of amphos enabled the preparation of water-soluble phosphines independent of solution pH and without inhibition through coordination with the functional group. The amphos-rhodium system provided olefin hydrogenation catalysis with comparable activities to that of the triphenylphosphine systems. The possibility for use in biphasic catalysis and attachment to anionic exchange resins also proved extremely interesting and has been an area of interest for many other groups over the last twenty years. However, one of the major disadvantages of amphos was the three-step approach to the quaternisation of the amino group. The first of these steps involved the protection of the phosphine using H_2O_2 to form the corresponding phosphine oxide, the amino group was then quaternised using methyl iodide with the final step being the reduction back to the phosphine using $HSiCl_3$. It was not until 1986

that Nagel and Kinzel reported a single step procedure for the quaternisation of (3R, 4R)-3, 4-bis(diphenylphosphino)-1-methylpyrrolidine using $(CH_3)_3OBF_4$. The key to the method was the protection of the phosphorus through coordination with rhodium. This was developed further by Toth et al. to include the selective quaternisation of aryl amino groups in tertiary or ditertiary phosphines.[103-106] Toth et al. prepared a series of dimethyl amino derivatives of asymmetric ligands such as DIOP (Fig. 5.1) and (BDPP) Skewphos. Through coordination to rhodium, as set out by Nagal and Kinsel, and use of $(CH_3)_3OBF_4$ it was possible to partially quaternise and in some cases fully quaternise all four amino sites. However, complete quaternisation of all four aryl amino groups of these functionalised ligands was not a facile task and although the extent of quaternisation had little effect on the enantioselectives achieved, the solubility requirements for a truly biphasic system and the need for exact characterisation of the complexes required complete quaternisation. Therefore the addition of HBF_4 to an acetone or methanol solution containing the aforementioned complexes was employed in order to achieve the complete protonation of all four amino groups. Toth also found that the protonation was completely reversible by the addition of weak bases such as Et_3N leading to a highly versatile catalyst system.

The following section describes an investigation using the above approach to give an improved level of solubility in the $MeOH/H_2O/AcOH$ media encountered in methanol carbonylation.

5.2 Results and discussion

5.2.1 Ligand synthesis

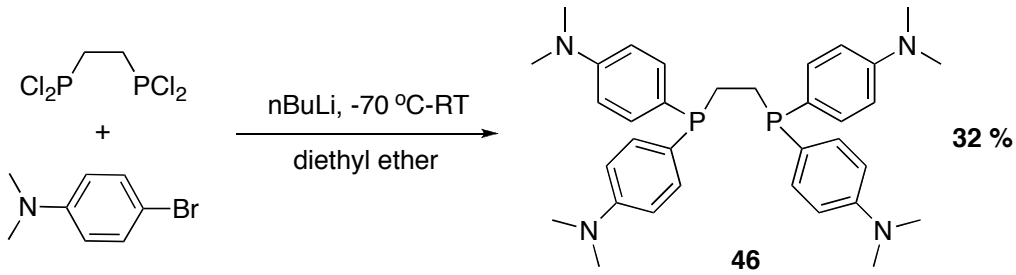

Scheme 5.1. The preparation a dimethyl amino substituted dppe analogue.

It was possible to synthesise a dimethyl amino derivative of dppe in a moderate yield of 32 % (lit. 28 %).[107] This involved the initial lithiation of 4-bromo-N,N-dimethylaniline and subsequently a reaction with the corresponding chloro phosphine. The desired product could be isolated in high purity as an air stable white solid and could be stored for a period of 18 months without oxidation.

5.2.2 Complexing with rhodium

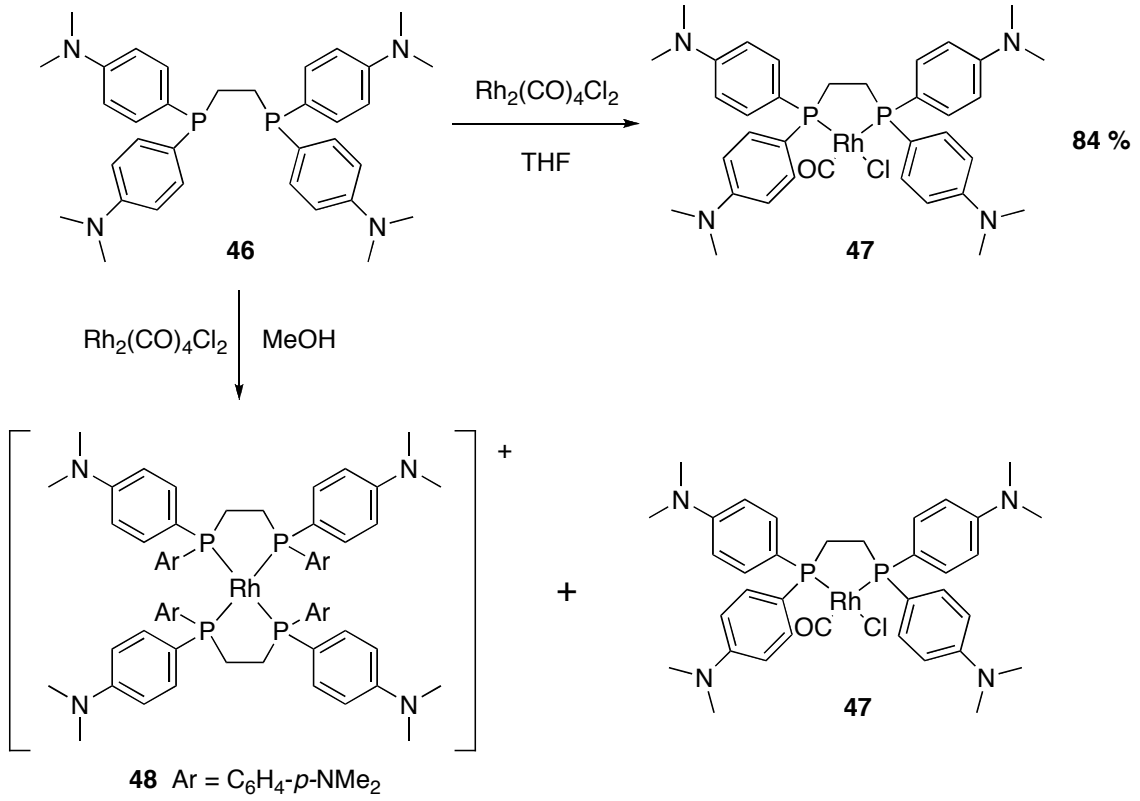

Scheme 5.2. The preparation of the mono-chelated rhodium carbonyl complex.

Due to the electron donating properties of the dimethyl amino substituents on the aryl rings the tendency to form bis-chelated species, analogous to that of $[Rh(dppe)_2]Cl$, has been significantly increased. Thus in the reaction of ligand **46** with $Rh_2(coe)_4Cl_2$, only a bis-chelated species was observed. The bis-chelated species $[Rh(dppe\text{-}(NMe_2)_4)_2]^+$ **48**, gives a sharp doublet in the $^{31}P\{^1H\}$ NMR spectrum at 56.0 ppm with a $J_{Rh\text{-}P}$ of 132.9 Hz with the FAB MS of 1243.8 $[M]^+$ agreeing with the proposed formulation. This is in direct comparison with the unsubstituted analogue $[Rh(dppe)_2]Cl$ for which the $^{31}P\{^1H\}$ NMR spectrum shows a doublet at 58.74 ppm with a $J_{Rh\text{-}P}$ of 132.9 Hz.

When ligand **46** was reacted with $Rh_2(CO)_4Cl_2$ in methanol a mixture of complexes resulted. A 4:1 ratio of mono-chelated rhodium carbonyl chloride complex to bis-chelated species was observed, showing that the formation of the bis-chelate species is also accentuated in protic solvents. To enable the isolation of solely the

desired mono-chelated carbonyl species [Rh(dppe-$(NMe_2)_4$)CO(Cl)], the ligand was reacted with $Rh_2(CO)_4Cl_2$ in a minimal amount of THF (scheme 5.2). After 15 minutes stirring under an inert atmosphere, a bright yellow precipitate had formed which could be removed by filtration and washed with a small amount of ice cold THF to remove any remaining bis-chelated complexes. Slow evaporation of this solution provided crystals suitable for X-ray diffraction from which the structure of complex **47** was fully determined (Fig. 5.2, Table 5.1).

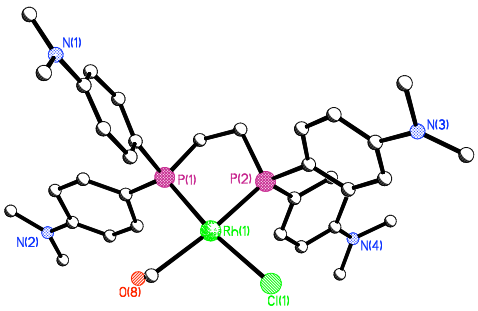

Figure 5.2. X-ray structure analysis of [Rh(dppe-$(NMe_2)_4$)CO(Cl)], **47**.

Table 5.1. X-ray data for [Rh(dppe-$(NMe_2)_4$)CO(Cl)]

	Rh-P[1]	Rh-P[2]	Rh-C	C-O	CO-Rh-Cl	P-Rh-P
47	2.297(3)	2.317(3)	1.866(4)	1.114(5)	101.0(13)	84.74(15)

5.2.3 Comparison of spectroscopic data for Rh(I) species

There are few examples of the X-ray structural analysis of monomeric rhodium carbonyl chloride diphosphine complexes available in the literature and so we are unable to make a direct comparison between the unsubstituted dppe analogue in this instance. However, the infrared spectrum shows a C-O stretch for the carbonyl group at 1987 cm^{-1} compared to a stretch of 2006 cm^{-1} for [Rh(dppe)CO(Cl)] **20**. This is indicative of the greater electron donating property of the substituted diphosphine ligand over that of dppe.

5.2.4 Reaction with methyl iodide

It was anticipated that [Rh(dppe-$(NMe_2)_4$)CO(Cl)] **47**, may be reacted with a large excess of methyl iodide in an attempt to quaternise the dimethyl amino substituents on the ligand while the phosphorus atoms were protected through their coordination with rhodium. **47** was dissolved in a solution of methyl acetate and methyl iodide and heated to 140 ^{o}C for 10 mins (Scheme 5.2). The complex showed a high degree of stability similar to that of the unsubstituted analogue, dppe (Chapter 3.3).

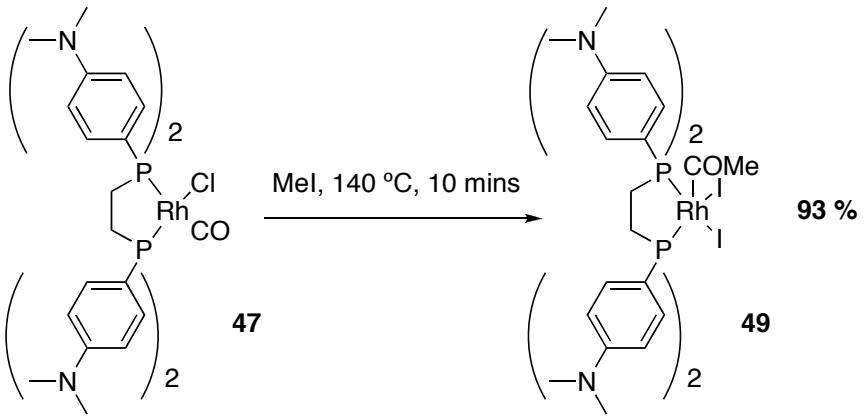

Scheme 5.3. Attempted quaternisation of **47** using methyl iodide and the subsequent formation of [Rh (dppe-$(NMe_2)_4$)COMe$(I)_2$], **49**.

The reaction with MeI (300 eq.) cleanly formed an acetyl species, crystals of which were grown by slowly blowing nitrogen over the solution (Scheme 5.3). Through the analysis of NMR spectroscopy and X-ray crystallography it was possible to prove that no quaternisation had occurred. It is concluded that the quaternisation of aryl amino groups was not easily achievable through the use of methyl iodide due to the poor nucleophilicity of the amino substituents. It was therefore concluded that the ionic, quaternised phosphines would not form directly under catalytic conditions.

5.2.3 Comparison of crystallographic data for C_2-Rh(III) acetyl species

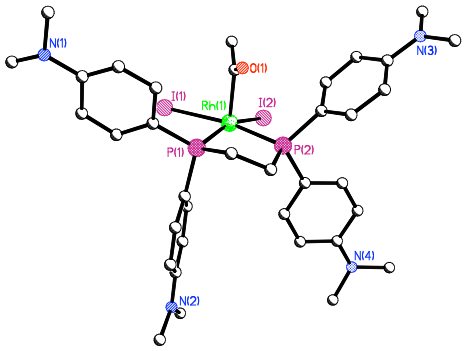

Figure 5.3. X-ray structure analysis of [Rh(dppe-$(NMe_2)_4$)COMe$(I)_2$], **49**.

Table 5.2. Comparison of X-ray data for [Rh(L)COMe$(I)_2$] complexes containing dppe and dppe-NMe_2 ligands

	Rh-P[1]	Rh-P[2]	C-O	I-Rh-I	P-Rh-P
dppe-NMe_2	2.280(3)	2.309(3)	1.206(8)	92.13(3)	85.75(10)
dppe[66]	2.267(2)	2.284(2)	1.178(9)	91.62(4)	84.74(7)

The structural data in Table 5.1 clearly show that, as expected, the complex containing the 4-dimethylaminophenyl substituted ligand shares many similarities in key bond lengths and angles as its unsubstituted dppe analogue. However, differences include longer Rh-P bond lengths and larger I-Rh-I and P-Rh-P bond angles.

5.2.4 Reaction with HBF_4

In order to prepare a catalyst with an improved solubility in protic media[108, 109] it was therefore necessary to employ the conditions set out by Toth et al. and attempt to quaternise the dimethyl amino groups via protonation with HBF_4.

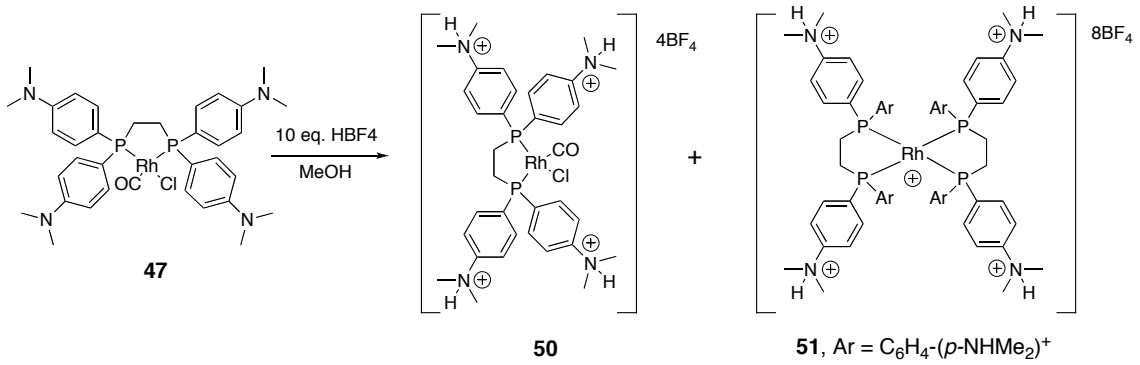

Scheme 5.4. Reaction of **47** with HBF_4 and the formation of protonated species **50** and **51**.

Reaction of **47** with HBF_4 gave a mixture of products with the $^{31}P\{^1H\}$ NMR spectrum showing two major sets of signals (Scheme 5.4). The first signals were a broadened set of indistinguishable multiplets at 69 ppm and 48 ppm, and have been tentatively assigned as the carbonyl complex at variable stages of protonation due to the similarities in shift patterns. The second set was a sharp doublet at 57.8 ppm with a $^1J_{P\text{-}P}$ coupling of 132 Hz assigned to the bis-chelated species and supports the view that bis-chelated species such as these have a higher tendency to form in protic solutions. Although only tentatively assigned, a few crystals were grown from this complicated mixture of differing species at variable states of protonation, and allowed the structural determination of the fully protonated bis-chelated species **51** (Fig. 5.4). This structure was somewhat disordered so no comments can be made regarding bond lengths and angles. However, the structure is consistent with a protonated ligand with counter ions also being observed.

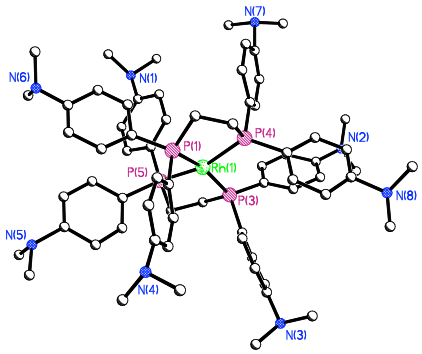

Figure 5.4. X-ray structure analysis of $[Rh(dppe\text{-}(HNMe_2)_4)_2]8(BF_4)Cl$, **51**.

5.2.5 The addition of HBF_4 under an atmosphere of CO

Although several species existed in the above solution these may be added to methyl iodide, HBF_4/H_2O and methanol and reacted at high temperature under an atmosphere of CO to produce a single detectable species tentatively assigned as $[Rh(dppe\text{-}(NHMe_2)_4)C(O)Me(I)_2]4BF_4$, **52** (Scheme 5.5). This product is also cleanly formed if **47** is treated with HBF_4, MeI and MeOH under CO. The $^{31}P\{^1H\}$ NMR spectrum showed a doublet at 71.4 ppm with a $^1J_{P\text{-}P}$ coupling of 138.9 Hz and the IR spectrum gave a strong ν(CO) of 1701 cm^{-1} characteristic of an acetyl species. In comparison the unprotonated acetyl gave a doublet at 69.0 ppm with a $^1J_{P\text{-}P}$ coupling of 139.6 Hz and $[Rh(dppe)COMe(I)_2]$ gives a doublet at 71.1 ppm with a $^1J_{P\text{-}P}$ coupling of 138.1 Hz.

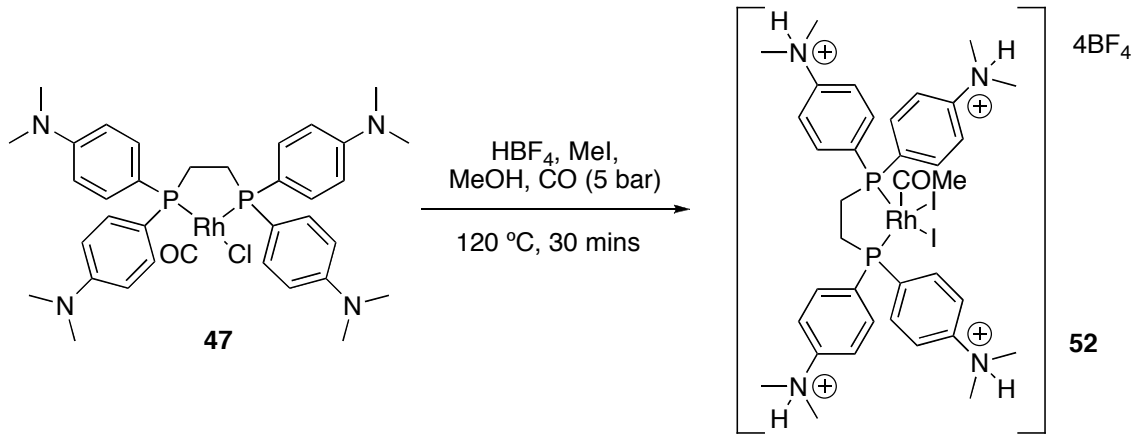

Scheme 5.5. Reaction of $[Rh(dppe\text{-}(NMe_2)_4)CO(Cl)]$ under catalytic conditions with the addition of HBF_4 gives a protonated acetyl species proposed to be **52**.

Due to the ionic nature of the complex the solubility properties had been dramatically changed, these cationic species now showed virtually no solubility in organic solvents in stark contrast to the unprotonated analogues. Instead they were extremely soluble in water and other hydroxylic media that make them ideal for the solvent mixture involved in the carbonylation of methanol ($MeOH/H_2O/AcOH$). However, their extreme solubility also made it difficult to isolate the catalytic species in a pure form as residual water and acid was not easily removed even through azotropic distillation. In addition it is possible that complex **52** is not fully protonated.

5.3 Solubility study

As a result of the interesting finds relating to the solubility of complex **49** in the presence of a strong acid such as HBF_4 a direct comparison was set up between [Rh(dppe)C(O)Me(I)$_2$] **22** and [Rh(dppe-(NMe$_2$)$_4$)C(O)Me(I)$_2$] **49**. In this experiment the solubility of 0.015 mmols of each complex in 2 cm^3 of a AcOH/MeOH/H_2O (40:45:15) mixture with and without the addition of acid was quantified. This was achieved using an external standard of tributylphosphine oxide in a similar manner to that of the stability tests in Chapters 2 and 3. In this instance two different acids were also tested, HBF_4 (pK_a -0.4) as for the previous experiment and HI (pK_a -10). HI is formed during the rhodium-catalysed carbonylation of methanol and therefore is potentially of greater significance if proven to be successful in promoting the solubility of amine-substituted ligand complexes.

Table 5.3. The solubility of complexes **22** and **49** in hydroxylic media with/without the addition of a strong acid.

	Complex **22**		Complex **49**	
	Approximate solubility (M)[a]	% in solution[b]	Approximate solubility (M)[a]	% in solution[b]
CH_2Cl_2	$7.73x10^{-3}$	100	$7.73x10^{-3}$	100
AcOH[c]	$<9x10^{-7}$	0	$<9x10^{-7}$	0
HBF_4 (50 eq.)	$<9x10^{-7}$	0	$5.81x10^{-3}$	75.1
HI (50 eq.)	$<9x10^{-7}$	0	$6.62x10^{-3}$	85.6

[a] Molar concentration calculated by the approximate integration of noise relative to an external standard of tributylphosphine oxide [b] % of complex in a solution of MeI/MeOAc relative to an external standard of tributylphosphine oxide [c] Solvent mixture consists of AcOH/H_2O/MeOH (40:45:15).

The differences in solubility between these complexes with and without the addition of acid are quite striking. Before the addition of acid both complexes possessed a poor solubility in the AcOH/MeOH/H_2O media, with the detection of no phosphorus species in the ^{31}P NMR. However, with the addition of 50 eq. of acid there was a clear difference between the unsubstituted dppe complex, whose solubility remained

undetectable in the ^{31}P NMR, and complex **49** whose previously insoluble precipitate was immediately taken into solution. There was also a small difference in the solubility of complex **49** when using either HBF_4 or HI. With only 50 eq. of HBF_4 it was calculated that ca. 75 % of the total starting material was soluble with the ^{31}P NMR now showing a strong doublet at 71.15 ppm with a $^{1}J_{Rh-P}$ coupling of 139.3 Hz, assigned to the protonated complex **52**. Whereas with the addition of 50 eq. of HI it was possible to achieve 85 % solubility. It was also shown that on addition of a further 50 eq. of both HBF_4 and HI the solubility of complex **49** was increased to 100 %.

5.4 Conclusions

We have shown that rhodium complexes of dimethylaminophenyl substituted phosphines are not quaternised by reaction with methyl iodide, which is of course already part of the reaction medium in methanol carbonylation. Therefore the use of HBF_4 and HI has been explored, similar to the approach used by Toth et al. in the asymmetric hydrogenation of dehydroamino acids, and found that it is possible to achieve protonation of dimethyl amino substituents. Although the protonated species were not isolated, they were identified in solution and the stark contrast in the solubility between the two acetyl complexes further demonstrates the protonation and shows the potential of such a procedure to improve the solubility of catalysts for the carbonylation of methanol. The use of a dppe analogue as our target phosphine was primarily as a model for future development of other catalysts (for details of further ligand design see Appendix I). Having proven HI to be an effective proton source for the quaternisation of amine-substituted phosphine ligand complex, this investigation has shown the potential of such a modification to overcome the solubility issues that currently exist in rhodium-phosphine systems. This is an area that I believe warrants further development as it is important to understand the impact of the change in solubility properties of the catalyst and how these novel highly cationic species affect the rate of reaction.

Chapter VI: Experimental

6.1 General

All manipulations were performed using standard Schlenk line techniques under nitrogen supplied by BOC. All chemicals and solvents were obtained through commercial sources. All complexes used were prepared by standard literature procedures. Microanalyses were by the University of St. Andrews microanalytical service. NMR spectra were recorded on Bruker Advance 300 instruments. Chemical shifts are reported in ppm with $^{1}H\{^{31}P\}$ and $^{13}C\{^{1}H\}$ NMR spectra referenced to tetramethylsilane (external). $^{31}P\{^{1}H\}$ NMR spectra were referenced externally to 85% H_3PO_4. Proton and carbon signal multiplicities are given as s (singlet), d (doublet), t (triplet), q (quartet), m (multiplet), b (broad) or a combination of them. All spectra were recorded at room temperature and the solvent for a particular spectrum is given in the parentheses. $^{13}C\{^{1}H\}$ and $^{31}P\{^{1}H\}$ NMR spectra were recorded with broad-band proton decoupling. IR spectra were recorded using a Perkin Elmer Spectrum GX FT-IR system. All solids were analysed as KBr disks. Microanalysis for carbon, hydrogen and nitrogen were performed using a EA 1110CHNS instrument at the University of St Andrews. CE Gas chromatography was carried out at BP PLC, Saltend. Mass spectroscopy data was obtained from the EPSRC National Mass Spectroscopy Service Centre, Swansea and the University of St Andrews Mass Spectroscopy service. In addition to detecting the ions shown, all Rh complexes showed excellent agreement between calculated and expected isotope patterns.

X-ray crystallography data was collected at 93 K by using a Rigaku MM007 High brilliance RA generator and Mercury/Saturn CCD systems using Mo K_α radiation. Intensities were corrected for Lorentz-polarisation and for absorption. The structures were solved by direct methods. All hydrogen atoms were refined as idealised riding geometries and structural refinements were obtained with full-matrix least-squares based on F^2 by using the program SHELXTL.

6.2 Catalysis experiments

These experiments were carried out at BP chemicals PLC in Hull in a 300 cm^3 Hastelloy high-pressure infrared (HPIR) autoclave fitted with a bursting disc, catalyst injector, overhead Magnedrive^{TM} stirrer, impeller with gas sparging facility, gas inlet, high pressure (195 bar) carbon monoxide reservoir and thermocouple. Additionally the apparatus featured equipment for pressure measurements and sampling. Carbon monoxide consumption was measured by monitoring the pressure drop in the reservoir. A computer collected the data automatically by use of a Dynamic Data Exchange (DDE) link between an Orsi process control package and a data logging package on Excel.

Safety note: These experiments were carried out using custom made facilities dedicated to methanol carbonylation. MeI and CO are extremely toxic and should be used with extreme care.

For the reactions carried out with an initial water level of 15 %w/w, methanol (100 g, 3.125 mol), water (19 g, 1.06 mol), $Rh_2(CO)_4Cl_2$ (150 mg, 0.386 mmol) and diphosphine ligand (2 eq, 0.772 mmol) were added to the autoclave under CO/syn-gas. The quantity of water was altered for the remaining reactions incorporating no initial water content. The autoclave was then sealed and pressurised with carbon monoxide (5 bar) and heated to 100 ºC, controlled by the use of a thermocouple in a thermowell in the reaction solution, whilst stirring at 900 rpm. Using the catalyst injector iodomethane (22.6 g, 0.159 mol) was then added to the autoclave with an over pressure of CO/syn-gas. Simultaneously, the autoclave was pressurised with CO/syn-gas (27 bar) from the high pressure ballast vessel. The autoclave was then heated to the desired temperature and the data collection activated. The pressure was maintained at 27 bar by a pressure regulating value which transferred CO/syn-gas from the high pressure ballast to the autoclave when the pressure dropped below the set-point.

After the reaction, the autoclave was allowed to cool before a gas sample was collected from the headspace in the autoclave. This gas sample was analysed by gas chromatography using in-house facilities. The autoclave was then disconnected from the kinetics rig and a liquid sample of the reaction solution was analysed by gas

chromatography. Liquid analysis was carried out for the main constituents that fall into the bulk liquids category, as well as a range of liquid by-products such as acetaldehyde.

For the stability tests run under a N_2 atmosphere, a Biotage™ microwave vial containing 0.0265 mmol of Rh(I)-phosphine ligand complex was charged with a solution of MeOAc/MeI (3:1) and heated at 140 ºC for 10 mins in a Biotage™ microwave. The % of Rh-P complex present was then calculated with respect to an external standard of tributylphosphine oxide using $^{31}P\{^{1}H\}$ NMR spectroscopy.

Safety note: These experiments were carried out using Biotage™ equipment purpose built to within pressures of up to 22 bar and temperatures in excess of 200 ºC. MeI is extremely toxic and should be used with extreme care.

The following compounds were prepared by exactly following the literature procedures, $[Rh(PPh_3)_2CO(Cl)]$ **7**[110], $[Rh(CO)(MeCN)(COMe)I_2]_2$ **8**[86], $[Rh(PPh_2(C_6H_4\text{-}2\text{-}Me))_2CO(Cl)]$ **13**[111, 112], $[Rh(PPh_2(C_6H_4\text{-}4\text{-}Me))_2CO(Cl)]$ **14**[113], $[Rh(P(C_6H_4\text{-}4\text{-}F)_3)_2CO(Cl)]$ **15**[113], $[Rh(PPh_2(C_6H_4\text{-}2\text{-}OMe))_2CO(Cl)]$ **17**[114], $[Rh(PPh_2(C_6H_4\text{-}4\text{-}OMe))_2CO(Cl)]$ **18**[115], $[Rh(P(C_6H_4\text{-}4\text{-}OMe)_3)_2CO(Cl)]$ **19**[113], Synthesis of [Rh(dppe)CO(Cl)] **20**[77], [Rh(BIPHEP)CO(Cl)] **21**, $[Rh(dppp)CO(Cl)]_2$ **22**[77], [Rh(Xantphos)CO(Cl)] **24**[116], $[Rh(Xantphos)CO]SbF_6$ **25**[116], [Rh(Nixantphos)CO(Cl)] **26**[116] and $[Rh(Nixantphos)CO]SbF_6$ **27**[116].

6.3 Selected data for Chapter II

General synthesis of $[Rh(L)CO(Cl)]_2$

Method A:

THF (2 cm^3) was charged into a Schlenk tube containing the precursor $Rh_2(CO)_4Cl_2$ and the diphosphine (2 eq.). After stirring for a short amount of time a pale yellow solid precipitated was filtered and washed with ice-cold methanol before drying under vacuum.

Method B:

THF (2 cm^3) was charged into a Schlenk tube containing the diphosphine (2 eq.) and the precursor $[Rh(coe)Cl]_2$. CO was then bubbled through the solution resulting in a pale yellow solid which was washed with ice cold methanol before drying under vacuum.

Method C:

THF (1.5 cm^3) was charged into a microwave vial containing the diphosphine (2 eq.) and the precursor $[Rh(coe)Cl]_2$. This was stirred for 10 minutes before adding the aldehyde (100 eq.) in THF (0.5 cm^3). The solution was then heated at 110 °C for 10 minutes in a Biotage™ microwave and the resulting yellow solution was then analysed.
Note: Several of these complexes were too insoluble to record meaningful $^{13}C\{^1H\}$ NMR data.

Synthesis of $[Rh(dppb)CO(Cl)]_2$ 1[85]

This compound has previously been reported.
(Method A) Yield: 90 % (136.8 mg, 0.116 mmol); IR (KBr), ν(CO)/cm^{-1}: 1960. LSIMS Found 1184.2 M^+; $C_{58}H_{56}Cl_2O_2P_4Rh_2$ requires 1184.1 M^+. $^{31}P\{^1H\}$ NMR (CD_2Cl_2): δ 24.0 (d, $^1J_{Rh\text{-}P}$ 124 Hz).

Synthesis of $[Rh(dppx)CO(Cl)]_2$ 3

(Method A) Yield: 79.3 % (48.4 mg, 0.041 mmol). IR (KBr), ν(CO)/cm^{-1}: 1970. LSIMS (FAB) Found 1224.1 [*M*-2CO]$^+$, 1245.2 [*M*-Cl]$^+$; $C_{64}H_{56}Cl_2P_4Rh_2$ requires 1224.1 [*M*-2CO] $^+$. $^{31}P\{^1H\}$ NMR (CD_2Cl_2): δ 30.7 (d, $^1J_{Rh\text{-}P}$ 127.7 Hz). $^1H\{^{31}P\}$ NMR (CD_2Cl_2): δ_H 8.00-6.00 (28H, m) , 3.85 (1H, s), 3.60 (1H, s), 2.95 (2H, s), 1.42 (2H, s), 1.25 (1H, s), 1.20 (1H, s).

Synthesis of $[Rh(dcpb)CO(Cl)]_2$ 4

(Method A) Yield: 74 % (117 mg, 0.095 mmol). IR (KBr), ν(CO)/cm^{-1}: 1949. LSIMS (FAB) Found 1232.3 M^+; $C_{58}H_{104}Cl_2O_2P_4Rh_2$ requires 1232.4 M^+. *Anal.* Calc. for $C_{58}H_{104}Cl_2O_2P_4Rh_2$: C, 56.45; H, 8.49%. Found: 56.22; H, 8.20%. $^{31}P\{^1H\}$ NMR (CD_2Cl_2): δ 31.5 (d, $^1J_{Rh\text{-}P}$ 118.8 Hz). $^1H\{^{31}P\}$ NMR (CD_2Cl_2): δ_H 1.99 (16H, bm) , 1.74 (48H, bm), 1.46 (16H, bm), 1.188 (16H, bm).

Synthesis of [Rh(BINAP)CO(Cl)] 5[81]

This compound has previously been reported.
(Method A) Yield: 79 % (95.6 mg, 0.121 mmol). IR (KBr), ν(CO)/cm^{-1}: 2007. LSIMS (FAB) Found 760.1 [M-CO]$^+$; $C_{44}H_{32}Cl_1P_2Rh_1$ requires 760.1 [M-CO]$^+$. $^{31}P\{^1H\}$ NMR (CD_2Cl_2): δ 46.8 (dd, $^1J_{Rh\text{-}P}$ 161.1 Hz, $^2J_{P\text{-}P}$ 43.59 Hz), δ 25.0 (dd, $^1J_{Rh\text{-}P}$ 127.7 Hz, $^2J_{P\text{-}P}$ 43.60 Hz).

Synthesis of [Rh(BINAP)CO(I)] 6

Acetone (5 cm^3) was added to a Schlenk tube containing [Rh(BINAP)CO(Cl)] (50 mg, 0.063 mmol) and NaI (1.9 eq.). This resulted in a colour change from a yellow to an orange solution which was filtered and dried under vacuum to give the iodo-complex [Rh(BINAP)CO(I)].
Yield: 96 % (53.6 mg, 0.061 mmol). IR (KBr), ν(CO)/cm^{-1}: 2007. LSIMS (FAB) Found 851.9 [M-CO]$^+$; $C_{44}H_{32}I_1P_2Rh_1$ requires 852.0 [M-CO]$^+$. $^{31}P\{^1H\}$ NMR (CD_2Cl_2): δ 42.9 (dd, $^1J_{Rh\text{-}P}$ 166 Hz, $^2J_{P\text{-}P}$ 42.3 Hz), δ 21.9 (dd, $^1J_{Rh\text{-}P}$ 126 Hz, $^2J_{P\text{-}P}$ 42.3 Hz). This compound was further characterised by X-ray crystallography.

Synthesis of [Rh(dppb)(C(O)Me)(I)$_2$] 7

1.5 cm^3 methyl acetate and 0.5 cm^3 methyl iodide was added to a 2.0 cm^3 Biotage™ microwave vial containing [Rh(dppb)CO(Cl)]$_2$ (15 mg, 0.013 mmol). The reaction mixture was then heated to 140 ºC for 10 minutes. High quality X-ray crystals were then formed from the slow evaporation of this solution.
Yield: 86 % (17.8 mg, 0.022 mmol). IR (KBr), ν(CO)/cm^{-1}: 1702. LSIMS (FAB) Found 825.8 M$^+$; $C_{30}H_{31}I_2OP_2Rh_1$ requires 825.9 M$^+$. *Anal.* Calc. for $C_{30}H_{31}I_2OP_2Rh_1$: C, 43.61; H, 3.78%. Found: C, 44.06; H, 3.76%. $^{31}P\{^1H\}$ NMR (CD_2Cl_2): δ 32.9 (d, $^1J_{Rh\text{-}P}$ 138.1 Hz. $^1H\{^{31}P\}$ NMR (CD_2Cl_2): δ 7.58 (4H, C*H*-Ar, dt), 7.23-7.41 (12H, C*H*-Ar, m), 3.19 (2H, CH_2, m), 2.58 (3H, COCH_3, s), 2.35 (2H, CH_2, m), 1.49 (2H, CH_2, m), 0.98 (2H, CH_2, m). $^{13}C\{^1H\}$ NMR (CD_2Cl_2): δ 212.85 (*C*OMe, dt, $^1J_{Rh\text{-}C}$ 25.77 Hz), 137.27, 136.54, 130.09, 130.27 (*C*-Ar), 136.44-127.30 (*C*H-Ar), 44.85 (*C*H$_2$, s), 23.53 (CH$_2$, d, $^1J_{Rh\text{-}C}$ 28.64 Hz), 21.46 (*C*H$_3$, s).

Synthesis of [Rh(dppx)(C(O)Me)(I)$_2$] 10

1.5 cm^3 methyl acetate and 0.5 cm^3 methyl iodide was added to a 2.0 cm^3 Biotage™ microwave vial containing [Rh(dppx)CO(Cl)]$_2$ (15 mg, 0.012 mmol). The reaction mixture was then heated to 140 ºC for 10 minutes. High quality X-ray crystals were then formed from the slow evaporation of this solution. Yield: 78.5 % (56.0 mg, 0.064 mmol). IR (KBr), ν(CO)/cm^{-1}: 1711. LSIMS (FAB) Found 873.8 M$^+$, 746.9 [M-I]$^+$; $C_{34}H_{31}I_2OP_2Rh_1$ requires 873.9 M$^+$. *Anal.* Calc. for $C_{34}H_{31}I_2OP_2Rh_1$: C, 46.71; H, 3.57%. Found: C, 46.56; H, 3.31%. $^{31}P\{^1H\}$ NMR (CD_2Cl_2): δ 11.0 (d, $^1J_{Rh-P}$ 138.7 Hz). $^1H\{^{31}P\}$ NMR (CD_2Cl_2): δ_H 7.86 (4H, C*H*, dt), 7.23-7.45 (12H, C*H*, m), 6.43 (4H, CH_2, m), 6.09 (2H, CH_2, m), 5.02 (2H, CH_2, m), 3.34 (2H, CH_2, m), 2.38 (3H, CH_3, s).

6.4 Selected data for Chapter III

General synthesis of [Rh(L)$_2$CO(Cl)]

Method A:

$RhCl_3.xH_2O$ (100 mg, 0.478 mmol) in 5 cm^3 absolute EtOH was slowly added to 20 cm^3 of boiling absolute ethanol containing the monodentate ligand (2 eq.). 2 cm^3 of 35% formaldehyde solution was then added causing a precipitation of a yellow crystalline solid. After cooling the solid was filtered and washed with ethanol.

Method B:

EtOH (4 cm^3) was charged into a microwave vial containing the monodentate ligand (2 eq.) and $RhCl_3.xH_2O$ (50 mg, 0.239 mmol). This was stirred for 10 minutes before adding 1 cm^3 35% formaldehyde solution. The solution was then heated at 110 °C for 10 minutes in a Biotage™ microwave and the resulting pale yellow solid was then analysed.

Method C:

EtOH (2 cm^3) was charged into a Schlenk tube containing the precursor $Rh_2(CO)_4Cl_2$ (20 mg, 0.0514 mmol) and the monodentate ligand (2 eq.). After stirring for a short amount of time a pale yellow solid precipitated was filtered and washed with ice-cold methanol before drying under vacuum.

Synthesis of [Rh(3, 4, 5-($C_6H_2F_3$)$_3$P)$_2$CO(Cl)] 16

The Rh(I) complex containing the above fluorinated ligand has not been previously reported.

(Method C) Yield: 76 % (79.4 mg, 0.078 mmol). IR (KBr), ν(CO)/cm^{-1}: 1985. *Anal.* Calc. for $C_{37}H_{12}ClF_{18}OP_2Rh_1$: C, 43.79; H, 1.19%. Found: C, 43.58; H, 1.01%. LSIMS (FAB) Found 985.7 $[M\text{-}CO]^+$; $C_{36}H_{12}F_{18}P_2Rh_1$ requires 985.9 $[M\text{-}CO]^+$. $^{31}P\{^1H\}$ NMR (CD_2Cl_2): δ 34.8 ppm (d, $^1J_{Rh\text{-}P}$ 134.4 Hz).

Synthesis of [Rh(κ^2-PPh$_2$(CH$_2$)$_2$PPh(CH$_2$)$_2$PPh$_2$CH$_3$)(COCH$_3$)I$_2$]$^+$I$^-$ 29a

MeI (0.1 cm^3, 1.06 mmol) was added to a 2.0 cm^3 Biotage™ microwave vial containing [Rh(TRIPHOS)(CO)$_2$]Cl prepared from $Rh_2(CO)_4Cl_2$ (15 mg, 0.039 mmol) and TRIPHOS ligand (41.3 mg, 0.077 mmol) in 2 cm^3 of dry degassed methanol. The reaction mixture was then heated to 140 ºC for 10 minutes. High quality X-ray crystals were then formed from the slow evaporation of this solution.

Yield: 75 % (54 mg, 0.058 mmol). IR (KBr), v(CO)/cm^{-1}: 1709. HRMS (ES) Found 948.9364 $[M]^+$; $C_{37}H_{39}I_3OP_3Rh$ requires 948.9353 $[M]^+$. *Anal.* Calc. for $C_{37}H_{39}I_3O_3P_3Rh$: C, 39.95; H, 3.90%. Found: C, 39.85; H, 3.75%. $^{31}P\{^1H\}$ NMR ($CDCl_3$): δ 79.55 (dd, $^1J_{Rh\text{-}P}$ 143.7 Hz, $^3J_{P\text{-}P}$ 47.2 Hz), 70.69 ($^1J_{Rh\text{-}P}$ 134.1 Hz), 26.50 ($^3J_{P\text{-}P}$ 47.2 Hz). $^1H\{^{31}P\}$ NMR ($CDCl_3$): δ 7.55 (25H, C*H*-Ar, m), 3.75 (1H, CH_2, m), 3.41 (2H, CH_2, m), 3.26 (1H, CH_2, m), 3.09 (1H, CH_2, m), 3.06 (2H, CH_2, m), 2.82 (3H, CH_3, s), 2.59 (3H, CH_3, s), 1.78 (1H, CH_2, m), 1.52 (4H, 2xH_2O, m). $^{13}C\{^1H\}$ NMR ($CDCl_3$): δ 211.12 (*C*OMe, dt, $^1J_{Rh\text{-}C}$ 26.54 Hz, $^1J_{P\text{-}C}$ 4.42 Hz), 135.30-128.29 (*C*H-Ar), 118.80 (*C*-Ar, d, $^1J_{Rh\text{-}C}$ 17.14 Hz), 117.67 (*C*-Ar, d, $^1J_{Rh\text{-}C}$ 17.14 Hz), 44.99 (CO*C*H$_3$), 29.08 (*C*H$_2$, ddd, $^1J_{P\text{-}C}$ 33.17 Hz, $^2J_{P\text{-}C}$ 12.16 Hz, $^2J_{Rh\text{-}C}$ 2.21 Hz), 27.61 (*C*H$_2$, dd, $^1J_{P\text{-}C}$ 32.07 Hz, $^2J_{P\text{-}C}$ 7.74 Hz), 21.43 (*C*H$_2$, dd, $^1J_{P\text{-}C}$ 25.98 Hz, $^2J_{Rh\text{-}C}$ 2.21 Hz), 20.74 (*C*H$_2$, d, $^1J_{P\text{-}C}$ 48.65 Hz), 8.98 (*C*H$_2$, d, $^1J_{P\text{-}C}$ 54.73 Hz).

Synthesis of [Rh(κ^2-PPh$_2$(CH$_2$)$_2$PPh(CH$_2$)$_2$PPh$_2$^{13}CH$_3$)(CO^{13}CH$_3$)I$_2$]$^+$I$^-$ 29c

Using the same procedure as described above the product was isolated in good yield.

Yield: 77 % (55.6 mg, 0.059 mmol). IR (KBr), v(CO)/cm^{-1}: 1709. $^{31}P\{^1H\}$ NMR ($CDCl_3$): δ 78.37 (d, $^1J_{Rh\text{-}P}$ 143.8 Hz, $^3J_{P\text{-}P}$ 47.0 Hz), 69.52 (d, $^1J_{Rh\text{-}P}$ 47.0 Hz), 25.26 (dd, $^3J_{P\text{-}P}$ 47.0 Hz, $^1J_{P\text{-}C}$ 54.6 Hz). $^1H\{^{31}P\}$ NMR ($CDCl_3$): δ 8.01-7.08 (25H, C*H*-Ar, m),

3.75 (1H, CH_2, m), 3.39 (1H, CH_2, m), 3.26 (2H, CH_2, m), 3.07 (2H, CH_2, m), 2.88 (3H, ^{13}CH_3, d, $^1J_{C\text{-}H}$ 98.4 Hz), 2.85 (1H, CH_2, m), 2.54 (3H, CH_3, d, $^1J_{C\text{-}H}$ 97.9 Hz), 1.86 (1H, CH_2, m). ^{13}C{^{1}H} NMR ($CDCl_3$): δ 44.97 (*C*O^{13}Me, s), 9.04 (^{13}*C*OMe, d, $^1J_{P\text{-}C}$ 54.6 Hz).

Synthesis of [Rh(TRIPHOS)Me(I)CO]I 30a[117]

MeI (1 cm^3, 16.06 mmol) was added to a solution of [Rh(TRIPHOS)$(CO)_2$]Cl prepared from $Rh_2(CO)_4Cl_2$ (30 mg, 0.077 mmol) and TRIPHOS ligand (82.5 mg, 0.154 mmol) in 5 cm^3 of dry degassed methanol. The solution was then stirred for 24 hrs to obtain a bright yellow solution. The solvent was removed under vacuum and the product isolated in good yield.

Yield: 91 % (113 mg, 0.140 mmol). IR (KBr), ν(CO)/cm^{-1}: 2075. LSIMS (ES) Found 779.06 [M-CO]$^+$; $C_{35}H_{36}IP_3Rh$ requires 779.01 [M-CO]$^+$. ^{31}P{^{1}H} NMR (CD_3OD): δ 108.73 (dt, $^1J_{Rh\text{-}P}$ 104.0 Hz, $^2J_{P\text{-}P}$ 2.97 Hz), 41.85 (dd, $^1J_{Rh\text{-}P}$ 92.1 Hz, $^2J_{P\text{-}P}$ 2.97 Hz). ^{1}H{^{31}P} NMR (CD_3OD): δ 7.78 (4H, C*H*-Ar, m), 7.45 (4H, C*H*-Ar, m), 7.16 (17H, C*H*-Ar, m), 3.51 (1H, CH_2, m), 2.99 (1H, CH_2, m), 2.74 (6H, CH_2, m), -0.14 (3H, CH_3, s).

Synthesis of [Rh(TRIPHOS)^{13}Me(I)CO]I 30b

Using the same procedure as described above the product was isolated in good yield.

Yield: 85 % (106 mg, 0.131 mmol). IR (KBr), ν(CO)/cm^{-1}: 2076. LSIMS (ES) Found 779.77 [M-CO]$^+$; $C_{34}{}^{13}CH_{36}IP_3Rh$ requires 780.02 [M-CO]$^+$. ^{31}P{^{1}H} NMR (CD_3OD): δ 108.9 (m, $^1J_{Rh\text{-}P}$ 103.7 Hz), 42.0 (d(dd), $^1J_{Rh\text{-}P}$ 92.45 Hz, $^2J_{P\text{-}P}$ 2.97 Hz, $^2J_{P\text{-}13C}$ 5.77 Hz). ^{1}H {^{31}P} NMR (CD_4OD): δ 8.12-7.31 (25H, C*H*-Ar, m), 3.82 (2H, CH_2, m), 3.05 (6H, CH_2, m), 0.17 (3H, ^{13}CH_3, d, $^1J_{13C\text{-}H}$ 135.7 Hz). ^{13}C{^{1}H} NMR (CD_3OD): δ 7.12 (^{13}*C*H$_3$, dq, $^1J_{Rh\text{-}13C}$ 14.4 Hz, $^1J_{P\text{-}13C}$ 6.1 Hz).

6.5 Selected data for Chapter IV

General synthesis of aminophosphine ligands

A solution of diphenylphosphinobenzaldehyde (0.1g, 0.344 mmol) in degassed absolute ethanol (15 cm^3) at 45 °C was added over a period of 4 hrs to a solution of amine (3.2 eq, 1.102 mmol) in 20 cm^3 at 0 °C. Sodium borohydride (4.2 eq, 54 mg, 1.447 mmol) was added to the reaction solution and stirred for a further 12 hrs at room temperature.

The reaction was then quenched with acetone (5 cm^3) and the solvent was removed under vacuum. The residue was dissolved by stirring with saturated ammonium hydrochloride solution (10 cm^3) and dichloromethane (20 cm^3). After extraction of the aqueous phase with dichloromethane (2 x 10 cm^3), the combined organic phases were washed with water (10 cm^3) followed by a further extraction. The organic phase was then dried using magnesium sulphate and filtered. The solvent was then removed under vacuum resulting in a clear oil.

Synthesis of 3-(2-(diphenylphosphino)benzylamino)propan-1-ol 34

Ligand **34** was obtained by following the general procedure as described above using diaminopropan-1-ol (3.2 eq, 1.102 mmol).

Imine: $^{31}P\{^1H\}$ NMR (C_6D_6): δ -12.21 (s, major), -17.24 (s, minor) (E/Z)
Amine: Yield: 96.4 % (58.0 mg, 0.164 mmol). HRMS (CI) Found 350.1674 [MH^+]; $C_{22}H_{25}NOP$ requires 350.1673 [MH^+]. $^{31}P\{^1H\}$ NMR ($CDCl_3$): δ -14.85 (s). $^1H\{^{31}P\}$ NMR ($CDCl_3$): δ_H 7.35-7.15 (12H, Ar*H*, m), 7.12-7.05 (1H, Ar*H*, dt), 6.84-6.78 (1H, Ar*H*, dd), 3.88 (2H, CH_2, s), 3.64 (2H, CH_2, t), 3.04 (1H, O*H*, br), 2.62 (2H, CH_2, t), 1.44 (2H, CH_2, quintet). $^{13}C\{^1H\}$ NMR (CD_2Cl_2): δ 143.6 (Ar*C*, d, $^1J_{P\text{-}C}$ 23.81 Hz), 136.40 (Ar*C*, d, $^1J_{P\text{-}C}$ 9.56 Hz) , 135.83 (Ar*C*, d, $^1J_{P\text{-}C}$ 13.25 Hz), 134.04-127.52 (Ar*C*, m), 64.12 (*C*H_2, s), 52.36 (*C*H_2, d, $^1J_{P\text{-}C}$ 20.74 Hz), 49.14 (*C*H_2, s), 30.76 (*C*H_2, s).

Synthesis of N1-(2-(diphenylphosphino)benzyl)propane-1,3-diamine 35

Ligand **35** was obtained by following the general procedure as described above using diaminopropane (3.2 eq, 1.102 mmol).

Imine: $^{31}P\{^1H\}$ NMR (C_6D_6): δ -13.29 (s), -16.42 (s) (E/Z)
Amine: Yield: 98.3 % (59 mg, 0.169 mmol). HRMS Found 349.1834 [MH^+]; $C_{22}H_{26}N_2P$ requires 349.1830 [MH^+]. $^{31}P\{^1H\}$ NMR (CD_3OD): δ -18.24 (s). $^1H\ \{^{31}P\}$ NMR (CD_3OD): δ_H 7.70-6.91 (14H, Ar*H*, m), 4.92 (2H, CH_2, s), 3.99 (2H, NH_2, s), 2.62 (2H, CH_2, t), 2.56 (2H, CH_2, t), 1.55 (2H, CH_2, quintet), 1.32 (1H, N*H*, m). $^{13}C\ \{^1H\}$ NMR (CD_3OD): δ 143.55 (Ar*C*, d, $^1J_{P\text{-}C}$ 24.05 Hz), 136.58 (Ar*C*, d, $^1J_{P\text{-}C}$ 9.43 Hz), 136.12 (Ar*C*, d, $^1J_{P\text{-}C}$ 13.35 Hz), 133.99-127.55 (Ar*C*, m), 51.9 (*C*H_2, d, $^1J_{P\text{-}C}$ 21.03 Hz), 46.50 (*C*H_2, s), 39.43 (*C*H_2, s), 31.60 (*C*H_2, s).

Synthesis of N-(2-(diphenylphosphino)benzyl)-3-(methylthio)propan-1-amine 36

Ligand **36** was obtained by following the general procedure as described above using 3-(methylthio)aminopropane (3.2 eq, 1.102 mmol).

Imine: $^{31}P\{^{1}H\}$ NMR (C_6D_6): δ -13.26 ppm

Amine: Yield: 93.3 % (61.0 mg, 0.161 mmol). HRMS(CI) Found 380.1602 ; $C_{23}H_{27}I_2NPS$ requires 380.1598 M^+. $^{31}P\{^{1}H\}$ NMR (CD_2Cl_2): δ 16.24 (s). $^{1}H\{^{31}P\}$ NMR (CD_3OD): δ_H 7.70-6.90 (14H, Ar*H*, m), 3.98 (2H, C*H*$_2$, s), 2.57 (2H, C*H*$_2$, t), 2.39 (2H, C*H*$_2$, t), 2.04 (3H, C*H*$_3$, s), 1.61 (2H, C*H*$_2$, quin). $^{13}C\{^{1}H\}$ NMR ($CDCl_3$): δ 143.53 (Ar*C*, d, $^{1}J_{P\text{-}C}$ 24.33 Hz), 135.7 (Ar*C*, d, $^{1}J_{P\text{-}C}$ 9.95 Hz) , 134.69 (Ar*C*, d, $^{1}J_{P\text{-}C}$ 13.82 Hz), 132.9-125.3 (Ar*C*H, m), 51.55 (*C*H$_2$, d, $^{1}J_{P\text{-}C}$ 20.46 Hz), 47.09 (*C*H$_2$, s), 30.90 (*C*H$_2$, s), 28.34 (*C*H$_2$, s), 14.40 (*C*H$_3$, s).

Synthesis of N1-(2-(diphenylphosphino)benzyl)ethane-1,2-diamine 37

Ligand **37** was obtained by following the general procedure as described above using diaminoethane (3.2 eq, 1.102 mmol).

Imine: $^{31}P\{^{1}H\}$ NMR (C_6D_6): δ -12.02 (s)

Amine: Yield: 81.6 % (47 mg, 0.141 mmol). HRMS Found 335.1677 [MH^+]; $C_{21}H_{24}N_2P$ requires 335.1687 [MH^+]. $^{31}P\{^{1}H\}$ NMR (CD_3OD): δ -18.15 (s). $^{1}H\{^{31}P\}$ NMR (CD_3OD): δ_H 7.72-6.90 (14H, Ar*H*, m), 4.90 (2H, C*H*$_2$, m), 4.00 (2H, N*H*$_2$, s), 2.64 (4H, C*H*$_2$, m), 1.31 (1H, N*H*, m). $^{13}C\{^{1}H\}$ NMR (CD_3OD): δ 143.64 (Ar*C*, d, $^{1}J_{P\text{-}C}$ 24.02 Hz), 136.65 (Ar*C*, d, $^{1}J_{P\text{-}C}$ 9.45 Hz), 136.12 (Ar*C*, d, $^{1}J_{P\text{-}C}$ 13.30 Hz), 133.97-127.55 (Ar*C*, m), 51.49 (*C*H$_2$, d, $^{1}J_{P\text{-}C}$ 21.05 Hz), 49.92 (*C*H$_2$, s), 40.28 (*C*H$_2$, s).

General synthesis of rhodium-aminophosphine complexes

MeOH (10 cm^3) was charged into a Schlenk tube containing the precursor $Rh_2(CO)_4Cl_2$ (50 mg, 0.129 mmol) and the aminophosphine ligand (2 eq, 0.258 mmol). After stirring for a short amount of time the solvent was removed under vacuum and the resulting yellow solid analysed.

Synthesis of [Rh(PNO-C_3)CO(Cl)] 38

Yield: 89 % (117 mg, 0.228 mmol). IR (KBr), ν(CO)/cm^{-1}: 1981. HRMS (ES+) Found 480.0600 $[M\text{-}Cl]^+$; $C_{23}H_{24}NO_2PRh$ requires 480.0592 $[M\text{-}Cl]^+$. $^{31}P\{^1H\}$ NMR (CD_2Cl_2): δ 43.12 (d, $^1J_{Rh\text{-}P}$ 179.53 Hz). $^1H\{^{31}P\}$ NMR ($CDCl_3$): δ_H 7.60-6.80 (14H, Ar*H*, m), 4.32 (1H, N*H*, br), 3.82 (1H, CH_2, m), 3.80 (2H, CH_2, s), 3.65 (1H, CH_2, m), 3.15 (1H, CH_2, m), 2.36 (1H, CH_2, m), 1.68 (2H, CH_2, m), 1.20 (1H, O*H*, br). $^{13}C\{^1H\}$ NMR ($CDCl_3$): δ 187.9 (*C*O, dd, $^1J_{Rh\text{-}C}$ 70.21 Hz, $^1J_{P\text{-}C}$ 18.80 Hz), 13.38 (*C*H_2, d, $^3J_{Rh\text{-}C}$ 14.93 Hz), 134.41-127.86 (Ar*C*, m), 61.16 (*C*H_2, s), 51.72 (*C*H_2, d, $^2J_{Rh\text{-}C}$ 11.61 Hz), 46.48 (*C*H_2, s), 28.20 (*C*H_2, s). This compound was also characterised by X-ray crystallography (see Appendix II).

Synthesis of [Rh(PNN-C_3)CO]Cl 39

Yield: 96 % (127 mg, 0.247 mmol). IR (KBr), ν(CO)/cm^{-1}: 1986. LSIMS (FAB) Found 480.0 $[M\text{-}Cl]+H^+$ and 537.0 [M]+Na; $C_{23}H_{25}N_2OPRh$ requires 480.0 $[M\text{-}Cl]+H^+$ and $C_{23}H_{25}ClN_2NaOPRh$ requires 537.0 [M]+Na. $^{31}P\{^1H\}$ NMR (CD_3OD): δ 40.85 (d, $^1J_{Rh\text{-}P}$ 151.5 Hz). $^1H\{^{31}P\}$ NMR (CD_3OD): δ_H 7.51 (13H, Ar*H*, m), 6.86 (1H, Ar*H*, m), 3.68 (2H, NH_2, m), 3.22 (1H, CH_2, m), 2.95 (1H, CH_2, m), 2.83 (1H, CH_2, m), 2.68 (1H, CH_2, m), 1.95 (2H, CH_2, m), 1.27 (2H, CH_2, m). $^{13}C\{^1H\}$ NMR (CD_3OD): δ 188.54 (Ar*C*O, dd, $^1J_{Rh\text{-}C}$ 71.85 Hz, $^1J_{P\text{-}C}$ 20.61 Hz), 139.99 (Ar*C*, d, $^1J_{P\text{-}C}$ 15.70 Hz), 134.26 (Ar*C*, t, $^1J_{P\text{-}C}$ 12.11 Hz), 131.80 (Ar*C*H, m), 129.13 (Ar*C*H, m), 56.58 (*C*H_2, d, $^1J_{P\text{-}C}$ 13.74 Hz), 51.54 (*C*H_2, s), 42.35 (*C*H_2, s), 28.14 (*C*H_2, s).

Synthesis of [Rh(PNS-C_3)CO]Cl 40

Yield: 92 % (129 mg, 0.237 mmol). IR (KBr), ν(CO)/cm^{-1}: 1985. HRMS Found 510.0528 [M-H]$^+$; $C_{24}H_{26}NORhPS$ requires 510.0530 [M-H]$^+$. $^{31}P\{^1H\}$ NMR (CD_3OD): δ 31.0 (d, $^1J_{Rh-P}$ 152.96 Hz). $^1H\{^{31}P\}$ NMR (CD_3OD): δ_H 7.91-7.52 (13H, Ar*H*, m), 6.97 (1H, CH_2, d), 4.90 (1H, CH_2, m), 3.77 (2H, CH_2, m), 3.24 (2H, CH_2, m), 2.79 (3H, CH_3, d, $^2J_{Rh-H}$ 1.79 Hz), 2.90-2.60 (2H, CH_2, m), 2.36-2.12 (2H, CH_2, m). $^{13}C\{^1H\}$ NMR (CD_3OD): δ 188.38 (Ar*C*, dd, $^1J_{P-C}$ 19.10 Hz, $^1J_{Rh-C}$ 68.96 Hz), 139.42 (Ar*C*, d, $^1J_{P-C}$ 15.41 Hz), 134.3-126.9 (Ar*C*H, m), 56.29 (*C*H_2, d, $^1J_{P-C}$ 14.67 Hz), 50.69 (*C*H_2, s), 35.21 (*C*H_2, s), 26.50 (*C*H_2, s), 21.79 (*C*H_3, s).

Synthesis of [Rh(PNN-C_2)CO]Cl 41

Yield: 79 % (102 mg, 0.203 mmol). IR (KBr), ν(CO)/cm^{-1}: 1989. LSIMS (FAB) Found 473.1 [M-CO]+H$^+$ and 466.2 [M-Cl]+H$^+$; $C_{21}H_{24}ClN_2PRh$ requires 473.0 [M-CO]+H$^+$ and $C_{22}H_{24}N_2OPRh$ requires 466.0 [M-Cl]+H$^+$. $^{31}P\{^1H\}$ NMR (CD_3OD): δ 39.62 (d, $^1J_{Rh-P}$ 153.0 Hz). ^1H $\{^{31}P\}$ NMR (CD_3OD): δ_H 8.10-6.95 (14H, Ar*H*, m), 4.90 (2H, CH_2, s), 3.89 (2H, NH_2, m), 3.28-2.70 (4H, CH_2, m), 1.31 (1H, N*H*, m). ^{13}C $\{^1H\}$ NMR (CD_3OD): δ 189.15 (Ar*C*O, dd, $^1J_{P-C}$ 18.83 Hz, $^1J_{Rh-C}$ 91.10 Hz), 181.47 (Ar*C*, d, $^1J_{Rh-C}$ 72.03 Hz), 141.31 (Ar*C*, d, $^1J_{P-C}$ 16.08 Hz), 134.44-128.75 (Ar*C*, m), 55.54 (*C*H_2, d, $^1J_{P-C}$ 8.44 Hz), 54.29 (*C*H_2, s), 42.41 (*C*H_2, s).

General synthesis for complexes 44 and 45

1.5 cm^3 methyl acetate and 0.5 cm^3 methyl iodide was added to a 2.0 cm^3 Biotage™ microwave vial containing [Rh(PNS-C_3)CO]Cl (30 mg, 0.055 mmol). The reaction mixture was then heated to 140 ºC for 10 minutes. The resulting mixture contained 2 complexes (**44** and **45)**. These were separated using a chromatatron and their structure tentatively assigned by $^{31}P\{^1H\}$ NMR, IR, HRMS and X-ray crystallography as discussed in Chapter IV.

6.6 Selected data for Chapter V

Synthesis of ligand dppe-NMe_2 46[107]

A solution of n-butyl-lithium (115 cm^3, 1.18 $moldm^{-3}$, 0.136 mol) in hexane was added dropwise over 90 mins to a stirred solution of *p*-$Me_2NC_6H_4Br$ (27.1 g, 0.136 mol) in diethyl ether (400 cm^{-1}) at RT. The mixture was then stirred for a further 15 mins and cooled to -70 ºC before $Cl_2PCH_2CH_2PCl_2$ (5.0 cm^3, 0.031 mol) in diethyl ether was added dropwise over 90 mins (always cooler than -30 ºC). The mixture was then allowed to warm to RT and stored for 12 h. The reaction mixture containing a white ppt was quenched with water (40 cm^3) and a yellow solid filtered off from both phases. This was redissolved in THF (400 cm^3) and combined with a solution obtained by dissolving the remaining solid in the reaction vessel in THF. The combined THF solutions were dried over anhydrous sodium sulphate, reduced to 50 cm^3 and the crude product precipitated with methanol (80 cm^3). Additional product was obtained with further addition of methanol.

Yield: 32 % (824 mg, 1.443 mmol). HRMS (ES) Found 571.3115 $[MH]^+$; $C_{34}H_{44}N_4P_2$ requires 571.3114 $[MH]^+$. $^{31}P\{^1H\}$ NMR (CD_2Cl_2): δ -17.68 (s). $^1H\{^{31}P\}$ NMR ($CDCl_3$): δ 7.10 (8H, C*H*-Ar, m), 6.55 (8H, C*H*-Ar, m), 2.82 (24H, NCH_3, s), 1.84 (4H, CH_2, s). $^{13}C\{^1H\}$ NMR (CD_2Cl_2): δ 151.12 (*C*N, s), 134.00 (*C*H-Ar, d, $^1J_{P-C}$ 9.95 Hz), 133.87 (*C*H-Ar, d, $^1J_{P-C}$ 9.95 Hz), 124.92 (*C*-Ar, d, $^1J_{P-C}$ 4.98 Hz), 112.61 (*C*H-Ar, d, $^1J_{P-C}$ 3.32 Hz), 112.56 (*C*H-Ar, d, $^1J_{P-C}$ 3.32 Hz), 47.47 (*C*H_3, s), 31.53 (*C*H_2-Ar, d, $^1J_{P-C}$ 3.32 Hz).

Synthesis of [Rh(dppe-NMe_2)CO(Cl)] 47

$[Rh_2(CO)_4Cl_2]$ (30 mg, 0.077 mmol) was dissolved up into 5 cm^3 of dry, degassed THF. The ligand (88 mg, 0.154 mmol) was also dissolved up into 25 cm^3 of dry, degassed THF and was added dropwise to the $[Rh_2(CO)_4Cl_2]$ and stirred for 4 hrs. After this time a bright yellow ppt had formed and was filtered under argon then washed with ice-cold pentane.

Yield: 84 % (95.2 mg, 0.129 mmol). IR (KBr), *v*(CO)/cm^{-1}: 1987. LSIMS (FAB) Found 708.1 $[M\text{-}CO]^+$, 701.2 $[M\text{-}Cl]^+$; $C_{35}H_{44}ClN_4OP_2Rh$ requires 708.2 $[M\text{-}CO]^+$, 701.2 $[M\text{-}Cl]^+$. HRMS (FAB) Found 708.1779 $[M\text{-}CO]^+$; $C_{34}H_{44}ClN_4P_2Rh$ requires 708.1771.

$^{31}P\{^{1}H\}$ NMR (CD_2Cl_2): δ 67.15 (dd, $^{1}J_{Rh-P}$ 157.4 Hz, $^{2}J_{P-P}$ 35.6 Hz), 45.69 (dd, $^{1}J_{Rh-P}$ 124.7 Hz, $^{2}J_{P-P}$ 35.6 Hz). $^{1}H\{^{31}P\}$ NMR (CD_2Cl_2): δ 7.49 (8H, C*H*-Ar, m), 6.61 (8H, C*H*-Ar, m), 2.89 (12H, NCH_3, s), 2.88 (12H, NCH_3, s), 2.21 (2H, CH_2, m), 1.93 (2H, CH_2, m). $^{13}C\{^{1}H\}$ NMR ($CDCl_3$): δ 191.38 (*C*O, dd, $^{1}J_{Rh-C}$ 102.8 Hz, $^{2}J_{P-C}$ 6.6 Hz), 152.44 (*C*N, s), 134.90 (*C*H-Ar, dd, $^{1}J_{P-C}$ 12.7 Hz, $^{2}J_{Rh-C}$ 1.11 Hz), 134.59 (*C*H-Ar, dd, $^{1}J_{P-C}$ 12.7 Hz, $^{2}J_{Rh-C}$ 1.11 Hz), 119.73 (*C*-Ar, d, $^{1}J_{P-C}$ 57.50 Hz), 117.66 (*C*-Ar, d, $^{1}J_{P-C}$ 47.55 Hz), 112.41 (*C*H, d, $^{1}J_{P-C}$ 17.1 Hz), 112.27 (*C*H, d, $^{1}J_{P-C}$ 17.7 Hz), 40.65 (*C*H_3, s), 31.53 (*C*H_2, m), 26.47 (*C*H_2, m).

Synthesis of [Rh(dppe-NMe$_2$)(COMe)(I)$_2$] 49

1.5 cm^3 methyl acetate and 0.5 cm^3 methyl iodide was added to a 2.0 cm^3 Biotage™ microwave vial containing [Rh(dppe-NMe_2)CO(Cl)] (15 mg, 0.013 mmol). The reaction mixture was then heated to 140 ºC for 10 minutes. High quality X-ray crystals were then formed from the slow evaporation of this solution.

Yield: 83 % (16.4 mg, 0.0169 mmol). IR (KBr), *ν*(CO)/cm^{-1}: 1702. LSIMS (ES) Found 969.9 $[M]^+$; $C_{36}H_{47}I_2N_4OP_2Rh$ requires 970.0 $[M]^+$. HRMS (FAB) Found 843.1324 $[M-I]^+$; $C_{36}H_{47}IN_4OP_2Rh$ requires 843.1324. *Anal.* Calc. for $C_{36}H_{47}I_2N_4OP_2Rh$: C, 44.56; H, 4.88; N, 5.77 %. Found: C, 44.61; H, 4.98; N, 5.34 %. $^{31}P\{^{1}H\}$ NMR (CD_2Cl_2): δ 69.04 (d, $^{1}J_{Rh-P}$ 139.6 Hz). $^{1}H\{^{31}P\}$ NMR (CD_2Cl_2):δ 7.54 (4H, *C*H-Ar, d, $^{1}J_{P-H}$ 8.96 Hz), 7.13 (4H, *C*H-Ar, d, $^{1}J_{P-H}$ 8.96 Hz), 6.61 (4H, *C*H-Ar, d, $^{1}J_{P-H}$ 8.96 Hz), 6.50 (4H, *C*H-Ar, d, $^{1}J_{P-H}$ 8.96 Hz), 2.92 (12H, NCH_3, s), 2.88 (12H, NCH_3, s), 2.66 (3H, COCH_3, s), 1.98 (1H, CH_2, m), 1.56 (1H, CH_2, m), 1.29 (2H, CH_2, m).

References

1. M. Gaub, A. Seidal, P. Torrance and P. Heymanns, in *Applied Homogeneous Catalysis with Organometallic Compounds*, eds. B. Cornils and A. Herrmann, VCH, New York, 1996, p. 104.
2. in *Chem. Eng. News*, 2005, pp. 67-76.
3. L. R. Partin and W. H. Heise, in *Acetic acid and its Derivatives*, eds. V. H. Agreda and J. R. Zoeller, Marcel Dekker, New York, 1993, p. 3.
4. G. Martin, in *Industrial and Manufacturing Chemistry, Part 1, Organic*, Crosby Lockwood, London, 1917, pp. 330-331.
5. D. Forster and T. W. Dekleva, *J. Chem. Ed.*, 1986, **63**, 204.
6. G. Irick, in *Acetic acid and its Derivatives*, eds. V. H. Agreda and J. R. Zoeller, Marcel Dekker, New York, 1993, p. 27.
7. R. Jira, W. Blau and D. Grimm, *Hydrocarbon Process*, 1976, **55**, 97.
8. H. Hohenschutz, N. Von Kutepow and W. Himmele, *Hydrocarbon Process*, 1966, **45**, 141.
9. N. Von Kutepow, W. Himmele and H. Hohenschutz, *Chem. Ing. Tech.*, 1965, **35**, 383.
10. F. E. Paulik and J. F. Roth, *Chem. Commun.*, 1968, 1578.
11. L. Vallarino, *Inorg. Chem.*, 1965, **4**, 161-165.
12. B. R. James and G. L. Rempel, *Chem. Commun.*, 1967, 158-159.
13. D. Forster, *Inorg. Chem.*, 1969, **8**, 2556-2558.
14. J. F. Roth, *Platinum Met. Rev.*, 1975, **19**, 12-14.
15. G. W. Adamson, J. J. Daly and D. Forster, *J. Organomet. Chem.*, 1974, **71**, C17-C19.
16. D. Forster, *J. Am. Chem. Soc.*, 1976, **98**, 846-848.
17. H. B. Tinker and D. E. Morris, *Rev. Sci. Instrum.*, 1972, **43**, 1024-1026.
18. H. B. Tinker and D. E. Morris, *J. Organomet. Chem.*, 1973, **52**, C55-C57.
19. D. E. Morris and H. B. Tinker, *J. Organomet. Chem.*, 1973, **49**, C53-C56.
20. H. Adams, N. A. Bailey, B. E. Mann, C. P. Manuel, C. M. Spencer and A. G. Kent, *J. Chem. Soc., Dalton Trans.*, 1988, 489-496.
21. A. Haynes, B. E. Mann, D. J. Gulliver, G. E. Morris and P. M. Maitlis, *J. Am. Chem. Soc.*, 1991, **113**, 8567-8569.

22. A. Haynes, B. E. Mann, G. E. Morris and P. M. Maitlis, *J. Am. Chem. Soc.*, 1993, **115**, 4093-4100.
23. P. M. Maitlis, A. Haynes, G. J. Sunley and M. J. Howard, *J. Chem. Soc., Dalton Trans.*, 1996, 2187-2196.
24. J. H. Jones, *Platinum Met. Rev.*, 2000, **44**, 94-105.
25. E. C. Baker, D. E. Hendriksen and R. Eisenberg, *J. Am. Chem. Soc.*, 1980, **102**, 1020-1027.
26. C.-H. Cheng, D. E. Hendriksen and R. Eisenberg, *J. Am. Chem. Soc.*, 1977, **99**, 2791-2792.
27. C. E. Hickey and P. M. Maitlis, *J. Chem. Soc., Chem. Commun.*, 1984, 1609-1611.
28. P. W. N. M. van Leeuwen, *Homogeneous Catalysis: Understanding the Art*, 2004.
29. D. Forster, *J. Chem. Soc., Dalton Trans.*, 1979, 1639-1645.
30. G. J. Sunley and D. J. Watson, *Catalysis Today*, 2000, **58**, 293-307.
31. G. J. Sunley, in *Manufacture of acetic acid by iridium-catalysed carbonylation of methanol using one or more metal iodides or iodide generating salts or complexes, GB Pat.*, 2003-16681, 2393437, 2004.
32. A. Haynes, P. M. Maitlis, G. E. Morris, G. J. Sunley, H. Adams, P. W. Badger, C. M. Bowers, D. B. Cook, P. I. P. Elliott, T. Ghaffar, H. Green, T. R. Griffin, M. Payne, J. M. Pearson, M. J. Taylor, P. W. Vickers and R. J. Watt, *J. Am. Chem. Soc.*, 2004, **126**, 2847-2861.
33. F. H. Jardine, J. A. Osborn, G. Wilkinson and J. F. Young, *Chem. Ind.*, 1965, 560.
34. N. Uematsu, A. Fujii, S. Hashiguchi, T. Ikariya and R. Noyori, *J. Am. Chem. Soc.,* 1996, **118**, 4916-4917.
35. B. H. Yang and S. L. Buchwald, *J. Organomet. Chem.,* 1999, **576**, 125-146.
36. C. A. Tolman, *J. Am. Chem. Soc.*, 1970, **92**, 2953-2956.
37. A. Roodt, S. Otto and G. Steyl, *Coord. Chem. Rev.*, 2003, **245**, 121-137.
38. C. A. Tolman, *Chem. Rev.*, 1977, **77**, 313-348.
39. L. E. Manzer and C. A. Tolman, *J. Am. Chem. Soc.*, 1975, **97**, 1955-1956.
40. C. P. Casey and G. T. Whiteker, *Isr. J. Chem.*, 1990, **30**, 299-304.
41. T. Hayashi, Y. Kawabata, T. Isoyama and I. Ogata, *Bull. Chem. Soc. Jpn.*, 1981, **54**, 3438-3446.
42. T. Hayashi, M. Konishi, Y. Kobori, M. Kumada, T. Higuchi and K. Hirotsu, *J. Am. Chem. Soc.*, 1984, **106**, 158-163.

43. C. P. Casey, G. T. Whiteker, M. G. Melville, L. M. Petrovich, J. A. Gavney, Jr. and D. R. Powell, *J. Am. Chem. Soc.*, 1992, **114**, 10680.
44. M. Kranenburg, Y. E. M. van der Burgt, P. C. J. Kamer, P. W. N. M. van Leeuwen, K. Goubitz and J. Fraanje, *Organometallics*, 1995, **14**, 3081-3089.
45. K. Yamamoto, S. Momose, M. Funahashi, S. Ebata, H. Ohmura, H. Komatsu and M. Miyazawa, *Chem. Lett.*, 1994, 189-192.
46. P. W. N. M. Van Leeuwen, P. C. J. Kamer, L. A. Van der Veen and J. N. H. Reek, *Chin. J. Chem.*, 2001, **19**, 1-8.
47. P. W. N. M. Van Leeuwen, P. C. J. Kamer and J. N. H. Reek, *Pure Appl. Chem.*, 1999, **71**, 1443-1452.
48. R. J. van Haaren, E. Zuidema, J. Fraanje, K. Goubitz, P. C. J. Kamer, P. W. N. M. van Leeuwen and G. P. F. van Strijdonck, *C. R. Chim.* 2002, **5**, 431-440.
49. L. A. van der Veen, P. K. Keeven, P. C. J. Kamer and P. W. N. M. van Leeuwen, *Dalton Trans.*, 2000, 2105-2112.
50. L. A. Van der Veen, P. H. Keeven, G. C. Schoemaker, J. N. H. Reek, P. C. J. Kamer, P. W. N. M. Van Leeuwen, M. Lutz and A. L. Spek, *Organometallics,* 2000, **19**, 872-883.
51. L. A. van der Veen, P. C. J. Kamer and P. W. N. M. van Leeuwen, *CATTECH*, 2002, **6**, 116-120.
52. L. A. Van der Veen, M. D. K. Boele, F. R. Bregman, P. C. J. Kamer, P. W. N. M. Van Leeuwen, K. Goubitz, J. Fraanje, H. Schenk and C. Bo, *J. Am. Chem. Soc.*, 1998, **120**, 11616-11626.
53. M. Schreuder Goedheijt, P. C. J. Kamer and P. W. N. M. van Leeuwen, *J. Mol. Catal. A: Chem.*, 1998, **134**, 243-249.
54. R. P. J. Bronger, P. C. J. Kamer and P. W. N. M. Van Leeuwen, *Organometallics*, 2003, **22**, 5358-5369.
55. W. Goertz, P. C. J. Kamer, P. W. N. M. Van Leeuwen and D. Vogt, *Chem. Commun.*, 1997, 1521-1522.
56. M. Kranenburg, P. C. J. Kamer, P. W. N. M. van Leeuwen, D. Vogt and W. Keim, *J. Chem. Soc., Chem. Commun.*, 1995, 2177-2178.
57. I. W. Davies, L. Gerena, L. Castonguay, C. H. Senanayake, R. D. Larsen, T. R. Verhoeven and P. J. Reider, *Chem. Commun.,* 1996, 1753-1754.
58. R. W. Wegman, A. G. Abatjoglou and A. M. Harrison, *J. Chem. Soc., Chem. Commun.*, 1987, 1891-1892.
59. J. Rankin, A. C. Benyei, A. D. Poole and D. J. Cole-Hamilton, *J. Chem. Soc., Dalton Trans.,* 1999, 3771-3782.

60. J. Rankin, A. D. Poole, A. C. Benyei and D. J. Cole-Hamilton, *Chem. Commun.,* 1997, 1835-1836.
61. D. K. Dutta, J. D. Woollins, A. M. Z. Slawin, D. Konwar, P. Das, M. Sharma, P. Bhattacharyya and S. M. Aucott, *Dalton Trans.*, 2003, 2674-2679.
62. C.-A. Carraz, A. G. Orpen, D. D. Ellis, P. G. Pringle, E. J. Ditzel and G. J. Sunley, *Chem. Commun.*, 2000, 1277-1278.
63. J. R. Dilworth, J. R. Miller, N. Wheatley, M. J. Baker and J. G. Sunley, *J. Chem. Soc., Chem. Commun.*, 1995, 1579-1581.
64. M. J. Baker, M. F. Giles, A. G. Orpen, M. J. Taylor and R. J. Watt, *J. Chem. Soc., Chem. Commun.*, 1995, 197-198.
65. L. Gonsalvi, H. Adams, G. J. Sunley, E. Ditzel and A. Haynes, *J. Am. Chem. Soc.*, 1999, **121**, 11233-11234.
66. L. Gonsalvi, H. Adams, G. J. Sunley, E. Ditzel and A. Haynes, *J. Am. Chem. Soc.*, 2002, **124**, 13597-13612.
67. S. Burger, B. Therrien and G. Suess-Fink, *Helv. Chim. Acta*, 2005, **88**, 478-486.
68. C. M. Thomas, R. Mafua, B. Therrien, E. Rusanov, H. Stoeckli-Evans and G. Suss-Fink, *Chem. Eur. J.*, 2002, **8**, 3343-3352.
69. C. M. Thomas and G. Suss-Fink, *Coord. Chem. Rev.*, 2003, **243**, 125-142.
70. Z. Freixa, P. C. J. Kamer, M. Lutz, A. L. Spek and P. W. N. M. van Leeuwen, *Angew. Chem., Int. Ed.*, 2005, **44**, 4385-4388.
71. C. Jimenez-Rodriguez, F. X. Roca, C. Bo, J. Benet-Buchholz, E. C. Escudero-Adan, Z. Freixa and P. W. N. M. van Leeuwen, *Dalton Trans.*, 2005, 268-278.
72. C. Jimenez-Rodriguez, P. J. Pogorzelec, G. R. Eastham, A. M. Z. Slawin and D. J. Cole-Hamilton, *Dalton Trans.*, 2007, 4160-4168.
73. K. G. Moloy and J. L. Petersen, *Organometallics*, 1995, **14**, 2931-2936.
74. K. G. Moloy and R. W. Wegman, *Organometallics*, 1989, **8**, 2883-2892.
75. S. Gaemers and G. J. Sunley, in *Carbonylation process using metal-polydentate ligand catalysts, WO Pat.*, 2004-GB1900, 2004101487, 2004.
76. S. Gaemers and G. J. Sunley, in *Carbonylation process using metal-tridentate ligand catalysts,Application: WO Pat.*, 2004-GB1943, 2004101488, 2004.
77. A. R. Sanger, *J. Chem. Soc., Chem. Commun.*, 1975, 893-894.
78. J. A. Osborn and G. Wilkinson, *Inorg. Synth.*, 1967, **10**, 67.
79. D. Evans, J. A. Osborn and G. Wilkinson, *Inorg. Synth.*, 1968, **11**, 99-101.
80. M. L. Clarke and G. J. Roff, *Chem. Eur. J.*, 2006, **12**, 7978-7986.
81. K. A. Bunten, D. H. Farrar, A. J. Poe and A. Lough, *Organometallics*, 2002, **21**, 3344-3350.

82. S. Jeulin, S. Duprat de Paule, V. Ratovelomanana-Vidal, J.-P. Genet, N. Champion and P. Dellis, *Angew. Chem., Int. Ed.*, 2004, **43**, 320-325.

83. A. Miyashita, A. Yasuda, H. Takaya, K. Toriumi, T. Ito, T. Souchi and R. Noyori, *J. Am. Chem. Soc.*, 1980, **102**, 7932-7934.

84. T. Yamagata, K. Tani, Y. Tatsuno and T. Saito, *J. Chem. Soc., Chem. Commun.*, 1988, 466-468.

85. A. R. Sanger, *J. Chem. Soc., Dalton Trans.*, 1977, 120-129.

86. A. Haynes, P. M. Maitlis, I. A. Stanbridge, S. Haak, J. M. Pearson, H. Adams and N. A. Bailey, *Inorg. Chim. Acta*, 2004, **357**, 3027-3037.

87. H. Adams, N. A. Bailey, B. E. Mann and C. P. Manuel, *Inorg. Chim. Acta*, 1992, **198-200**, 111-118.

88. P. Kuhn, D. Semeril, D. Matt, M. J. Chetcuti and P. Lutz, *Dalton Trans.*, 2007, 515-528.

89. C. Hillairet, G. Michaud and S. Sirol, in *Polymerisation of ethylene and alpha-olefins with phosphine-iminophenol ligand, catalyst components and its preparation, EP Pat.*, 2006-110967, 1832597, 2007.

90. M. Doering and M. Bluhm, in *Manufacture of polyethane and catalyst precursor, EP Pat.*, 2004-25259, 1574529, 2005.

91. M. E. Bluhm, O. Walter and M. Doering, *J. Organomet. Chem.,* 2005, **690**, 713-721.

92. M. L. Clarke, M. B. Diaz-Valenzuela and A. M. Z. Slawin, *Organometallics*, 2007, **26**, 16-19.

93. S. Laue, L. Greiner, J. Woltinger and A. Liese, *Adv. Synth. Catal.*, 2001, **343**, 711-720.

94. J.-X. Gao, T. Ikariya and R. Noyori, *Organometallics*, 1996, **15**, 1087-1089.

95. J. Best, J. M. Wilson, H. Adams, L. Gonsalvi, M. Peruzzini and A. Haynes, *Organometallics*, 2007, **26**, 1960-1965.

96. M. L. Clarke and J. A. Fuentes, *Angew. Chem., Int. Ed.*, 2007, **46**, 930-933.

97. *German Pat.*, 2 627 354, 1976.

98. F. R. Hartley and P. N. Vezey, *Adv. Organomet. Chem.,* 1977, **15**, 189-234.

99. W. H. Lang, A. T. Jurewicz, W. O. Haag, D. D. Whitehurst and L. D. Rollmann, *J. Organomet. Chem.*, 1977, **134**, 85-94.

100. A. F. Borowski, D. J. Cole-Hamilton and G. Wilkinson, *Nouv. J. Chim.*, 1978, **2**, 137-144.

101. R. T. Smith and M. C. Baird, *Inorg. Chim. Acta*, 1982, **62**, 135-139.

102. R. T. Smith, R. K. Ungar, L. J. Sanderson and M. C. Baird, *Organometallics*, 1983, **2**, 1138-1144.

103. I. Toth and B. E. Hanson, *Tetrahedron: Asymmetry*, 1990, **1**, 895-912.

104. I. Toth, B. E. Hanson and M. E. Davis, *J. Organomet. Chem.,* 1990, **397**, 109-117.

105. I. Toth, B. E. Hanson and M. E. Davis, *Tetrahedron: Asymmetry*, 1990, **1**, 913-930.

106. I. Toth, B. E. Hanson and M. E. Davis, *J. Organomet. Chem.*, 1990, **396**, 363-373.

107. J. Chatt, W. Hussain, G. J. Leigh, H. M. Ali, C. J. Pickett and D. A. Rankin, *J. Chem. Soc., Dalton Trans.*, 1985, 1131-1136.

108. T. S. Koblenz, H. L. Dekker, C. G. De Koster, P. W. N. M. Van Leeuwen and J. N. H. Reek, *Chem. Commun.*, 2006, 1700-1702.

109. A. Buhling, P. C. J. Kamer, P. W. N. M. van Leeuwen, J. W. Elgersma, K. Goubitz and J. Fraanje, *Organometallics*, 1997, **16**, 3027-3037.

110. J. A. McCleverty and G. Wilkinson, *Inorg. Synth.*, 1966, **8**, 214-217.

111. P. Suomalainen, H. Riihimaki, S. Jaaskelainen, M. Haukka, J. T. Pursiainen and T. A. Pakkanen, *Catal. Lett.*, 2001, **77**, 125-130.

112. M. A. Bennett and P. A. Longstaff, *J. Am. Chem. Soc.*, 1969, **91**, 6266-6280.

113. S. Otto and A. Roodt, *Inorg. Chim. Acta*, 2004, **357**, 1-10.

114. P. Suomalainen, S. Jaaskelainen, M. Haukka, R. H. Laitinen, J. Pursiainen and T. A. Pakkanen, *Eur. J. Inorg. Chem.*, 2000, 2607-2613.

115. H. Gulyas, Z. Bacsik, A. Szollosy and J. Bakos, *Adv. Synth. Catal.*, 2006, **348**, 1306-1310.

116. A. J. Sandee, J. N. H. Reek, P. C. J. Kamer and P. W. N. M. van Leeuwen, *J. Am. Chem. Soc.*, 2001, **123**, 8468-8476.

117. M. M. Taqui Khan and A. E. Martell, *Inorg. Chem.*, 1974, **13**, 2961.

118. C. Dusemund, M. Mikami and S. Shinkai, *Chem. Lett.,* 1995, 157-158.

119. A. M. Choudhury, I. G. C. Coutts, A. K. Durbin, K. Schofield and D. J. Humphreys, *J. Chem. Soc. C*, 1969, **16**, 2070-2077.

Appendix I: Attempted preparation of an amine containing phosphine ligand

AI.1 Preparation of a morpholine substituted phosphine ligand

Initial investigations into soluble catalysts for the carbonylation of methanol led us to attempt to prepare the following morpholine substituted phosphine ligand **60**. We were successful in preparing the first five synthetic intermediates shown in Fig. AI.1, however were not able to achieve the final P-C coupling step. Poor results in the stability of BIPHEP and BINAP complexes (Chapter V), coupled with the difficulties in preparing the desired ligand **60** led us to focus on more accessible amine-containing ligands such as dppe-NMe_2 **47**.

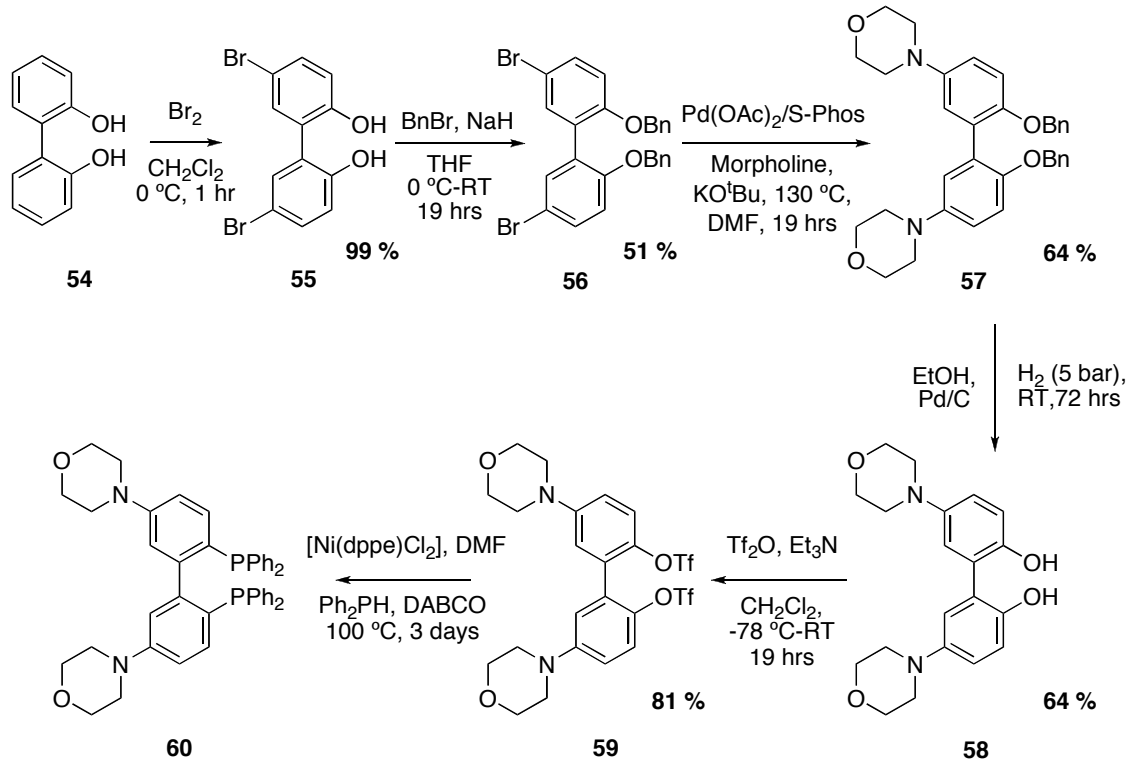

Figure AI.1. The synthetic steps involved in the attempted preparation of the amine-containing phosphine ligand.

AI.2 Experimental for the attempted synthesis of an amine-containing phosphine ligand

5,5'-Dibromo-biphenyl-2,2'-diol 55[118]

This compound was prepared from a modification of the literature procedure. A solution of biphenol **54** (10 g, 53.7 mmol) in dry CH_2Cl_2 was cooled to 0 ºC. To this solution bromine (2.5 eq, 21.5 g, 134 mmol) was added dropwise over a period of 30 mins. After stirring for a further 45 mins a precipitate had formed. This solution was then worked-up using several additions of sodium hydrogen sulphite to remove any remaining HBr. A colour change was observed; from a red/brown to a clear solution containing a pale brown precipitate. This was then filtered to obtain the precipitate. A further re-slurrying of the filtered material in a solution of sodium hydrogen sulphite followed by a second filtration increased the purity of the final solid.

Yield: 99 % (18.3 g, 53 mmol). *Anal.* Calc. for $C_{12}H_8Br_2O_2$: C, 41.9 %; H, 2.34 %. Found: C, 42.30 %; H, 2.07 %. mp: 183-184 ºC (Lit: 188-189 ºC). $^1H\{^{31}P\}$ NMR (acetone-d_6): δ 6.95 (2H, d, *J* = 8.71 Hz, C*H*), 7.36 (2H, dd, *J* = 2.56 & 8.72 Hz, C*H*), 7.40 (2H, d, *J* = 2.56 Hz, C*H*); $^{13}C\{^1H\}$ NMR ($CDCl_3$): δ 114.14 (s, *C*Br), 119.08 (s, *C*H), 125.50 (s, *C*-Ph), 133.39 (s, *C*H), 134.18 (s, *C*H), 152.29 (s, *C*OH). LRMS (ES-) Found 340.8, 342.8, 344.8 [M-H^+]; $C_{12}H_7Br_2O_2$ requires 340.8, 342.8, 344.8 [M-H^+].

2,2'-Dibenzyloxy-5,5'-dibrom-biphenyl 56[119]

Benzyl bromide (3 eq, 0.75 g, 4.36 mmol) was added to a solution containing **55** (0.5 g, 1.45 mmol) and NaH (4 eq, 0.14 g, 5.81mmol) in dry THF at 0 ºC under nitrogen. The reaction was then allowed to proceed at 0 ºC for 25 mins before removing the ice bath, and with continued stirring was allowed to warm to room temperature over the period of 19 hrs. After this time the reaction mixture under went an organic work-up with $NaHCO_3$, then the product was extracted into CH_2Cl_2 and dried over $MgSO_4$. The solvent was then removed under vacuum. The light yellow crystalline solid that was produced was then analysed by TLC to show an excess of benzyl bromide remaining and this was simply removed by washing with petroleum ether. This left a bright white crystalline solid.

Yield: 51 % (0.39 g, 0.74 mmol). *Anal.* Calc. for $C_{26}H_{20}Br_2O_2$: C, 59.57 %; H, 3.85 %. Found: C, 59.39 %; H, 3.85 %. mp: 130-131 ºC (Lit: 134-135 ºC). $^1H\{^{31}P\}$ NMR

($CDCl_3$): δ 4.91 (4H, s, CH_2), 6.78 (2H, d, *J* = 8.49 Hz, *Ph*), 7-7.5 (14H, m, *Ph*); $^{13}C\{^1H\}$ NMR ($CDCl_3$): δ 70.84 (s, *C*H_2), 113.26 (s, *C*-Br) 114.86 (s, *Ph*), 127.03 (s, *Ph*), 128.05 (s, *C*H), 128.84 (s, *Ph*), 129.45 (s, *Ph*), 132.02 (s, *C*H), 134.02 (s, *C*H), 137.13 (s, *C*-Ph), 155.62 (s, *C*-OBn). LRMS (ES+): 544.92, 546.90, 548.92 [M+Na^+]. LRMS (ES+) 544.9, 546.9, 548.9 [M+Na^+]; $C_{26}H_{20}Br_2O_2Na$ requires 545.0, 547.0, 549.0 [M+Na^+].

2,2'-Dibenzyl-biphenyl-5,5'-dimorpholine 57

A solution containing **56** (100 mg, 0.19 mmol), morpholine (8 eq, 133 mg, 1.53 mmol), $Pd(OAc)_2$ (5 %mol/mol, 2.134 mg), S-Phos (5 %mol/mol, 3.917 mg), and 0.1 M ^{t}BuOK (5 eq, 0.95 ml) in DMF was heated to 130 ºC for 19 hrs. The resulting mixture was then allowed to cool to room temperature before an organic workup and an extraction using ethyl acetate. The organic portions were then washed with H_2O and brine then dried over K_2CO_3. The solvent was then removed from the filtered solution on the rotary evaporator to leave a dark brown residue. This was further purified by passing through a column of silica gel eluting with a solution of 3:1 ethyl acetate/hexane, to give a brown residue that solidified under high vacuum for 2 days to allow the complete removal of DMF.

Yield: 64 % (65.5 mg, 0.12 mmol). $^1H\{^{31}P\}$ NMR ($CDCl_3$): δ 2.95 (8H, t, *J* = 4.61 Hz, CH_2), 3.76 (8H, t, *J* = 4.61 Hz, CH_2), 4.84 (4H, s, CH_2), 6.77 (2H, dd, *J* = 2.82 & 8.96 Hz, C*H*), 6.86 (2H, d, *J* = 8.96 Hz, C*H*), 6.89 (2H, d, J = 2.82 Hz, C*H*), 7.16 (10H, m, C*H*, Ph); $^{13}C\{^1H\}$ NMR ($CDCl_3$): δ 50.99 (s, *C*H_2), 67.46 (s, CH_2), 71.53 (s, *C*H_2), 114.90 (s, *C*H) 116.7 (s, *C*H), 120.89 (s, *C*H), 127.37 (s, *Ph*), 127.87 (s, *Ph*), 128.63 (s, *Ph*), 129.72 (s, *C*-NR), 138.12 (s, *Ph*), 145.80 (s, *C*-Ph), 150.96 (s, *C*-OBn). HRMS Found 537.2748 [MH^+]; $C_{34}H_{37}N_2O_4$ requires 537.2748 [MH^+].

2,2'-Dihydroxyl-biphenyl-5,5'-dimorpholine 58

57 (100 mg, 0.19 mmol) and 10 % Pd on carbon (10 %mol/mol, 1.99 mg, 0.19 mmol) in a solution of ethanol (3 cm^3) was put under a hydrogen pressure of 5 atm. This was left to stir for 3 days then filtered through a bed of celite, which was then washed with a further addition ethanol. The solvent was then removed under vacuum to obtain an off-white powder.

Yield: 63.6 % (42 mg, 0.12 mmol). $^{1}H\{^{31}P\}$ NMR ($CDCl_3$): δ 3.00 (8H, t, *J* = 4.35 Hz, C*H*$_2$), 3.79 (8H, t, *J* = 4.35 Hz, C*H*$_2$), 6.84 (6H, m, C*H*); $^{13}C\{^{1}H\}$ NMR ($CDCl_3$) δ 51.06 (4C, s, *C*H$_2$), 67.36 (4C, s, CH$_2$), 117.99 (2C, s, *C*H) 118.56 (2C, s, *C*H), 119.55 (2C, s, *C*H), 125.63 (2C, s, *C*-NR), 147.42 (4C, s, *C*OH). HRMS Found 357.1811 [MH^+]; $C_{20}H_{25}N_2O_4$ requires 357.1814 [MH^+].

2,2'-Ditriflate-biphenyl-5,5'-dimorpholine 59

Tf_2O (3 eq, 118 mg, 0.42 mmol) was added drop-wise to a solution containing **58** (50 mg, 0.14 mmol) and dry Et_3N (3 eq, 43 mg, 0.42 mmol) in dry CH_2Cl_2 at -78 ºC under nitrogen. The cooling bath was then removed and the reaction and with continued stirring was allowed to warm to room temperature over the period of 19 hrs. After completion this was poured into ice cold 0.1 M HCl. The product was then extracted using CH_2Cl_2 followed by an organic workup comprising $NaHCO_3$ and NaCl saturated solutions, then dried over Na_2SO_4. The solvent was then removed on a rotary evaporator to leave the crude product. This was further purified by passing through a short column of silica gel eluting with a solution of 3:1 ethyl acetate/hexane, to give an orange/light brown crystalline solid.

Yield: 80.8 % (59 mg, 0.095 mmol). *Anal.* Calc. for $C_{22}H_{22}F_6N_2O_8S_2$: C, 42.98 %; H, 3.57 %; N, 4.51; Found: C, 42.58 %; H, 3.62 %; N, 4.44 %. $^{1}H\{^{31}P\}$ NMR ($CDCl_3$): δ 3.12 (8H, t, *J* = 4.68 Hz, C*H*$_2$), 3.81 (8H, t, *J* = 4.68 Hz, C*H*$_2$), 6.82 (2H, d, *J* = 3.07 Hz, C*H*), 6.88 (2H, dd, *J* = 3.07 & 8.96 Hz, C*H*), 7.20 (2H, d, *J* = 8.96 Hz, C*H*); $^{19}F\{^{1}H\}$ NMR ($CDCl_3$) δ -74.56 (s, CF_3). HRMS Found 643.0604 [$M+Na^+$]; $C_{22}H_{22}F_6N_2NaO_8S_2$ requires 643.0614 [$M+Na^+$].

Appendix II: X-ray crystallographic data

AII.1 X-ray crystallography

X-ray crystallography data was collected at 93 K by using a Rigaku MM007 High brilliance RA generator and Mercury/Saturn CCD systems using Mo K_α radiation. Intensities were corrected for Lorentz-polarisation and for absorption. The structures were solved by direct methods. All hydrogen atoms were refined as idealised riding geoemetries and structural refinements were obtained with full-matrix least-squares based on F^2 by using the program SHELXTL. Where appropriate solvent molecules were omitted for clarity. Full crystallographic data in CIF format is available on the CD attachment. Complex **51** was somewhat disordered so no comments can be made regarding bond lengths and angles.

Crystal data and structure refinement for [Rh(BINAP)(CO)I] 6

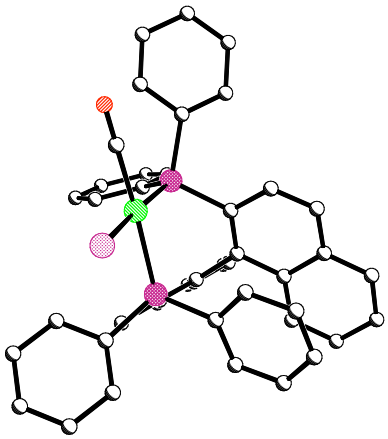

Empirical formula	C45 H32 I O P2 Rh	
Formula weight	880.46	
Temperature	93(2) K	
Wavelength	0.71073 Å	
Crystal system	Triclinic	
Space group	P-1	
Unit cell dimensions	a =11.15776(12) Å	α= 84.203(7)°.
	b =11.5084(16) Å	β= 71.704(7)°.
	c =14.6153(15) Å	γ = 89.593(10)°.
Volume	1772.1(4) $Å^3$	
Z	2	
Density (calculated)	1.650 Mg/m^3	
Absorption coefficient	1.480 mm^{-1}	
F(000)	876	
Crystal size	0.1000 x 0.0300 x 0.0100 mm^3	
Theta range for data collection	2.02 to 25.33°.	
Index ranges	-13<=h<=10, -13<=k<=10, -17<=l<=15	
Reflections collected	11550	
Independent reflections	6105 [R(int) = 0.0409]	
Completeness to theta = 25.00°	94.7 %	
Absorption correction	Multiscan	
Max. and min. transmission	1.0000 and 0.5353	
Refinement method	Full-matrix least-squares on F^2	
Data / restraints / parameters	6105 / 0 / 452	
Goodness-of-fit on F^2	1.002	
Final R indices [I>2sigma(I)]	R1 = 0.0474, wR2 = 0.0781	
R indices (all data)	R1 = 0.0645, wR2 = 0.0865	
Largest diff. peak and hole	0.875 and -1.667 $e.Å^{-3}$	

Crystal data and structure refinement for [Rh(dppb)(COMe)I_2] 7

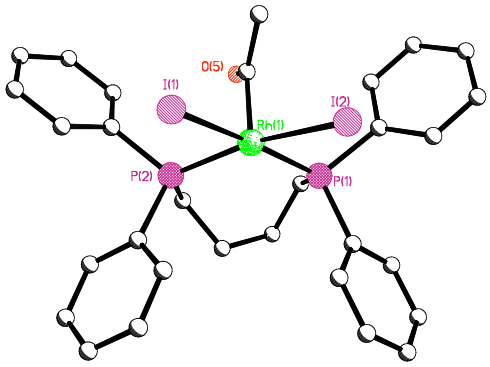

Empirical formula	C30 H31 I2 O P2 Rh	
Formula weight	825.90	
Temperature	93(2) K	
Wavelength	0.71073 Å	
Crystal system	Monoclinic	
Space group	P2(1)/c	
Unit cell dimensions	a = 21.540(4) Å	α= 90°.
	b = 8.1514(14) Å	β= 96.662(3)°.
	c = 18.908(4) Å	γ = 90°.
Volume	3297.5(11) $Å^3$	
Z	4	
Density (calculated)	1.739 Mg/m^3	
Absorption coefficient	2.513 mm^{-1}	
F(000)	1680	
Crystal size	0.0300 x 0.0200 x 0.0200 mm^3	
Theta range for data collection	2.27 to 25.36°.	
Index ranges	-25<=h<=23, -9<=k<=9, -22<=l<=22	
Reflections collected	22888	
Independent reflections	5963 [R(int) = 0.0310]	
Completeness to theta = 25.00°	98.9 %	
Absorption correction	Multiscan	
Max. and min. transmission	1.0000 and 0.4715	
Refinement method	Full-matrix least-squares on F^2	
Data / restraints / parameters	5963 / 0 / 354	
Goodness-of-fit on F^2	1.098	
Final R indices [I>2sigma(I)]	R1 = 0.0258, wR2 = 0.0486	
R indices (all data)	R1 = 0.0337, wR2 = 0.0519	
Largest diff. peak and hole	0.670 and -0.568 $e.Å^{-3}$	

Crystal data and structure refinement for $[Rh(dppx)(COMe)I_2].CHCl_3$ 10

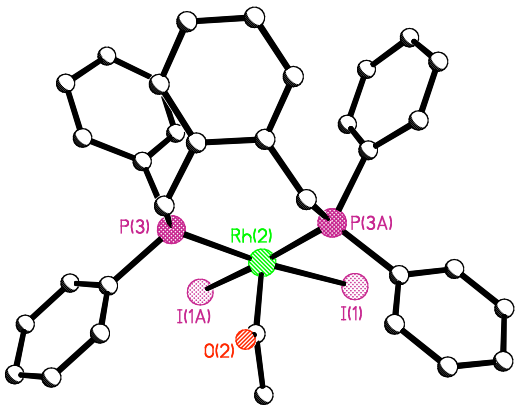

Empirical formula	C34 H31 I2 O P2 Rh.CHCl3	
Formula weight	993.61	
Temperature	93(2) K	
Wavelength	0.71073 Å	
Crystal system	Orthorhombic	
Space group	Pnma	
Unit cell dimensions	a = 24.241(4) Å	α= 90°.
	b = 18.209 Å	β= 90°.
	c = 8.1431(14) Å	γ = 90°.
Volume	3594.5(11) $Å^3$	
Z	4	
Density (calculated)	1.836 Mg/m^3	
Absorption coefficient	2.533 mm^{-1}	
F(000)	1928	
Crystal size	0.1100 x 0.0300 x 0.0300 mm^3	
Theta range for data collection	1.68 to 25.31°.	
Index ranges	-18<=h<=29, -21<=k<=21, -9<=l<=7	
Reflections collected	21819	
Independent reflections	3338 [R(int) = 0.1380]	
Completeness to theta = 25.00°	98.4 %	
Absorption correction	Multiscan	
Max. and min. transmission	1.0000 and 0.6069	
Refinement method	Full-matrix least-squares on F^2	
Data / restraints / parameters	3338 / 0 / 210	
Goodness-of-fit on F^2	1.041	
Final R indices [I>2sigma(I)]	R1 = 0.0641, wR2 = 0.1186	
R indices (all data)	R1 = 0.1037, wR2 = 0.1316	
Largest diff. peak and hole	1.244 and -1.1357 $e.Å^{-3}$	

Crystal data and structure refinement for 29a.2H_2O

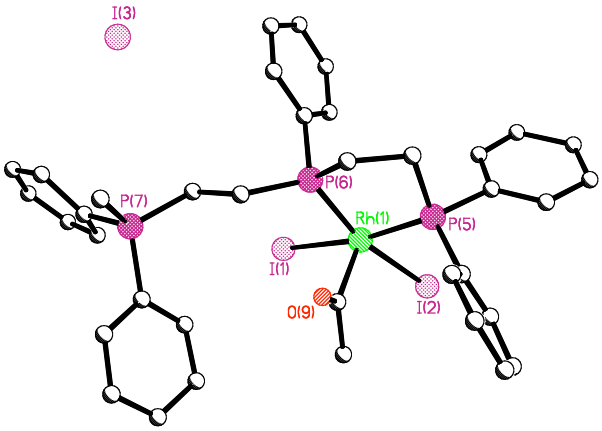

Empirical formula	C37 H39 I3 O P3 Rh. 2[H2O]	
Formula weight	1112.23	
Temperature	93(2) K	
Wavelength	0.71073 Å	
Crystal system	Monoclinic	
Space group	P2(1)/n	
Unit cell dimensions	a = 18.916(3) Å	α= 90°.
	b = 11.4403(17) Å	β= 115.263(8)°.
	c = 20.007(4) Å	γ = 90°.
Volume	3915.4(12) $Å^3$	
Z	4	
Density (calculated)	1.887 Mg/m^3	
Absorption coefficient	2.959 mm^{-1}	
F(000)	2152	
Crystal size	0.100 x 0.080 x 0.010 mm^3	
Theta range for data collection	2.80 to 25.34°.	
Index ranges	-22<=h<=17, -10<=k<=13, -23<=l<=23	
Reflections collected	22382	
Independent reflections	6829 [R(int) = 0.0886]	
Completeness to theta = 25.00°	96.7 %	
Absorption correction	Multiscan	
Max. and min. transmission	1.0000 and 0.7815	
Refinement method	Full-matrix least-squares on F^2	
Data / restraints / parameters	6829 / 0 / 427	
Goodness-of-fit on F^2	1.141	
Final R indices [I>2sigma(I)]	R1 = 0.0840, wR2 = 0.1749	
R indices (all data)	R1 = 0.1165, wR2 = 0.1949	
Largest diff. peak and hole	1.766 and -2.592 $e.Å^{-3}$	

Crystal data and structure refinement for [Rh(PNO-C_3)CO(Cl)].CH_3OH 38

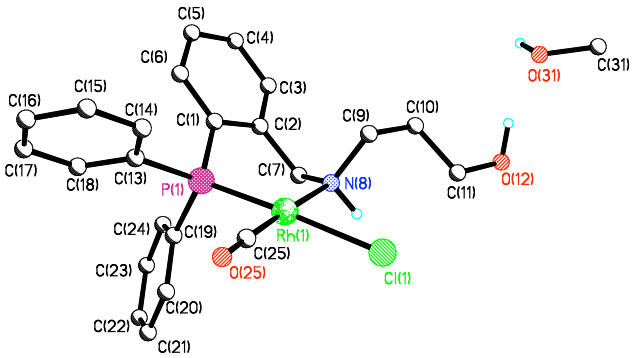

Empirical formula	C23 H24 Cl N O2 P Rh.CH3OH	
Formula weight	547.80	
Temperature	93(2) K	
Wavelength	0.71073 Å	
Crystal system	Triclinic	
Space group	P-1	
Unit cell dimensions	a = 9.2996(15) Å	α= 103.365(11)°.
	b = 9.9027(17) Å	β= 95.038(12)°.
	c = 13.758(2) Å	γ = 91.805(12)°.
Volume	1226.1(4) $Å^3$	
Z	2	
Density (calculated)	1.484 Mg/m^3	
Absorption coefficient	0.895 mm^{-1}	
F(000)	560	
Crystal size	0.200 x 0.200 x 0.050 mm^3	
Theta range for data collection	3.14 to 25.35°.	
Index ranges	-11<=h<=11, -11<=k<=11, -16<=l<=16	
Reflections collected	11293	
Independent reflections	4319 [R(int) = 0.0821]	
Completeness to theta = 25.00°	97.4 %	
Absorption correction	Multiscan	
Max. and min. transmission	1.0000 and 0.8850	
Refinement method	Full-matrix least-squares on F^2	
Data / restraints / parameters	4319 / 2 / 291	
Goodness-of-fit on F^2	1.286	
Final R indices [I>2sigma(I)]	R1 = 0.0728, wR2 = 0.1689	
R indices (all data)	R1 = 0.0776, wR2 = 0.1710	
Largest diff. peak and hole	1.274 and -1.018 e.$Å^{-3}$	

Crystal data and structure refinement for $[Rh(PNO\text{-}C_3)Cl_3].CHCl_3$ 42

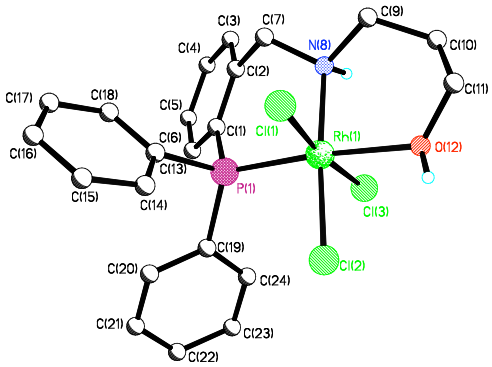

Empirical formula	C22 H24 Cl3 N O P Rh.CHCl3	
Formula weight	678.02	
Temperature	93(2) K	
Wavelength	0.71073 Å	
Crystal system	Triclinic	
Space group	P-1	
Unit cell dimensions	a = 10.490(3) Å	α= 77.38(6)°.
	b = 11.131(3) Å	β= 84.17(6)°.
	c = 12.635(4) Å	γ = 65.18(5)°.
Volume	1306.5(6) $Å^3$	
Z	2	
Density (calculated)	1.723 Mg/m^3	
Absorption coefficient	1.347 mm^{-1}	
F(000)	680	
Crystal size	0.0600 x 0.0300 x 0.0300 mm^3	
Theta range for data collection	2.06 to 25.35°.	
Index ranges	-12<=h<=11, -13<=k<=13, -15<=l<=14	
Reflections collected	13100	
Independent reflections	4728 [R(int) = 0.0370]	
Completeness to theta = 25.00°	99.0 %	
Absorption correction	Multiscan	
Max. and min. transmission	1.0000 and 0.8812	
Refinement method	Full-matrix least-squares on F^2	
Data / restraints / parameters	4728 / 2 / 307	
Goodness-of-fit on F^2	1.044	
Final R indices [I>2sigma(I)]	R1 = 0.0364, wR2 = 0.0746	
R indices (all data)	R1 = 0.0487, wR2 = 0.0812	
Largest diff. peak and hole	1.555 and -0.469 $e.Å^{-3}$	

Crystal data and structure refinement for $[Rh(PNN\text{-}C_3)Cl_3].1/2CH_3COCH_3$ 43

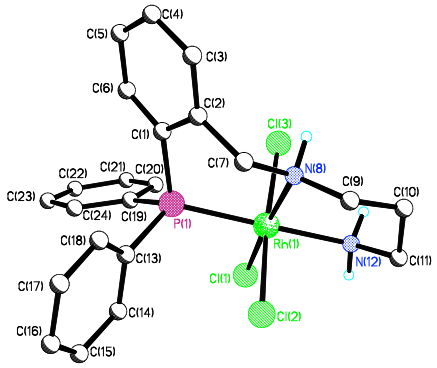

Empirical formula	C22 H25 Cl3 N2 P Rh. ½[CH3COCH3]	
Formula weight	586.71	
Temperature	93(2) K	
Wavelength	0.71073 Å	
Crystal system	Monoclinic	
Space group	P2(1)/c	
Unit cell dimensions	a = 16.4609(14) Å	α= 90°.
	b = 8.0615(6) Å	β= 107.967(4)°.
	c = 20.6366(17) Å	γ = 90°.
Volume	2604.9(4) $Å^3$	
Z	4	
Density (calculated)	1.496 Mg/m^3	
Absorption coefficient	1.041 mm^{-1}	
F(000)	1192	
Crystal size	0.100 x 0.100 x 0.100 mm^3	
Theta range for data collection	3.27 to 25.35°.	
Index ranges	-17<=h<=19, -9<=k<=9, -24<=l<=23	
Reflections collected	24148	
Independent reflections	4716 [R(int) = 0.1671]	
Completeness to theta = 25.00°	98.9 %	
Absorption correction	Multiscan	
Max. and min. transmission	1.0000 and 0.8978	
Refinement method	Full-matrix least-squares on F^2	
Data / restraints / parameters	4716 / 3 / 279	
Goodness-of-fit on F^2	1.266	
Final R indices [I>2sigma(I)]	R1 = 0.1510, wR2 = 0.3109	
R indices (all data)	R1 = 0.1629, wR2 = 0.3171	
Largest diff. peak and hole	1.680 and -1.243 e.Å-3	

Crystal data and structure refinement for $[Rh(PNS\text{-}C_3)I_3].CHCl_3$ 44

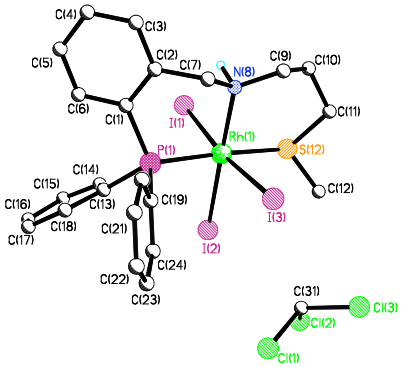

Empirical formula	C23 H26 I3 N P Rh S. CH Cl3	
Formula weight	982.46	
Temperature	93(2) K	
Wavelength	0.71073 Å	
Crystal system	Triclinic	
Space group	P-1	
Unit cell dimensions	a = 9.005(2) Å	α= 88.472(10)°.
	b = 11.649(3) Å	β= 84.231(9)°.
	c = 14.320(3) Å	γ = 83.564(11)°.
Volume	1484.9(6) $Å^3$	
Z	2	
Density (calculated)	2.197 Mg/m^3	
Absorption coefficient	4.104 mm^{-1}	
F(000)	928	
Crystal size	0.030 x 0.030 x 0.030 mm^3	
Theta range for data collection	3.27 to 25.35°.	
Index ranges	-10<=h<=10, -9<=k<=14, -16<=l<=14	
Reflections collected	8585	
Independent reflections	5104 [R(int) = 0.0914]	
Completeness to theta = 25.00°	95.6 %	
Absorption correction	Multiscan	
Max. and min. transmission	1.0000 and 0.8606	
Refinement method	Full-matrix least-squares on F^2	
Data / restraints / parameters	5104 / 0 / 310	
Goodness-of-fit on F^2	1.091	
Final R indices [I>2sigma(I)]	R1 = 0.0826, wR2 = 0.2249	
R indices (all data)	R1 = 0.0975, wR2 = 0.2387	
Largest diff. peak and hole	2.779 and -1.817 $e.Å^{-3}$	

Crystal data and structure refinement: [Rh(dppe-(NMe_2)$_4$)CO(Cl)].2H_2O 47

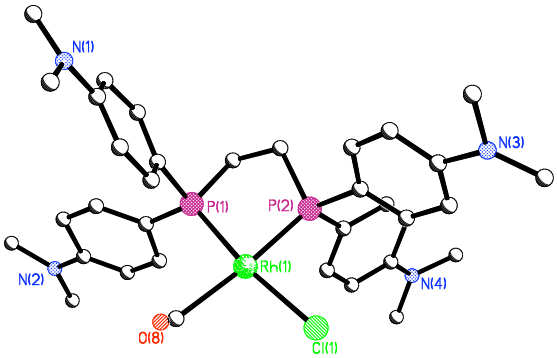

Empirical formula	C35 H44 Cl N4 O P2 Rh.2(H2 O)	
Formula weight	773.07	
Temperature	93(2) K	
Wavelength	0.71073 Å	
Crystal system	Monoclinic	
Space group	C2	
Unit cell dimensions	a = 25.6933(18) Å	α= 90°.
	b = 8.1263(6) Å	β= 98.610(4)°.
	c = 21.3538(15) Å	γ = 90°.
Volume	4408.2(5) Å^3	
Z	4	
Density (calculated)	1.165 Mg/m^3	
Absorption coefficient	0.553 mm^{-1}	
F(000)	1608	
Crystal size	0.100 x 0.030 x 0.010 mm^3	
Theta range for data collection	2.84 to 25.35°.	
Index ranges	-23<=h<=30, -9<=k<=9, -25<=l<=25	
Reflections collected	21301	
Independent reflections	7887 [R(int) = 0.0520]	
Completeness to theta = 25.00°	98.7 %	
Absorption correction	Multiscan	
Max. and min. transmission	1.0000 and 0.9562	
Refinement method	Full-matrix least-squares on F^2	
Data / restraints / parameters	7887 / 24 / 428	
Goodness-of-fit on F^2	1.094	
Final R indices [I>2sigma(I)]	R1 = 0.0904, wR2 = 0.2439	
R indices (all data)	R1 = 0.0940, wR2 = 0.2469	
Absolute structure parameter	0.06(7)	
Largest diff. peak and hole	1.505 and -0.597 e.Å^{-3}	

Crystal data and structure refinement for [Rh(dppe-(NMe$_2$)$_4$)COMe(I)$_2$] 49

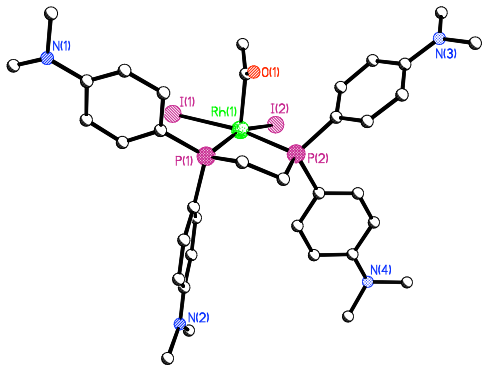

Empirical formula	C36 H47 I2 N4 O P2 Rh. ¼(CH2 Cl2)	
Formula weight	991.66	
Temperature	93(2) K	
Wavelength	0.71073 Å	
Crystal system	Monoclinic	
Space group	C2/c	
Unit cell dimensions	a = 34.391(3) Å	α= 90°.
	b = 10.3769(7) Å	β= 112.234(4)°.
	c = 26.060(2) Å	γ = 90°.
Volume	8608.5(11) Å^3	
Z	8	
Density (calculated)	1.530 Mg/m^3	
Absorption coefficient	1.967 mm^{-1}	
F(000)	3924	
Crystal size	0.100 x 0.100 x 0.010 mm^3	
Theta range for data collection	2.14 to 25.35°.	
Index ranges	-41<=h<=40, -12<=k<=12, -30<=l<=31	
Reflections collected	38816	
Independent reflections	7790 [R(int) = 0.1067]	
Completeness to theta = 25.00°	99.3 %	
Absorption correction	Multiscan	
Max. and min. transmission	1.0000 and 0.7995	
Refinement method	Full-matrix least-squares on F^2	
Data / restraints / parameters	7790 / 10 / 429	
Goodness-of-fit on F^2	1.221	
Final R indices [I>2sigma(I)]	R1 = 0.0888, wR2 = 0.1993	
R indices (all data)	R1 = 0.1018, wR2 = 0.2073	
Largest diff. peak and hole	2.733 and -1.486 e.Å^{-3}	